

THESIS FOR THE DEGREE OF DOCTOR OF PHILOSOPHY

Collisional effects and attosecond diagnostics in laser-generated plasmas

ANDRÉAS SUNDSTRÖM

Department of Physics
CHALMERS UNIVERSITY OF TECHNOLOGY
Göteborg, Sweden 2022

Collisional effects and attosecond diagnostics in laser-generated plasmas

ANDRÉAS SUNDSTRÖM

ISBN 978-91-7905-743-5

© ANDRÉAS SUNDSTRÖM, 2022.

Doktorsavhandlingar vid Chalmers tekniska högskola

Ny serie nr 5209

ISSN 0346-718X

Division of Subatomic, High Energy and Plasma Physics

Department of Physics

Chalmers University of Technology

SE-412 96 Göteborg

Sweden

Telephone: +46 (0)31-772 1000

Cover: Illustration of a laser-plasma experiment, with a high-intensity optical laser pulse hitting a thin-foil plasma, and an extreme-ultraviolet probe pulse to diagnose the laser plasma. In the plasma, Coulomb collisions are illustrated through various particle trajectories.

Typeset in L^AT_EX

Printed in Sweden by

Chalmers digitaltryck

Göteborg, Sweden 2022

Collisional effects and attosecond diagnostics in
laser-generated plasmas

ANDRÉAS SUNDSTRÖM

Department of Physics
Chalmers University of Technology

Abstract

When matter is radiated by laser light of extreme intensity, it is rapidly ionized, thereby forming a plasma. Such laser-generated plasmas can be used as sources of energetic particles and radiation, or to study astrophysically relevant phenomena in the laboratory and the behavior of matter under extreme conditions. This thesis considers the dynamics and diagnosis of laser-induced plasmas, with focus on the effect of Coulomb collisions on electrostatic shocks and laser-energy absorption, as well as ultra-rapid plasma diagnostics using attosecond pulses.

Electrostatic shocks in plasmas have the potential to accelerate ions with a very narrow energy spread. First, collisional effects on electrostatic shocks are studied in two regimes of low and high collisionality. In the former, we show that even rare collisions can significantly affect the structure of the electrostatic shock over long time scales due to an accumulation of trapped ions. The high-collisionality case was studied using particle-in-cell simulations of laser foil targets. Effective ion acceleration by electrostatic shocks relies on a high electron temperature. Heating of the upstream ions, through collisions with the shock-accelerated ions, creates a self-amplifying process that increases the fraction of accelerated ions. However, this unstable condition rapidly depletes the energy of the shock, which transitions into a blast wave, unable to accelerate ions.

An additional study of the same laser–solid interaction shows that, unlike the commonly held knowledge, collisions may dominate the energy absorption of ultraintense laser pulses through inverse bremsstrahlung, and also causing rapid thermalization of the target electrons.

Finally, two diagnostic methods for the electron density utilizing attosecond extreme-ultraviolet pulses, are presented. The first method is based on the dispersion of a probe pulse, which can be used to infer information about the peak density and line-integrated density of the probed plasma. The second method is based on stimulated Raman scattering, which uses two pulses, and can give a localized reading of the electron density in the interaction regions where the two pulses meet.

Keywords: plasma physics, laser-plasmas, electrostatic shocks, Coulomb collisions, attosecond pulses, extreme-ultraviolet, plasma diagnostics

List of publications

This thesis is based on the work contained in the following publications:

- A** SUNDSTRÖM, A., JUNO, J., TENBARGE, J. M. & PUSZTAI, I. 2019 “Effect of a weak ion collisionality on the dynamics of kinetic electrostatic shocks”. *Journal of Plasma Physics* **85** (1), 905850 108, DOI: 10.1017/S0022377819000023
- B** SUNDSTRÖM, A., GREMILLET, L., SIMINOS, E. & PUSZTAI, I. 2020a “Fast collisional electron heating and relaxation with circularly polarized ultraintense short-pulse laser”. *Journal of Plasma Physics* **86** (2), 755860 201, DOI: 10.1017/S0022377820000264
- C** SUNDSTRÖM, A., GREMILLET, L., SIMINOS, E. & PUSZTAI, I. 2020b “Collisional effects on the ion dynamics in thin-foil targets driven by an ultraintense short pulse laser”. *Plasma Physics and Controlled Fusion* **62** (8), 085 015, DOI: 10.1088/1361-6587/ab9a62
- D** SUNDSTRÖM, A., PUSZTAI, I., ENG-JOHNSON, P. & FÜLÖP, T. 2022a “Attosecond dispersion as a diagnostics tool for solid-density laser-generated plasmas”. *Journal of Plasma Physics* **88** (2), 905880 211, DOI: 10.1017/S0022377822000307
- E** SUNDSTRÖM, A., GRECH, M., PUSZTAI, I. & RICONDA, C. 2022b “Stimulated-Raman-scattering amplification of attosecond XUV pulses with pulse-train pumps and application to local in-depth plasma-density measurement”. *Physical Review E* **106**, 045 208, DOI: 10.1103/PhysRevE.106.045208

Publications not included in this thesis

- F** PUSZTAI, I., JUNO, J., BRANDENBURG, A., TENBARGE, J. M., HAKIM, A., FRANCISQUEZ, M. & SUNDSTRÖM, A. 2020 “Dynamo in weakly collisional nonmagnetized plasmas impeded by Landau damping of magnetic fields”. *Physical Review Letters* **124**, 255 102, DOI: 10.1103/PhysRevLett.124.255102
- G** TINGUELY, R. A., IZZO, V. A., GARNIER, D. T., SUNDSTRÖM, A., SÄRKIMÄKI, K., EMBRÉUS, O., FÜLÖP, T., GRANETZ, R. S., HOPPE, M., PUSZTAI, I. & SWEENEY, R. 2021 “Modeling the complete prevention of disruption-generated runaway electron beam formation with a passive 3D coil in SPARC”. *Nuclear Fusion* **61** (12), 124 003, DOI: 10.1088/1741-4326/ac31d7
- H** IZZO, V. A., PUSZTAI, I., SÄRKIMÄKI, K., SUNDSTRÖM, A., GARNIER, D. T., WEISBERG, D., TINGUELY, R. A., PAZ-SOLDAN, C., GRANETZ, R. S. & SWEENEY, R. 2022 “Runaway electron deconfinement in SPARC and DIII-D by a passive 3D coil”. *Nuclear Fusion* **62** (9), 096 029, DOI: 10.1088/1741-4326/ac83d8
- I** TINGUELY, R. A., PUSZTAI, I. IZZO, V. A., , SÄRKIMÄKI, K., FÜLÖP, T., GARNIER, D. T., GRANETZ, R. S., HOPPE, M., PAZ-SOLDAN, C., SUNDSTRÖM, A. & SWEENEY, R. 2022 “On the minimum transport required to passively suppress runaway electrons in SPARC”. *Submitted to Plasma Physics and Controlled Fusion*

Statement of contribution

- Paper A:** I implemented the kinetic shock model numerically in a MATLAB library for numerically computing shock parameters based on a given set of input arguments. The library was used in the computations for the paper. I wrote the majority of the manuscript with input from the co-authors; I produced all the figures (except fig. 8).
- Paper B:** I ran all simulations for the paper. The results were analyzed and discussed in close collaboration with the co-authors. I produced all the figures and wrote the manuscript.
- Paper C:** I ran all simulations for the paper. The results were analyzed and discussed in close collaboration with the co-authors. I produced all the figures and wrote the manuscript.
- Paper D:** I implemented the pseudo-spectral solver in a Python package, which includes methods for extracting relevant data directly from output from Smilei particle-in-cell simulations. I ran all simulations for the paper. The results were analyzed and discussed in close collaboration with the co-authors. I produced all the figures and wrote the manuscript.
- Paper E:** I ran all simulations for the paper. The results were discussed and analyzed in close collaboration with the co-authors. I produced all the figures and wrote the manuscript.

*And all I've done for want of wit
To memory now I can't recall
So fill to me the parting glass
Good night and joy be to you all*
“The parting glass” (trad. Irish folk song)

Acknowledgments

I would first and foremost like to extend my warmest gratitude to my main supervisor István Pusztai, whose enormous patience, the failure of which I have never witnessed despite my many silly and ridiculous ideas, suggestions and flat-out failure to listen to sound advice throughout the years. Besides István, I would also like to express my deepest gratefulness to my co-supervisors Laurent Gremillet and Evangelos Siminos, the insights of whom have been invaluable in the pursuance the various research projects. Next, I must also express my strongest gratitude to Tünde Fülöp, the leader of our plasma-physics group here at Chalmers, who not only provided me with the opportunity to pursue doctoral studies, but also supported and guided me through these studies. Last, but not least, I wish to send a heartfelt thanks to Caterina Riconda and her research group for their warm hospitality during my visit to Paris.

I would of course also like to send out my warmest appreciation to all the other, present and former, members of our research group – no one named, no one left out – who have given meaning to all the coffee breaks and Friday fikas that I have forced upon them. A special thanks also goes out to hr Dr-Ing Algehed, for all the days and evenings spent on the Water and all the liters of grape juice and barley malt consumed. Then, there is one last group of people here at Chalmers that I would like to thank: the students that I have had the pleasure of teaching. At the risk of beating the already over-used cliché to death, following their learning journey has been the most fun and rewarding experience during my time here – my only regret is that I didn't get to follow them further.

Finally, I cannot thank my family enough for the support that they have given me through out my whole life, and especially these last four years. I have previously thanked my father and sister, and this time I want to especially thank my dear sweet mother, who has always encouraged and supported me – too often without adequate gratitude.

Andréas Sundström, Göteborg, 2022-11-09

Contents

Abstract	iii
List of publications	v
Statement of contribution	vii
1 Introduction	1
1.1 Laser-based particle acceleration	3
1.2 High energy density and plasma heating	7
1.3 High-harmonic generation and plasma optics	8
1.4 Simulating and diagnosing laser plasmas	10
2 Basics of plasma physics	15
2.1 Kinetic theory	15
2.1.1 Maxwell–Jüttner distribution	18
2.1.2 Moments and fluid quantities	19
2.1.3 Electromagnetic waves in plasmas	20
2.2 Fluid theory	23
2.2.1 Debye shielding	24
2.2.2 Ion-acoustic waves	25
2.2.3 Langmuir electron waves	26
2.3 Collisions	27
2.4 Simulating plasmas	29
2.4.1 Continuum Vlasov–Maxwell solvers	29
2.4.2 Particle-in-cell methods	31
3 Laser–plasma interactions	35
3.1 Basic concepts of laser–plasma interactions	35
3.1.1 Particle motion in an electromagnetic plane wave	36
3.1.2 Undercritical plasmas	39
3.1.3 Overcritical plasmas	42

3.2 Laser-induced plasma heating	46
4 Plasma diagnostics using attosecond pulses	49
4.1 Diagnosing electron density with dispersion	49
4.1.1 Quantifying dispersion using group delay	50
4.1.2 The pseudo-spectral wave solver	52
4.2 Using stimulated Raman scattering to measure density . . .	53
5 Summary and outlook	57
5.1 Summary of papers	57
5.2 Outlook	61
References	65
Included papers A–E	83

*Je n'ai fait celle-ci plus longue que parce que
je n'ai pas eu le loisir de la faire plus courte.*

*I have made this longer only because I have
not had time to make it shorter.*

Blaise Pascal (1657)

Chapter 1

Introduction

Broadly speaking, physics is the study of matter and energy, how they interact and behave in relation to time and space. Our knowledge of physics has been a fundamental cornerstone in the advancements of technology made throughout human history – from the quantum mechanical effects that govern the behavior of the semi-conductors in our computers, to Newton’s and Maxwell’s laws which let us understand the “ordinary” world around us, like the behavior of mechanical structures under load or the transmission of radio waves. The perhaps greatest manifestation of this knowledge lies in the predictive power of mathematical modeling of physical systems. However, while precise and accurate modeling may be very powerful, a physicist must also master a second very powerful tool: the approximation. When there are more variables than we can control or even be aware of, knowing what level of detail in the modeling is “good enough” becomes crucial. Likewise, knowing the limitations of a model based on approximations – which all models and physical laws are – is just as essential as the predictions of the model itself. Another, related, powerful tool for the physicist is the generalization – in the prejudicious sense of the word – to bunch together similar systems under one class. We can then develop laws and intuitions for each class of systems.

One such class of physical systems is the *plasma* state of matter. In the progression from solid, to liquid, to gaseous, the atoms and molecules become less and less bound to each other, from being bound in a lattice when solid to flying around more or less freely in a gas. In the plasma state – the next step on the ladder – the electrons are no longer bound to their atomic nuclei. The fact that the negatively charged electrons and positively charged ions are separated from each other in a plasma, means that each individual charged particle contributes and responds to

the electromagnetic fields present. A plasma, therefore, reacts to external and internal electromagnetic fields in a way which is fundamentally different to the behavior the other states of matter.

In order to reach a plasma state, the matter must either have sufficiently high internal energy (have high enough temperature) or be subjected to an electric field that can overcome the atomic binding potential that keeps the electrons bound to the atomic nuclei, so that the atoms can be ionized. In the latter, with a sufficiently strong field, ionization can occur on sub-femtosecond ($<10^{-15}$ s) timescales, faster than the electromagnetic oscillations of visible light. It is therefore not surprising that intense light can be used to create plasmas. In practice, high-power laser pulses are used in laser-plasma experiments every day across the globe. The laser pulses are focused to a few micrometer sized spots, reaching the extremely high intensities required to ionize the target – similar to if all the sunlight that hits Earth was focused down to a few centimeters.

These laser-plasma experiments are performed with a broad range of applications in mind. Among others, laser plasmas can be used to accelerate electrons (Tajima, Yan & Ebisuzaki, 2020) or ions (Daido, Nishiuchi & Pirozhkov, 2012; Macchi, Borghesi & Passoni, 2013), both of which in setups much more compact than conventional radio-frequency particle accelerators. Laser-generated plasmas can also provide compact radiation sources spanning a wide band of frequencies, from terahertz pulses (Liao & Li, 2019; Thiele *et al.*, 2018; Yi & Fülöp, 2019) in the very low frequency range, via extreme ultra violet (XUV) radiation from high-harmonic generation (HHG) from gaseous (Ferray *et al.*, 1988; Hentschel *et al.*, 2001; Paul *et al.*, 2001) or solid (Gibbon, 1996; Gordienko *et al.*, 2004; an der Brügge *et al.*, 2012) laser targets, all the way into the x-ray regime from betatron radiation (Rousse *et al.*, 2004; Ferri *et al.*, 2018; Horný *et al.*, 2020). We shall come back to some of these subjects later on, especially ion acceleration and HHG.

Besides the above applications, where the goal is to make the laser plasma emit either particles or radiation of certain energies, laser plasmas are also gaining interest for the possibility to study the conditions and processes inside them. In various laboratory-astronomy experiments, intense laser pulses can be used to recreate astrophysical phenomena and plasma conditions (Remington *et al.*, 1999; Remington, 2005; Takabe & Kuramitsu, 2021). These conditions include the interiors of planets (Ross, 1981; Knudson, Desjarlais & Dolan, 2008) and stars (Bailey *et al.*, 2007; Casey *et al.*, 2017), black-hole accretion disks (Fujioka *et al.*, 2009; Law *et al.*, 2020), supernovae explosions (Gremillet & Lemoine,

2020; Fiuza *et al.*, 2020), as well as magnetic-field generation (Tzeferacos *et al.*, 2018; Bott *et al.*, 2021) and reconnection events in solar flares (Nilson *et al.*, 2006; Zhong *et al.*, 2010; Yi *et al.*, 2018).

For some of the above applications, it is crucial that the laser target is heated rapidly, before it has time to expand due to its extremely high pressures ($>$ Mbar). If such *isochoric heating* is achieved, the resulting high-energy-density (HED) state of matter can be used for experimental verification of HED atomic-physics models (Hoarty *et al.*, 2013a; Fausurier & Blancard, 2019) or equations of state (Renaudin *et al.*, 2003; Nettelmann *et al.*, 2008; Dyer *et al.*, 2008), i.e. how temperature and pressure are related under these extreme conditions. Fast heating and compression by ultra-intense laser irradiation is also the base of inertial confinement fusion (Le Pape *et al.*, 2018; Drake, 2018; Zylstra *et al.*, 2022), the goal of which is to reach temperatures and pressures similar to stellar interiors so that the atomic nuclei will fuse and release large amounts of energy. The work in this thesis also touches upon the subject of isochoric heating, which we will discuss further in following chapters.

Beside the experimental effort and advances presented above, considerable theoretical work has also been put into developing mathematical models as well as developing and running simulation software for laser plasmas – all with the goal to aid our understanding of the laser-plasma interactions. This thesis contains aspects of all three of the above-mentioned kinds of theoretical work. It is, however, very important for the theoretical and experimental works to interact and supplement each other. In order to do that, we must be able to diagnose the laser-plasma experiment, which will be the closing topic of this thesis. We will explore the use of XUV pulses to diagnose the electron density of laser plasmas.

1.1 Laser-based particle acceleration

Since the invention of the laser in 1960 by Maiman, the laser technology has advanced rapidly, with increasing intensities and decreasing laser-pulse durations. Early on, the invention of Q-switching (McClung & Hellwarth, 1962) and mode locking (Hargrove, Fork & Pollack, 1964) paved the way for several orders of magnitude increase in laser power. Not long after, Treacy (1968) found that the pulses produced from mode-locked lasers had a positive frequency *chirp* – the carrier frequency of the pulses increased with time – which results in rather long pulses of nanosecond duration. This chirp could, however, be counteracted via a clever arrangement of optical gratings, in order to produce sub-picosecond pulses.

After these rapid developments in the 60's, improvements stagnated around a focused laser intensity of $\sim 10^{14}$ W/cm². The intensities reached inside the laser systems were starting to damage the optical amplification stages, so that the only viable option for higher laser power was to spread out the light transversally with larger and larger apertures – and then focus the light. These devices became increasingly complex and sensitive due to their large sizes. It was not until 1985, when Strickland & Mourou – with inspiration from radar technology (Brookner, 1985) – had the idea to use the temporal stretching of the chirped pulse to their advantage. By first inducing, or accentuating, the chirp in the carrier wave, the pulse can be spread out longitudinally, and the peak intensity is lowered below the damage threshold of the optical amplifiers. Then, the amplified pulse can be compressed back to its original duration using the same technique as Treacy (1968). This scheme is called *chirped pulse amplification* (CPA) and it paved the way for a new era of laser development. For this achievement, Strickland & Mourou were recognized with the 2018 Nobel prize in physics.

Long before the invention of CPA, but inspired by the rapid developments in the 60's, the possibility of using lasers to accelerate electrons were discussed in various configurations by, e.g. Chan (1971) and Palmer (1972). Almost a decade later, Tajima & Dawson (1979) put forth the, to this day, most successful and prevalent electron-acceleration scheme, *laser-wakefield acceleration* (LWFA). When a strong laser pulse passes through a plasma, the electrons in its path are pushed away, but quickly rush back behind the laser pulse – similar to the wake behind a boat making way*. And like a surfer on a boat wake, if some electrons are injected into the laser wake at the right position and with the right momentum, the electron can be accelerated to the speed of the laser pulse as it passes through the plasma (close to the speed of light in vacuum). Although it would take another two decades of laser development, including CPA, before LWFA could first be experimentally demonstrated by Amiranoff *et al.* (1998), based on simulations by Joshi *et al.* (1984).

In addition to electrons, intense lasers have also been used to accelerate ions. Indeed, already the year after Q-switching was invented, Linlor (1963) reported energetic ions from metal-foil targets were. Up

*The boat analogy can be taken further by considering the length of the laser pulse or boat, which is important for an efficient wake formation. In the case of a boat it is the ratio between boat speed and length, the *Froude number*, that governs the wake (Rabaud & Moisy, 2013), while in the plasma it is the ratio between pulse length and plasma-oscillation wavelength that is important.

until the invention of CPA, accelerated ion energies had reached the MeV level (Gitomer *et al.*, 1986), although requiring the use of relatively long-duration (nanosecond) laser pulses. With the rapid developments in laser technology and the understanding of various ion acceleration mechanisms, more recent experiments by Kim *et al.* (2016) and Higginson *et al.* (2018) reported maximum proton energies close to 100 MeV.

What makes laser-based accelerators attractive is the potential for high-intensity lasers to deliver large amounts of energy to a small volume in very short times. In the right conditions accelerating field strengths in the GV/m to TV/m regime can be achieved (Higginson *et al.*, 2018; Tajima, Yan & Ebisuzaki, 2020). Because the laser-based acceleration occurs inside a plasma, the collective effects of the charged particles help build these enormous field strengths, significantly higher than the $\lesssim 100$ MV/m level that can be reached before damage occurs in conventional, non-plasma accelerators. With the higher field strengths achieved with laser-plasma accelerators, particles can be accelerated in a much shorter distance than in conventional, potentially reducing the cost and real estate required for particle accelerators.

Besides the practical advantages of being more compact, laser-based particle accelerators possess other unique features such as a high number of accelerated particles in very short-duration bunches (Cowan *et al.*, 2004; Lundh *et al.*, 2011; Zhang *et al.*, 2017a). Potential applications of these kinds of bunches include imaging of transient electromagnetic fields in other plasmas (Borghesi *et al.*, 2002; Romagnani *et al.*, 2005), useful for diagnostic purposes, or to generate *warm dense matter* (Patel *et al.*, 2003; Dyer *et al.*, 2008; Mančić *et al.*, 2010; Malko *et al.*, 2022), using fast ions. Wakefield-accelerated electrons can also be used as intense sources of electromagnetic radiation in a broad range of frequencies (Albert & Thomas, 2016), which may be used in medical and imaging applications. Laser-accelerated protons could also be used in nuclear reactions to produce neutrons (Roth *et al.*, 2013; Martinez *et al.*, 2022); these neutron bunches would be of similar duration and intensity as the proton bunches, something which is not achievable otherwise by conventional means.

In terms of medical applications, laser-based accelerators has received significant attention due to their potential to provide small-scale and low-cost alternatives to conventional accelerators (Giulietti & Tajima, 2016). While laser-accelerated electrons gather some interest due to the relative maturity of the LWFA scheme (Richter *et al.*, 2011), electron-radiation therapy is limited to tumors on or near the surface of the skin due to the low penetration depth of electron beams (Hogstrom & Almond, 2006).

Fast ions, on the other hand, can penetrate deeper into the tissue; furthermore, high-energy ions deposit a large fraction of their energy at a well-defined depth – at the so called Bragg peak – which makes ion-beam radiotherapy extremely interesting since deep-seated tumors can be targeted with little damage in front of or behind the cancerous tissue (Bulanov *et al.*, 2002; Linz & Alonso, 2007; Hoskin & Bhattacharya, 2014; Karsch *et al.*, 2017). However, laser-based ion accelerators are not yet mature enough for such applications; ion energies of several hundred MeV per nucleon with very narrow energy spread and excellent repeatability are the minimum requirements before they can be used medically.

The first part of the work in this thesis covers *electrostatic shocks*; such shocks feature one of the above requirements: accelerating ions with low energy spread. These shock waves are also often called *collisionless* because they are governed by *kinetic* rather than fluid effects – meaning that the plasma dynamics is not dominated by the effects of particle collisions. The collisionless epithet might, however, be somewhat deceiving; as we shall see in paper A, even a very low rate of collisions can significantly impact the evolution of the shock. Next, in paper C, the behavior and evolution of electrostatic shocks are studied in a high-collisionality regime – at the intersection of kinetic and fluid plasma physics.

The mechanism by which electrostatic shocks accelerate ions was first described by Moiseev & Sagdeev (1963), and later numerically investigated by Forslund & Shonk (1970). The shock wave consists of a supersonic wave structure with a steep rise in ion density, with an accompanying equally steep rise in electrostatic potential due to the charge imbalance set up by the high ion density. Because the high-density structure moves faster than the so called *ion-acoustic wave*, which governs the speed at which the ion population reacts to subsonic perturbations, the ions do not have time to react to the strong fields of the shock wave. Therefore, most ions are simply swept up by the shock wave, thus contributing to the high ion density behind the shock front. However, a fraction of the upstream ions are instead reflected, to twice the velocity of the shock wave, by the steep electrostatic potential barrier – similar to how rubber ball hitting the front of a high-speed train would be bounced off the train with double the velocity of the train. Since all the shock-reflected ions will have a speed very close to twice the shock velocity, the energy spread of these accelerated ions can be very small.

Following the interest high-intensity lasers enabled by CPA, the use of lasers for initiating the shock waves was investigated in a variety of conditions via numerical simulations (Denavit, 1992; Silva *et al.*, 2004;

Fiuza *et al.*, 2012, and many more), showing the feasibility of laser-induced electrostatic shock waves. The shock is formed when the laser pulse hits the front of the plasma surface, which pushes it into the bulk plasma – in what is referred to as a *laser piston* (Macchi *et al.*, 2005). If the piston velocity is supersonic, an electrostatic shock wave can be driven by the laser. These kind of shocks were observed in experiments by Romagnani *et al.* (2008). Soon after, the narrow energy spread of the accelerated ions were reported by Haberberger *et al.* (2012), and in recent experiments by Zhang *et al.* (2017a), Pak *et al.* (2018) and Puyuelo-Valdes *et al.* (2019).

While the low energy spread of shock accelerated ions can be attractive, the top energies reach only around $\lesssim 50$ MeV for protons (Antici *et al.*, 2017). Meanwhile, there are other ion-acceleration mechanisms, such as *target normal sheath acceleration* (TNSA) first described by Wilks *et al.* (2001) and *radiation pressure acceleration* proposed by Esirkepov *et al.* (2004), which are both capable of producing protons with top energies around twice that of shock acceleration (Kim *et al.*, 2016; Wagner *et al.*, 2016; Higginson *et al.*, 2018). However, the energy spectra of ions accelerated employing these techniques are very broad, so they would require some form of spectral filtering if low energy spread is required.

1.2 High energy density and plasma heating

As we have seen, the capability of modern high-intensity lasers to quickly deliver relatively large amounts of energy to a small volume of target material have opened up the possibility for new and compact particle accelerators, but that same laser energy can also be used to heat up the target to extreme temperatures. In our every-day experience, matter expands when heated. So too will the laser targets when they are irradiated by extreme-intensity light. However, because the energy can be delivered to the laser target within tens of femtoseconds, the inertia of the ions prevent the newly-formed plasma from expanding significantly when heated, to up to millions of degrees. This process is named *isochoric heating*, i.e. heating at constant volume.

Once heated, the target plasma is in a state of *high energy density* (HED), characterized by high temperatures and densities at the same time – resulting in extremely high pressures. Such conditions can be found in planetary and stellar cores (Paquette *et al.*, 1986; Guillot, 1999;

Remington, 2005; Casey *et al.*, 2017) and inertial-confinement-fusion plasmas (Le Pape *et al.*, 2018; Zylstra *et al.*, 2022). Laser-plasma experiments could therefore be used to further our knowledge of this HED state of matter, such as understanding atomic physics (Hoarty *et al.*, 2013a; Faussurier & Blancard, 2019) or the relation between density, pressure and temperature (Renaudin *et al.*, 2003; Nettelmann *et al.*, 2008; Dyer *et al.*, 2008) under these conditions. Indeed, over the years, several such experiments have been performed on very high-power (petawatt) laser systems (Evans *et al.*, 2005; Gregori *et al.*, 2005; Nilson *et al.*, 2009; Brown *et al.*, 2011; Hoarty *et al.*, 2013b; Matsuo *et al.*, 2020), as well as smaller scale lasers with the use of nano-structured targets to increase the absorption efficiency (Purvis *et al.*, 2013; Bargsten *et al.*, 2017).

The importance of efficient coupling of laser energy to the plasma is not limited to isochoric heating applications. For instance, the efficiency of ion acceleration mechanisms, such as TNSA or electrostatic-shock acceleration, also greatly depends on the ability to heat up the electrons in the plasma. However, there is a problem here in that high-density plasmas block optical-wavelength light, thus limiting the potential for laser-plasma interaction. The laser pulse will only be able to penetrate a few *skin depths* into the plasma – normally only a few tens of nanometers – as it is reflected by the plasma. In that region, energy must be transferred from the laser to the electrons, which may later heat the rest of the plasma. Over the years, various such laser-plasma heating mechanisms have been proposed in different interaction regimes; some of these mechanisms are described in §3.2. In paper B, we revisit the so called *inverse bremsstrahlung* heating mechanism, which is based on laser-energy absorption through collisional friction.

1.3 High-harmonic generation and plasma optics

As CPA technology developed, the laser power has increased and the pulse duration has decreased, both by several orders of magnitude. There are currently university-lab laser systems that can generate pulses that are several tens of terawatts in power for tens of femtoseconds – resulting a pulse energy of a couple of joules. The fastest such systems can reach as short pulses as a few femtoseconds (Rivas *et al.*, 2017), which amounts to only a couple of oscillations of the electromagnetic field at optical frequencies. We are therefore now reaching the limit of how short pulses that can be made in the optical spectrum. If we want to use sub-

femtosecond pulses, then we must go to shorter wavelengths. There are, however, no readily available high-power laser technologies that can directly generate laser pulses with wavelengths below ~ 100 nm – in the *extreme ultraviolet* (XUV) spectral range of radiation.

Instead of generating XUV light directly, it is possible to convert high-intensity optical light, from a *pump* laser pulse, through a process called *high-order harmonic generation* (HHG), to generate XUV pulses. There are two main branches of HHG. The first is based on rapid ionization and recombination in noble gas targets (Ferry *et al.*, 1988; Paul *et al.*, 2001; Calegari *et al.*, 2016). In gas HHG, the pump laser has sufficiently high intensity that the target atoms can be ionized during the peaks of the electric field oscillation, but the electrons recombine within half a laser cycle, thus emitting high-energy (XUV) photons. The second method, is based on the relativistic Doppler effect, where the pump pulse is reflected from a plasma surface that oscillates back and forth due to the varying radiation pressure as the laser field oscillates. As the plasma surface moves towards the incoming laser pulse, the reflected light is Doppler shifted to XUV frequencies (Gibbon, 1996; an der Brügge *et al.*, 2012; Gonoskov *et al.*, 2011; Yi, 2021).

As the name suggests, both mechanisms generate discrete high-order harmonics of the original pump-laser frequency. Therefore, the generated radiation normally has the form of a train of attosecond XUV pulses, with the current record duration being 43 attoseconds, reported by Gaumnitz *et al.* (2017). Through various pumping and filtering techniques it is possible to generate continuous-spectrum isolated attosecond pulses, both with gas HHG (Christov, Murnane & Kapteyn, 1997; Hentschel *et al.*, 2001; Itatani *et al.*, 2002; Xue *et al.*, 2020) and solid HHG (Wheeler *et al.*, 2012; Hammond *et al.*, 2016). However, the conversion efficiency, from the pump laser to the XUV pulses, is very low with attosecond-pulse energies in the range of tens of nanojoules with gas HHG (Manschuetus *et al.*, 2016) and millijoules with relativistic mirrors (Zepf, 2011) – compared to the joule level pulses that the optical pump laser has.

One possibility, that is explored in paper E, to obtain XUV pulses with higher intensity is to amplify them. Because of the high photon energies, normal optical amplification would not work – the amplifying elements would be ionized and destroyed. However, as with the strong-field acceleration, a plasma is already ionized and will not suffer from ionization damage. This use of plasma optics to amplify laser pulses was demonstrated already in 1966 by Maier, Kaiser & Giordmaine, through a process called *stimulated Raman scattering* (SRS). Since then, SRS has

gathered attention for its potential to significantly amplify short laser pulses to very high energies (Ping *et al.*, 2000; Ren *et al.*, 2007; Trines *et al.*, 2011*a,b*), especially in the non-linear regime (Cheng *et al.*, 2005; Trines *et al.*, 2020). The SRS mechanism is based on the stimulated energy transfer from a pump laser pulse to a seed laser pulse, via scattering off induced electron waves in the plasma. In our paper (E), we investigate the efficacy of using attosecond XUV pulse trains as the pump and an isolated attosecond pulse as the seed, which may provide a pathway to higher-intensity XUV pulses. It is especially interesting to amplify isolated attosecond pulses, since they generally have lower intensity than their pulse-train counterparts.

1.4 Simulating and diagnosing laser plasmas

The next, and final, part of this thesis touches upon how to diagnose a laser plasma. None of the above-mentioned applications would be possible if we do not have any information about the outcome of the experiments. The first step in understanding some aspect of a laser-plasma experiment – often taken before the experiment itself – is to consult mathematical models and numerical simulations. These models are based on experience and fundamental principles of physics, but the behavior of plasmas can very complex and often require extensive non-linear modeling to portray accurately. Analytically solving the non-linear integro-differential *Vlasov–Maxwell equations* that govern the *distribution function* – which represent the *phase-space* density of each particle species in both configuration (“normal”) and momentum (or velocity) space – in kinetic plasma physics is in the vast majority of cases impossible without extensive simplifications.

The other option at hand is to find numerical solutions to the governing equations. In laser-plasma situations, the most commonly used numerical tool are the so called *particle-in-cell* (PIC) codes. The PIC method is based on the dynamics of individual charged particles – how they interact with and affect the electromagnetic fields. By simulating a large number of macroparticles, representing the electrons and ions in the plasma, most laser–plasma interactions can be fairly accurately captured. Another method to simulate the plasma is to discretize the distribution function on a fixed grid and numerically solving the Vlasov–Maxwell equations on that grid. The latter represents an *Eulerian* description of the flow phase-space fluid, across the phase-space cells at

fixed phase-space locations, specified by the discretized grid. The PIC method, on the other hand, represents a *Lagrangian* description of the phase-space flows, where “fluid packets” are followed along their phase-space trajectories.

The PIC method can also be thought of as a Monte-Carlo sampling of phase space, which may significantly reduce the computation cost compared to resolving all of phase space – that can be up to six dimensional – in the Eulerian specification. The drawback is, however, a significant level of numerical noise due to the limited number of macroparticles, which might even lead to unphysical behavior (Juno *et al.*, 2020). However, the most important advantage of PIC algorithm is that its simplicity lends itself well for including special relativity in its particle dynamics, which is much more complicated to implement in Eulerian continuum Vlasov–Maxwell solvers. Since the field strengths involved with modern high-intensity lasers readily accelerates electrons to relativistic energies, it would be impossible to accurately describe such a laser–plasma interaction in a non-relativistic framework. The simplicity of the PIC algorithm also makes it easier to implement other physical phenomena, not captured by the Vlasov–Maxwell equations, such as Coulomb collisions (Nanbu, 1997; Nanbu & Yonemura, 1998; Pérez *et al.*, 2010), ionization from collisions (Pérez *et al.*, 2010) or strong fields (Nuter *et al.*, 2011), as well as various quantum electro-dynamical effects (Di Piazza *et al.*, 2012; Lobet *et al.*, 2016).

Of course, in the end, it is not feasible nor possible to include every physical phenomenon in your simulation, and some educated exclusions must be made. Because of this limitation, combined with numerical artifacts such as noise – or simply because of errors in the models or their implementation – the results of the simulations tools must in some way be compared with and verified by real-life experimental results. Toward this end, there are many different diagnostics techniques that can be used on laser plasmas. If the plasma density is sufficiently low, e.g. in LWFA plasmas, optical probing methods, such as shadowgraphy, have been used to image these plasmas in high detail (Evans *et al.*, 1996; Schwab *et al.*, 2013; Sävert *et al.*, 2015; Siminos *et al.*, 2016). If, on the other hand, the plasma density is above the critical density of optical wavelengths, i.e. that these frequencies cannot propagate through the plasma, other types of probing beams must be used, such as beams of high-energy ions (Borghesi *et al.*, 2002; Romagnani *et al.*, 2008) or electrons (Zhang *et al.*, 2017b), but also x-rays (Kluge *et al.*, 2018; Allen *et al.*, 2022). Besides the active probing methods above, it is, of course, also possible

to passively utilize particles (Neely *et al.*, 2006; Nürnberg *et al.*, 2009) or x-ray radiation (Renner & Rosmej, 2019; Sawada *et al.*, 2019) emitted by the plasma itself to diagnose high-density plasmas.

Common for the methods mentioned above, is that the probing or emitted beams are able to penetrate through the plasma. For electromagnetic radiation, the criterion for propagation is that the frequency of the radiation is higher than the plasma frequency – determined by the electron density. That means, in principle, that you could probe a high-density plasma with a sufficiently high-frequency electromagnetic wave, such as x-rays; just below that in frequency, we find XUV radiation, that can be generated through HHG, which is able to penetrate some solid-density plasmas (Koliyadu *et al.*, 2017).

The penultimate paper of this thesis, paper **D**, details a scheme for diagnosing laser plasmas using the dispersion of attosecond XUV pulses. Because the duration of the pulse is only a few oscillations of the electromagnetic fields, its spectrum will be broad. The pulse is therefore susceptible to dispersion, which in a plasma depends on the density profile. In the paper, we develop such a scheme for generating synthetic dispersion diagnostics, based on PIC simulations, but, importantly, there are also experimental methods available to perform the same dispersion diagnostics as in the paper – the RABBIT[†] (“*Reconstruction of Attosecond Beating By Interference of Two-photon transitions*”; Paul *et al.*, 2001) and attosecond streak camera (Itatani *et al.*, 2002) methods.

The idea of using XUV pulses in diagnostic purposes has, however, been explored to some degree before. Early on, several groups demonstrated spectral interference techniques to measure electron densities, where small relative shifts and dispersion of individual pulses in a pulse train can greatly affect the spectrum of the train (Salières *et al.*, 1999; Descamps *et al.*, 2000; Merdji *et al.*, 2000; Hergott *et al.*, 2003). It is also possible to gauge the electron density by the relative transmission of the high harmonics (Hergott *et al.*, 2001; Dobosz *et al.*, 2005), or by measuring the XUV refractive index (Williams *et al.*, 2013). With the proposed technique in paper **D**, it is possible to probe the density and, to some degree, the shape of the density profile along the line of flight of the XUV probe pulse.

We continue our exploration of how XUV pulses and pulse trains can be used to diagnose plasmas in the final paper of this thesis, paper **E**, where we also investigate the diagnostic possibilities of SRS with XUV

[†]Note that the alternative abbreviation RABITT is also used sometimes.

pulses and pulse trains. As an XUV pulse propagates through a plasma, it is not only dispersed by the plasma, the pulse can also affect the plasma. In particular, if two counterpropagating laser pulses – the *pump* and *seed* pulses – meet in the plasma, they can induce waves in the electron density, which in turn can cause scattering of the pump pulse in the so called SRS process. More details of SRS will be laid out in §4.2, but for the moment, one important feature is that the frequency of the scattered light is downshifted by an amount equal to the plasma frequency. It is therefore possible to gauge the electron density, based on a spectral comparison of the original and scattered light, as has, indeed, been proposed by Jang *et al.* (2008) and later experimentally demonstrated by Vieux *et al.* (2013).

Our contribution in paper E is that we explore the use of an XUV pulse-train as the SRS pump. For diagnostic purposes, not only does XUV pulses allow for probing plasmas of higher densities, but they also increase the spatiotemporal resolution compared to using optical wavelengths. Furthermore, by using a train of XUV pulses as the pump, which has a spectrum consisting of fairly distinct individual peaks, the accuracy of the density measurement may be as good as a few percent. Lastly, unlike the other density-probing methods, this SRS-based diagnostic gives a density measurement at a certain depth instead of a line-of-sight averaged reading. Because SRS only occurs in the region where the pump and seed pulses interact, the density values that the SRS provides is that of the interaction region only, which can be as small as a few microns when using XUV pulses.

The ionized gas contains ions and electrons in about equal numbers so that the resultant space charge is very small. We shall use the name plasma to describe this region containing balanced charges of ions and electrons.

Irving Langmuir (1928)

Chapter 2

Basics of plasma physics

The papers in this thesis all connect to laser-plasma physics, and specifically to the behavior of the *plasma* in the laser–plasma interaction. The concept of plasmas encompasses many different physical systems – from the extremely hot and dense stellar cores, to cold and partially ionized plasmas at atmospheric pressure, via hot and low density magnetic–fusion plasmas, and many more – all of which have their differences which require separate theoretical treatment. Yet, they still fall under the umbrella term of “plasma” because they all share the fact that they contain free charged particles. The important difference between a plasma and a neutral gas is that the charged particles in the plasma experience long-range interaction via electric and magnetic fields in the plasma – hence giving rise to the *collective behavior* of the particles – while the neutral gas particles only interact with each other in close-range collisions. In this chapter, we will focus on some of the more general aspects of plasmas, how to theoretically model them and their behaviors.

2.1 Kinetic theory – from many particles to one distribution

Plasmas, like most other forms of matter, consist of a very large number of individual particles. These particles can be described more or less classically, depending on parameters such as density and temperature. In what follows, we will therefore, unless stated otherwise, treat the problem of modeling plasmas classically. Because quantum effects are ignored, we can develop a statistical theory of plasma physics based on the classical – albeit relativistic – equations of motion. In this theory, the

plasma is described by the statistical distribution of particles in *phase space* – consisting of the normal configuration space and momentum space. This distribution describes the number of particles with a certain momentum, at a certain point in configuration space. The theory of how this distribution behaves is called *kinetic plasma physics*, and it plays a central role in this thesis. We will, therefore, explore the basics of this kinetic plasma physics in this section.

In the most basic formulation of kinetic theory, the *one-particle distribution function* f_a plays the central role by describing the phase-space density of particles belonging to some species, denoted by a – these species include electrons and various kinds of ions. The distribution is a function of time t , space \mathbf{x} , and momentum \mathbf{p} , and the quantity $f_a(\mathbf{x}, \mathbf{p}; t) d^3x d^3p$ represents the number of particles in the infinitesimal phase-space volume $d^3x d^3p$ at the phase-space coordinate (\mathbf{x}, \mathbf{p}) . Following this representation, the distribution function is normalized such that the full phase-space integral

$$N_a = \int d^3x d^3p f_a(\mathbf{x}, \mathbf{p}; t) \quad (2.1)$$

is the total number of particles of species a (at time t) in the system under consideration. Consequently, the momentum-only integral

$$n_a(x, t) = \int d^3p f_a(\mathbf{x}, \mathbf{p}; t) \quad (2.2)$$

is the number density of particles of species a at position \mathbf{x} and time t . In this interpretation, the phase-space is sufficiently coarse grained, and number of particles N_a sufficiently large, so that individual particles are not visible in the distribution*, and $f_a(\mathbf{x}, \mathbf{p}; t)$ is (mostly) smooth.

Ignoring effects that can change the number of particles N_a – such as ionization/recombination or nuclear reactions – the distribution function is *conserved along phase-space trajectories*, a continuity equation in phase space

$$0 = \frac{df_a}{dt} \equiv \frac{\partial f_a}{\partial t} + \mathbf{v} \cdot \frac{\partial f_a}{\partial \mathbf{x}} + \tilde{\mathbf{K}}_a \cdot \frac{\partial f_a}{\partial \mathbf{p}}, \quad (2.3)$$

where dots denote time derivatives, e.g. $\dot{\mathbf{x}} \equiv d\mathbf{x}/dt \equiv \mathbf{v}$, and the partial derivative with respect to the coordinate vectors are gradient like vectors in the respective coordinate, e.g. $\partial f_a / \partial \mathbf{p} = [\partial_{p_x}, \partial_{p_y}, \partial_{p_z}] f_a$, and $\tilde{\mathbf{K}}_a =$

*Formally, the distribution is derived from an ensemble average, which removes the contribution of each individual particle.

$\tilde{\mathbf{K}}_a(\mathbf{x}, \mathbf{v}; t) \equiv \dot{\mathbf{p}}_a$ represents the forces acting on the particles of species a at that point in phase space.

The conservation statement in (2.3) is true for all forces $\tilde{\mathbf{K}}_a$, such that particles being acted upon by $\tilde{\mathbf{K}}_a$ obey Hamiltonian mechanics – viz. all physical forces – and is known as *Liouville’s theorem*. In the case of a plasma, the particles are charged, so the dominant force at play is the Lorentz force, $\tilde{\mathbf{K}}_a(\mathbf{x}, \mathbf{v}; t) = eZ_a[\tilde{\mathbf{E}}(\mathbf{x}, t) + \mathbf{v} \times \tilde{\mathbf{B}}(\mathbf{x}, t)]$, where $\tilde{\mathbf{E}}$ and $\tilde{\mathbf{B}}$ are the electric and magnetic fields; e is the elementary charge and Z_a is the charge number of species a (for electrons, $Z_e = -1$). These fields are in turn linked to the distribution functions of all species via Maxwell’s equations, since the distribution functions determine the charge and current sources.

The smoothing of the distribution, such that individual particles become “invisible”, presents a slight problem, however. Since the particles still interact with each other on the microscopic scale – through *Coulomb collisions* – the effects of these collisions are lost in the smoothing operation. The effect of these interactions can, however, be modeled through a (binary) *collision operator* \tilde{C}_{ab} . The result is a form of mean-field treatment of (2.3), which becomes

$$\frac{\partial f_a}{\partial t} + \mathbf{v} \cdot \frac{\partial f_a}{\partial \mathbf{x}} + eZ_a(\mathbf{E} + \mathbf{v} \times \mathbf{B}) \cdot \frac{\partial f_a}{\partial \mathbf{p}} = \sum_{\ell} \tilde{C}_{a\ell}, \quad (2.4)$$

where $\tilde{C}_{a\ell}$ is the collision operator that accounts for binary collisions[†] between species a and ℓ , and the sum goes over every species ℓ (including a itself). Next, the mean fields, \mathbf{E} and \mathbf{B} (denoted by the removal of the “tilde”), are then given by Maxwell’s (1865) equations

$$\nabla \cdot \mathbf{E} = \frac{\rho}{\epsilon_0}, \quad (2.5a) \quad \nabla \times \mathbf{E} = -\frac{\partial \mathbf{B}}{\partial t}, \quad (2.5c)$$

$$\nabla \cdot \mathbf{B} = 0, \quad (2.5b) \quad \nabla \times \mathbf{B} = \mu_0 \mathbf{j} + \frac{1}{c^2} \frac{\partial \mathbf{E}}{\partial t}, \quad (2.5d)$$

where these equations are given using the SI convention for electromagnetism, so ϵ_0 are μ_0 the permittivity and permeability of free space, respectively, and $c = (\epsilon_0 \mu_0)^{-1/2}$ is the speed of light in vacuum. The charge and current densities in (2.5) are computed from the distribution

[†]For a more general treatment, where collisions between more than two particles are included, one can resort to the BBGKY hierarchy (after Bogoljubov, 1960; Born & Green, 1946; Green, 1952; Kirkwood, 1946 and Yvon, 1935).

function as

$$\rho(\mathbf{x}, t) = \sum_a eZ_a \int d^3p' f_a(\mathbf{x}, \mathbf{p}'; t) = \sum_a \rho_a(\mathbf{x}, t), \quad (2.6a)$$

$$\mathbf{j}(\mathbf{x}, t) = \sum_a eZ_a \int d^3p' \mathbf{v}' f_a(\mathbf{x}, \mathbf{p}'; t) = \sum_a \mathbf{j}_a(\mathbf{x}, t), \quad (2.6b)$$

respectively, where the sums are over all species a , $\mathbf{v}' = \mathbf{p}'/(m_a\gamma')$ is the velocity of a particle with momentum \mathbf{p}' and mass m_a , with the Lorentz factor $\gamma' = [1 + p'^2/(m_a c)^2]^{1/2}$. These equations (2.4, 2.5 & 2.6) constitute the closed and self-consistent system that is the basis for kinetic plasma physics.

If collisional effects are ignored in the *kinetic equation* (2.4), it is instead called the *Vlasov* (1968) *equation*, and the whole system (2.4, 2.5 & 2.6) is then referred to as *Vlasov–Maxwell equations* and describes a plasma dominated by the collective behavior of its particles. This simplification can, in some instances, be well motivated, e.g. in a sufficiently tenuous or hot plasma, where the particles rarely come in close contact with each other, or when the process of interest is much faster than the timescales of collisions. Later, in §2.3, we shall come back to collisions. For now, though, we will concentrate on the collisionless Vlasov equation and the effects seen with it on the distribution function.

2.1.1 Example: The Maxwell–Jüttner distribution

Let us illustrate the kinetic framework with a simple example calculation to find the distribution corresponding to local thermodynamic equilibrium, using the kinetic system of equations. We will consider a one-dimensional (1D) plasma under the influence of some *electrostatic* field E , without any magnetic fields. In this case, we can use the electrostatic potential Φ to express the electric field $E = -\partial\Phi/\partial x$. Furthermore, since we are searching for an equilibrium distribution, we require a steady-state solution, i.e. $\partial f_a/\partial t = 0$. Finally, we will ignore the effects of collisions here.

With these restrictions set, the kinetic equation (2.4) is simplified to

$$\frac{p}{\gamma m_a} \frac{\partial f_a}{\partial x} - eZ_a \frac{\partial \Phi}{\partial x} \frac{\partial f_a}{\partial p} = 0, \quad (2.7)$$

where we have kept the relativistic formulation, using $v = p/(\gamma m_a)$. If we further assume that the solution can be separated as $f_a(x, p) =$

$\mathcal{X}(x)\mathcal{P}(p)$, it is possible to solve (2.7) to give,

$$f_a(x, p) = \mathcal{F}_0 \exp\{-\mathcal{C}_a [eZ_a\Phi(x) - m_a c^2 \gamma(p)]\}, \quad (2.8)$$

with effectively two unknown constants \mathcal{F}_0 and $\mathcal{C}_a = 1/T_a$. The latter we can, at least heuristically, identify as an inverse temperature, and the former can easily be determined using the normalization (2.2).

The final result is the so called the *Maxwell–Jüttner distribution* (after Jüttner, 1911),

$$f_a^{(\text{MJ})}(\mathbf{x}, \mathbf{p}; t) = \frac{n_a(\mathbf{x})}{4\pi(m_a c)^3 \Theta_a K_2(1/\Theta_a)} \exp\left(-\frac{\gamma(p)}{\Theta_a}\right), \quad (2.9)$$

where $\Theta_a = T_a/m_a c^2$ and K_2 is the (second-order) modified Bessel function of the second kind. In the non-relativistic limit, (2.9) recovers the *Maxwell–Boltzmann distribution* (after Maxwell, 1860; Boltzmann, 1872)

$$f_a^{(\text{MB})}(\mathbf{x}, \mathbf{v}; t) = \frac{n_a(\mathbf{x})}{(2\pi T_a/m_a)^{d/2}} \exp\left(-\frac{m_a v^2}{2T_a}\right), \quad (2.10)$$

in d dimensions. The configuration-space density of this distribution, n_a , depends on the electrostatic potential according to the *Boltzmann distribution* (after Boltzmann, 1868)

$$n_a(\mathbf{x}) = n_{a,0} \exp\left(-\frac{eZ_a\Phi(\mathbf{x})}{T_a}\right), \quad (2.11)$$

where $n_{a,0}$ is the unperturbed density at $\Phi = 0$. We have here arrived at the momentum and spatial dependencies of a steady-state distribution, subject to an electrostatic potential Φ . As a consequence of this, the Maxwell–Jüttner (or Maxwell–Boltzmann) distribution must be the distribution of a plasma at local thermodynamic equilibrium. As such they have maximum entropy, and a collision operator acting on them should have no effect, since otherwise entropy would drive changes to the distribution, and the system would not be in steady state.

2.1.2 Moments and fluid quantities

The distribution function holds a large amount of information about the plasma, and at some points, not all the details of the exact distribution are necessary to understand some physical effects or certain plasma phenomena. In those cases, we can take averages over momentum space to get certain *moments* of the distribution. Indeed, we have already seen

examples of these moments when prescribing the charge and current densities (2.6).

Formally, these so called *fluid* quantities are extracted from the distribution via integration. Given some microscopic – that is valid for individual particles – quantity $\chi = \chi(\mathbf{x}, \mathbf{p}'; t)$, its fluid counterpart is computed as an average of χ over momentum weighted with the distribution,

$$\chi_a(\mathbf{x}, t) \equiv \langle \chi(\mathbf{x}, \mathbf{p}'; t) \rangle_a = \frac{1}{n_a} \int d^3p' \chi(\mathbf{x}, \mathbf{p}'; t) f_a(\mathbf{x}, \mathbf{p}'; t), \quad (2.12)$$

where the density n_a is given by (2.2). Through this averaging, we can compute a multitude of fluid quantities, e.g. fluid flow velocity $\mathbf{v}_a = \langle \mathbf{v} \rangle_a$.

2.1.3 Electromagnetic waves in plasmas

We will end this section with a short discussion about electromagnetic waves in plasmas. This topic will be highly relevant for the further discussion about laser–plasma interactions, since the laser is precisely an electromagnetic wave.

The propagation of electromagnetic waves is governed by Maxwell's equations (2.5), which can be reformulated using the magnetic *vector potential* \mathbf{A} such that $\mathbf{B} = \nabla \times \mathbf{A}$ and $\mathbf{E} = -\partial \mathbf{A} / \partial t - \nabla \Phi$ in the *Coulomb/radiation gauge* ($\nabla \cdot \mathbf{A} = 0$). The wave equation in this gauge becomes (c.f. Jackson, 1999, eqn. 6.30)

$$\nabla^2 \mathbf{A}_\perp - c^{-2} \frac{\partial^2 \mathbf{A}_\perp}{\partial t^2} = -\mu_0 \mathbf{j}_\perp, \quad (2.13)$$

where \mathbf{A}_\perp and \mathbf{j}_\perp are the components transverse to the wave-propagation direction of the vector potential and current density, respectively.

In a 1D geometry, and with *plane waves*, the transverse canonical momentum, $\mathbf{P}_{a,\perp} = \mathbf{p}_{a,\perp} + eZ_a \mathbf{A}_\perp$, of each particle is conserved (see also §3.1.1). Because of the conservation of the transverse canonical momentum, and assuming an initially cold and stationary plasma, we can express the current density in terms of the vector potential $\mathbf{j}_\perp = -en_e \mathbf{v}_{e,\perp} = -e^2 n_e \mathbf{A}_\perp / (\bar{\gamma}_e m_e)$, where $\bar{\gamma}_e$ is an effective Lorentz factor for the electron population, linking the fluid velocity response $\mathbf{v}_{e,\perp}$ to the momentum response $\mathbf{p}_{e,\perp} = e \mathbf{A}_\perp$. The wave equation (2.13) now reads

$$\frac{\partial^2 \mathbf{A}_\perp}{\partial x^2} - c^{-2} \frac{\partial^2 \mathbf{A}_\perp}{\partial t^2} = \frac{\omega_p^2}{\bar{\gamma}_e c^2} \mathbf{A}_\perp, \quad (2.14)$$

introducing the non-relativistic (electron) *plasma frequency*

$$\omega_p^2 \equiv \frac{e^2 n_e}{\epsilon_0 m_e}. \quad (2.15)$$

From this wave equation, we obtain the *plasma dispersion relation*

$$\omega^2 = \tilde{\omega}_p^2 + c^2 k^2, \quad (2.16)$$

where we have set $\tilde{\omega}_p^2 \equiv \omega_p^2 / \bar{\gamma}_e$ as the effective plasma frequency. The electric field, which is the physical quantity of interest, is simply given by $\mathbf{E}_\perp = -\partial \mathbf{A}_\perp / \partial t$ since $\nabla_\perp = 0$.

From this dispersion relation (2.16), we find one of the major features in laser-plasma physics: *that waves with frequencies $\omega < \tilde{\omega}_p$ below the plasma frequency cannot propagate through the plasma*. Since the plasma frequency is determined by the electron density, it is customary to talk about laser-plasma densities in terms of the *critical density*

$$n_c \equiv \frac{\epsilon_0 m_e \omega^2}{e^2}, \quad (2.17)$$

which is the density at which the (non-relativistic) plasma frequency equals the (laser) frequency considered, ω . Plasmas with densities $n_e > n_c$ ($n_e < n_c$) above (below) the critical density are said to be *over-(under-)dense* or *over-(under-)critical*.

Relativistic birefringence and transparency

For the moment, we have either ignored or swept relativistic effects under the “effective Lorentz factor” $\bar{\gamma}_e$, and no consideration has been given to kinetic effects. From what we can see from the dispersion relation (2.16), if the conditions are such that $\bar{\gamma}_e$ is large, or at least non-negligible, the propagation characteristics of an electromagnetic wave may be significantly altered. Indeed, there are two named phenomena that relate to this effect.

The first of which, *relativistically induced* or *self-induced transparency* (Kaw & Dawson, 1970), is the more widely known phenomenon. In this case, the wave amplitude is so large that the collective electron motion becomes relativistic, and their high Lorentz factor can thereby allow for transmission through an otherwise overcritical plasma. This process has been leveraged to enhance TNSA ion acceleration via increased electron energization (Henig *et al.*, 2009; Roth *et al.*, 2013; Higginson *et al.*, 2018).

This topic will, however, not be discussed further in this thesis; more detail can be found in the literature, e.g. by Siminos *et al.* (2012) and Fernández *et al.* (2017).

The other phenomenon, which has some bearing on the work in paper **D**, is called *relativistic birefringence* (Stark *et al.*, 2015; Arefiev *et al.*, 2020). It relates to the fact that the current response of the electrons is different for different polarizations if the electron momentum distribution is anisotropic. Basically, if the electrons are already moving near the speed of light in one direction, an electric field in that same direction will not be able to change their velocity by much, thereby generating a weaker current response than for initially stationary electrons; whereas the velocity and current response to an electric field perpendicular to the initial velocity of the electrons is not limited in the same way.

The work in paper **D** concerns the propagation and dispersion of low-amplitude waves through plasmas, so we will now briefly explore how relativistic birefringence might affect such low-amplitude waves $eA \ll m_e c$ (or $e\omega E \ll m_e c$ in terms of the electric field amplitude). Consider a wave with vector potential $\mathbf{A}_\perp = A\hat{\mathbf{e}}$. The corresponding change in momentum each electron experience from this wave would be $\delta\mathbf{p} = eA\hat{\mathbf{e}}$, due to conservation of transverse canonical momentum. Importantly this change in momentum is independent of the initial momentum of the electron. However, the velocity response – and thus the current in (2.13) – is highly dependent on the initial momentum \mathbf{p} of the electron. Since the amplitude is low, we can treat the velocity response perturbatively,

$$\delta\mathbf{v} \cdot \hat{\mathbf{e}} \simeq \delta\mathbf{p} \cdot \frac{d(\mathbf{v} \cdot \hat{\mathbf{e}})}{d\mathbf{p}} = \frac{eA}{\gamma m_e} \left(1 - \frac{(\mathbf{p} \cdot \hat{\mathbf{e}})^2}{\gamma^2 m_e^2 c^2} \right), \quad (2.18)$$

where we have here only considered the contribution to the velocity (current) in the polarization direction. As we can see, the corresponding change in velocity indeed depends on the initial momentum and the relative direction of the momentum perturbation.

In order to get the perturbed current response, we must take the $\delta\mathbf{v}$ moment over the electron distribution to give

$$\delta\mathbf{j} \cdot \hat{\mathbf{e}} = -en_e \langle \delta\mathbf{v} \cdot \hat{\mathbf{e}} \rangle_e = -\frac{e^2 A}{m_e} \int d^3p \frac{f(\mathbf{p})}{\gamma} \left(1 - \frac{(\mathbf{p} \cdot \hat{\mathbf{e}})^2}{\gamma^2 m_e^2 c^2} \right). \quad (2.19)$$

From this expression, we can identify the effective gamma factor, as used in (2.14),

$$\bar{\gamma}_{\hat{\mathbf{e}}}^{-1} \equiv \frac{1}{n_e} \int d^3p \frac{f(\mathbf{p})}{\gamma} \left(1 - \frac{(\mathbf{p} \cdot \hat{\mathbf{e}})^2}{\gamma^2 m_e^2 c^2} \right) = \left\langle \frac{1}{\gamma} \left(1 - \frac{(\mathbf{p} \cdot \hat{\mathbf{e}})^2}{\gamma^2 m_e^2 c^2} \right) \right\rangle_e. \quad (2.20)$$

We also see here that, if the distribution is anisotropic, $\bar{\gamma}_{\hat{\mathbf{e}}}$ will be dependent on the polarization direction $\hat{\mathbf{e}}$; hence the name relativistic *birefringence*, since the effective plasma frequency – and thereby the propagation properties – will be polarization dependent, $\tilde{\omega}_{\mathbf{p},\hat{\mathbf{e}}}^2 = \omega_{\mathbf{p}}^2/\bar{\gamma}_{\hat{\mathbf{e}}}$.

2.2 Fluid theory – when the exact details of the distribution can be ignored

As already noted, it is not always necessary to use all the information contained in the distribution functions, and, as we just saw in §2.1.2, fluid quantities can be extracted from moments of the distributions. If we want a simpler model than the kinetic one, it is, however, not sufficient to extract the fluid quantities; we also have to come up with governing equations for these quantities. In this respect, we can again turn to moments, but this time of the Vlasov equation as a whole. For if the left-hand side of the Vlasov equation (2.4, with $\tilde{C}_{ab} \rightarrow 0$) is zero at all values of \mathbf{p} , then so must any moment of it also be

$$\int d^3p \chi \left[\frac{\partial f_a}{\partial t} + \mathbf{v} \cdot \frac{\partial f_a}{\partial \mathbf{x}} + \mathbf{K}(\mathbf{x}, \mathbf{p}; t) \cdot \frac{\partial f_a}{\partial \mathbf{p}} \right] = 0, \quad (2.21)$$

for any arbitrary quantity χ , and with $\mathbf{K} = eZ_a(\mathbf{E} + \mathbf{v} \times \mathbf{B})$.

It is possible to derive the *fluid equations* by taking moments with consecutive powers of $\chi = \mathbf{p}^n$, which can be solved through integration by parts. In the end, (2.21) is resolved as

$$\frac{\partial}{\partial t} \left[n_a \langle \chi \rangle_a \right] + \frac{\partial}{\partial \mathbf{x}} \cdot \left[n_a \langle \chi \mathbf{v} \rangle_a \right] = n_a \left\langle \mathbf{K} \cdot \frac{\partial \chi}{\partial \mathbf{p}} \right\rangle_a, \quad (2.22)$$

where $\langle \cdot \rangle_a$ is as in (2.12). Of course, the field–plasma interaction is still governed by Maxwell’s equations (2.5) through the charge and current density determined by the fluid densities and velocities.

Taking the first few powers of \mathbf{p} in (2.22), we get the beginning of the fluid system of equations. Each power generates a new equation, but also a new variable. As the powers grow, the equations become more complicated. So, while in theory, the system contains an infinite number of equations, various *closures* are used to terminate the series of equations (Hakim, Loverich & Shumlak, 2006; Wang *et al.*, 2020). These closures might be externally motivated, e.g. based on heat flux (Allmann-Rahn, Trost & Grauer, 2018; Hunana *et al.*, 2018), or simply neglecting higher order quantities if the temperature is low enough.

Since the work in this thesis mainly concerns kinetic effects, we will not go into too much detail about fluid modeling of plasmas. There are, however, some largely fluid effects which are relevant to this thesis, which we will discuss in the remainder of this section. For simplicity, we will ignore relativistic effects, so that we may use $\mathbf{v} = \mathbf{p}/m_a$ in (2.22). The first power, $\chi(\mathbf{p}) = 1$, then gives the *continuity equation* (which is the same in the relativistic formulation)

$$\frac{\partial n_a}{\partial t} + \frac{\partial}{\partial \mathbf{x}} \cdot [n_a \mathbf{v}_a] = 0, \quad (2.23a)$$

where \mathbf{v}_a is the fluid flow velocity. Next, with $\chi(\mathbf{v}) = \mathbf{v}$, we obtain

$$m_a n_a \frac{\partial \mathbf{v}_a}{\partial t} + m_a n_a \left(\mathbf{v}_a \cdot \frac{\partial}{\partial \mathbf{x}} \right) \mathbf{v}_a = e Z_a n_a \mathbf{K} - \frac{\partial}{\partial \mathbf{x}} \cdot \overleftrightarrow{\Pi}_a, \quad (2.23b)$$

where the last term contains the *pressure tensor* $\overleftrightarrow{\Pi}_a$ which represents the covariance (spread) of the velocity distribution. For our purposes, we will only consider an isotropic distribution, which renders the last term as $\partial \Pi_a / \partial \mathbf{x}$. We will furthermore use the *adiabatic closure* for the pressure,

$$\Pi_a n_a^{-\gamma_a} = \text{const.} \quad \text{and} \quad \Pi_a = T_a n_a, \quad (2.23c)$$

where T_a is the temperature of the fluid and γ_a is the adiabatic constant; for 1D motion, $\gamma_a = -3$.

2.2.1 Debye shielding

As has been mentioned before, the main difference between a plasma and neutral gas is that the charged particles in a plasma interact with, and generate their own, electric and magnetic fields. The interactions between particles are also said to be long range in a plasma due to the long-range nature of the electrostatic interaction between charged particles. It is, however, only partially true that the electrostatic field of a charged particle is “long range” inside a plasma. As we saw in §2.1.1, a population of free charged particles will react and adjust its density in response to an electrostatic potential. The reaction is such that the charges tend to counteract the existing potential, which will generate a shielding effect.

The length scale of the of this shielding effect is called the *Debye length* λ_D , and it is governed by the response of the particles to the electrostatic disturbance. As we saw in §2.1.1, a thermal population

of charged particles reacts to an electrostatic potential according to the Boltzmann distribution, through which the Debye length (2.11)

$$\lambda_D = \sqrt{\frac{\epsilon_0 T_e}{e^2 n_{e,0}}} \quad (2.24)$$

can be calculated, where T_e and $n_{e,0}$ are the electron temperature and (unperturbed) density, respectively. So when we talk about “long-range” interaction or distances, we mean lengths comparable to or larger than λ_D . The Debye length is also the relevant length scale for electrostatic shocks, as is apparent in the semi-analytical model in paper A, mainly, but also in paper C.

While a plasma consists of both free electrons as well as free ions, and, theoretically, both can contribute to the Debye shielding effect. Often, we only consider the electrons when calculating λ_D – as we did in (2.24) above. In practice, however, the disturbances are rarely completely static, and mostly they vary faster than the time scales of the ion reaction. This ion time scale is analogous to the (electron) plasma frequency in (2.15),

$$\omega_{p,i} = \sqrt{\frac{e^2 Z_i^2 n_{i,0}}{\epsilon_0 m_i}}, \quad (2.25)$$

where the ion charge, eZ_i , density $n_{i,0}$, and mass m_i have replaced those of the electron in (2.15). It is therefore often justified to only consider the electrons when computing the Debye length.

2.2.2 Ion-acoustic waves

The second fluid effect that we will discuss concerns the *ion-acoustic waves*, so called because they are longitudinal compression waves – much like the gas-acoustic waves – mediated mainly through ion-density oscillations. Because the ions carry the oscillation, it is reasonable to say that the time scales involved should be on the scale of the ion plasma frequency (2.25), and since the response of the electrons to the electrostatic field created by the wave will be on the length scale of the Debye length, we can now identify a characteristic velocity

$$c_s \equiv \omega_{p,i} \lambda_D = \sqrt{\frac{Z_i T_e}{m_i}}. \quad (2.26)$$

In this expression, we have assumed a single-ion-species plasma, which means that $n_{e,0} = Z_i n_{i,0}$ due to quasi-neutrality.

While the reasoning above is clearly heuristic, the characteristic velocity c_s defined in (2.26) is actually the propagation speed found for (long-wavelength) ion acoustic waves in a more careful derivation using the fluid system of equations. If you solve for (low-amplitude) longitudinal ion waves in the fluid system of equations is the dispersion relation (for a single-ion-species plasma)

$$\omega^2(1 + k^2\lambda_D^2) = c_s^2k^2. \quad (2.27)$$

We therefore see that both the phase and group velocities of the ion-acoustic wave are c_s , in the long-wavelength limit, $k^2\lambda_D^2 \ll 1$. This dispersion relation also reveals an upper frequency limit of $c_s/\lambda_D = \omega_{p,i}$, justifying the reasoning in the previous paragraph.

Also analogous to sound waves in gases, if an electrostatic perturbation moves through the plasma faster than the ion-acoustic wave speed, an electrostatic shock is created, corresponding to the sonic boom in air. In the context of shocks, their speed is often measured relative to the sound speed, in terms of the *Mach number*

$$\mathcal{M} = \frac{v_{\text{shock}}}{c_s}. \quad (2.28)$$

For a wave to actually be a shock wave, its Mach number must be greater than unity, $\mathcal{M} > 1$. Then, the shock moves faster through the ion population than any information about it, thus arriving before the ions can react to it, and the result is a steep – on the order of λ_D – gradient in both electrostatic potential and ion density at the *shock front*.

2.2.3 Langmuir electron waves

The final fluid phenomenon that we will discuss are *electron (density) waves*, also known as *Langmuir waves* after Langmuir (1928) and Tonks & Langmuir (1929). These waves are central to the phenomenon stimulated Raman scattering (SRS), which play a central role in paper E. In SRS, two counterpropagating laser pulses induce electron waves, on which one of the laser pulses back-scatters. In this way, energy can be transferred from one of the pulses to the other. Here we will, however, only set up the basics of the electron wave, SRS will be discussed further in §§ 3.1.2 and 4.2.

The electron waves are, like the ion-acoustic waves, longitudinal density waves, which means that they can be treated in a 1D geometry – and that there is no oscillating magnetic field associated with the wave. We

can find a perturbative solution by linearizing the fluid system of equations (2.23). After linearization in the perturbed quantities, we obtain a wave equation for the perturbative density fluctuation n_1 ,

$$3v_{te}^2 \frac{\partial^2 n_1}{\partial x^2} - \frac{\partial^2 n_1}{\partial t^2} = \omega_{p,0}^2 n_1, \quad (2.29)$$

where $v_{te} = (T_e/m_e)^{1/2}$ is the electron thermal velocity, and $\omega_{p,0}$ is the equilibrium plasma frequency associated with the background electron density n_0 . Note the interesting similarity between this wave equation and that of the electromagnetic wave in a plasma (2.14), that the plasma frequency appears in (2.29) the same way as in (2.14), further demonstrating that the plasma frequency is the response timescale of the electrons. We also get a similar dispersion relation

$$\omega^2 = \omega_{p,0}^2 + 3v_{te}^2 k^2, \quad (2.30)$$

which also shows that only oscillations with frequency at or above $\omega_{p,0}$ are allowed.

2.3 Collisions – reintroducing microscopic interactions in kinetic theory

While the Vlasov system of equations (2.5, 2.6 & 2.4 with $\tilde{C}_{ab} \rightarrow 0$) is entirely self-contained and can be integrated as is, we are still lacking an adequate description of the cases where collisions cannot be neglected. While inter-particle collisions are microscopic events, we can still approximate their effect on the macroscopic scale, based on the information contained in the distribution functions – that will be the collision operator. Depending on the complexity required in the modeling, different collision operators have been devised; naturally, these will result in different levels of accuracy depending on situation and intended usage. In this section, we will present a short overview of particle collisions in plasmas, which are often described using the *Fokker–Planck operator*. A detailed account of collisions in plasmas can be found in the book by Helander & Sigmar (2002).

The Fokker–Planck operator is based on the *Coulomb interaction* between charged particles. Unlike the hard-sphere, close collisions that Maxwell (1860) and Boltzmann (1872) considered, which result in large-angle scattering, the long-range nature of the Coulomb force results in the prevalence of small-angle, grazing collisions, where the momenta of

the colliding particles are only slightly changed. Therefore, the collision operator, which acts on the distribution function, should only directly affect the *momentum space* portion of the distribution. In fact, each collision can be viewed as a step in a momentum-space random walk for the colliding particles. In turn, considering the statistics of all particles, these random walks may be viewed as a type of momentum-space diffusion of the distribution function. Indeed, we may write a general form of the collision operator consisting of a *diffusion* term and an *advection* or *friction* term. The advection term is added to account for such effects as friction, e.g. when a particle is moving relative to the plasma background. Intuitively, we would expect a population of particles that is moving relative to the background to slow down when they collide with the background, not only diffuse.

The other main consequence of the coulombic nature of particle collisions in a plasma is that the effect of the collisions – the *collisionality* – generally decreases when the relative velocities of the colliding particles increase. On the level of individual particles, this relation means that fast particles are generally not affected much by the effects of collisions. Accordingly, on the level of the whole distribution function, if there are many high-energy particles – for example at high temperatures – the collisional effects decrease. This decreased collisionality in a hot population affects both how much the population itself is affected by collisions, as well as how much this population collisionally can affect other populations of particles.

The collisionality of a given plasma system is commonly gauged by the so-called *collision frequency* ν , which describes the inverse time scale of the changes to the distribution due to collisions. There are many different collision frequencies, related to *friction* or the two types of momentum-space diffusion that occur, *parallel diffusion* and *pitch-angle scattering*. The former is the diffusion of the magnitude of the particle momenta, whereas pitch-angle scattering is the process by which a population with a directed momentum is scattered along the sphere of constant energy – i.e. the distribution spreads out in the direction of the particle momenta. It is often useful to consider how these collision frequencies scale with physical parameters. As we already mentioned, the collision frequencies decrease if the temperatures increase. Other important scalings are the linear scaling with the densities and the quadratic scaling with the charges of the particles of the colliding populations.

In paper A, we consider the effect of parallel diffusion of ions across a phase-space separatrix, using a perturbative approach in the smallness

of the diffusion collision frequency in a very low-collisionality plasma. This approach can thus be motivated for very low-density plasmas, such as astrophysical plasmas. In papers B and C, on the other hand, we consider the effects of collisions in plasmas that were chosen to have high collisionalities, through high density and ions with high charge numbers. However, in this limit of high density or low temperature, where the scalings above give high collisionality, the derivation of the Fokker–Planck operator is no longer valid – small-angle collisions no longer dominate. Some of the issues that arise in such situations are discussed in paper C.

2.4 Simulating plasmas – using numerical tools to solve the complex behavior of plasmas

While we are able to describe and capture many aspects of plasma physics through either the fluid or kinetic systems of equations, we are not able to solve the equations analytically, except in a very limited number of idealized cases. Both the descriptions are, after all, sets of coupled partial differential equations (PDEs), which we can only solve using numerical. In this section we will take a brief overview of two possible ways to numerically solve the kinetic system of equations (2.4, 2.5 & 2.6): the Continuum Vlasov–Maxwell solver (§ 2.4.1) and particle-in-cell method (§ 2.4.2). In both cases, we will also present the simulation tools used in the various works in this thesis.

2.4.1 Continuum Vlasov–Maxwell solvers

One way to numerically solve the Vlasov–Maxwell system of equations is to discretize them in time and onto an *Eulerian*[‡] simulation grid in phase space, and then use numerical PDE solvers to find a solution for $f_a(\mathbf{r}, \mathbf{p}; t)$. These methods are called *continuum* or *Vlasov–Maxwell/kinetic solvers*, because they solve the Vlasov/kinetic equation coupled with Maxwell’s equations in a framework where the plasma is considered as a continuum medium – unlike the particle-in-cell (PIC) approach, in which the plasma is modeled as discrete particles. Addi-

[‡]The denomination “Eulerian” stems from the two flow specifications of a fluid, *Eulerian* and *Lagrangian*, where the fluid flow field is either specified on a fixed coordinate system or along the trajectories of “packets” of fluid, respectively. In the case of a continuum Vlasov–Maxwell solver, the “fluid” in question is the phase-space distribution.

tional reading on these types of simulation frameworks can be found in the book by Shoucri (2011), or in the thesis by Juno (2020).

The fact that the full phase space is discretized is, however, one of the main drawbacks of the continuum methods. Since the phase space has up to twice the number of dimensions (both \mathbf{r} and \mathbf{p}) as the configuration space modeled, that means that we may have to simulate up to six dimensions, plus time. In addition, not all areas of phase space are of the same physical relevance, e.g. some areas might be devoid of plasma or have a very low phase-space density; yet, these less important phase-space volumes are still part of the whole computation and incur a similar computational cost as the densely populated volumes. The computational cost can therefore grow prohibitively fast for simulation of more than a few dimensions.

Often, this high computational cost of continuum methods forces the users to run simulations with comparatively small system sizes or low resolution (Pusztai *et al.*, 2020). However, depending on the numerical methods used, continuum solvers do not suffer from discretization noise in the same way as PIC methods, and can thus be used at much lower resolution than PIC. In some cases, where continuum solvers have been used successfully, it might not be feasible to use PIC codes due to the high resolution requirement to suppress the noise (Juno *et al.*, 2020).

Another complication that might arise due to the complexity of continuum methods is that of code development. A numerical scheme optimized to solve the (collisionless) Vlasov–Maxwell equations, might not be suitable for a slightly modified system of equations, such as including a collision operator (Hakim *et al.*, 2020). Effectively incorporating new features into a continuum code may therefore be rather challenging.

In summary, for applications which require a fully kinetic description and can be simulated with one or two spatial dimensions, or requiring very low noise levels, continuum solvers for the Vlasov–Maxwell system of equations can be powerful tools. A selection of such applications are electrostatic shocks (Svedung Wettervik, DuBois & Fülöp, 2016; Pusztai *et al.*, 2018; paper A), which will be examined further in this thesis, kinetic plasma instabilities (Cagas *et al.*, 2017; Skoutnev *et al.*, 2019), and kinetic effects in magnetic dynamos (Rincon *et al.*, 2016[§]; Pusztai *et al.*, 2020). Furthermore, Vlasov–Maxwell solvers may also be used as a reference; thanks to their low noise and possibly high fidelity, their

[§]Although Rincon *et al.* (2016) used a Vlasov–Maxwell method, they reduced the computational cost by treating the electrons with a fluid model.

output from a standardized problem could be used as a benchmark for other types of simulation codes, such as fluid or PIC codes.

Gkeyll

One of the simulation tools used in paper A was Gkeyll[¶] (Juno *et al.*, 2018). Gkeyll is a simulation framework containing, among others, an Eulerian solver for the (non-relativistic) Vlasov–Maxwell equations. Beyond the collisionless Vlasov–Maxwell system, Gkeyll also supports effects of collisions with either the BGK operator (Bhatnagar, Gross & Krook, 1954) or the Dougherty (1964) (Dougherty & Watson, 1967) operator – the latter is sometimes also referred to as a Lenard–Bernstein (1958) operator. These operators are not as advanced as the Fokker–Planck operator and lack the complex velocity dependence found therein, which means that their scope of application is limited to near-thermal distributions. A detailed account of the implementation of the collisions in Gkeyll can be found in the recent paper by Hakim *et al.* (2020).

2.4.2 Particle-in-cell methods

A more widely used framework to simulate kinetic plasmas is the particle-in-cell (PIC) technique (Langdon, 2014; Pukhov, 2016). This method goes back to the basic idea to compute the trajectories of individual particles, although with limited number of computational *macroparticles*. Instead of the relatively complicated system of non-linear PDEs that is used in kinetic theory, PIC methods integrate the equations of motion for the finite number of macroparticles, albeit with every macroparticle weighted to represent a large number of “real” *microparticles*, i.e. q_a and m_a are scaled up by some factor, while keeping the charge-to-mass ratio q_a/m_a constant. The macroparticles usually also have a finite spatial extent – their *shape function* – which reduces discretization noise. When the Lorentz force on the macroparticle is computed, the (discretized) field is interpolated together with the shape function; for more detail, see for instance the appendix of Derouillat *et al.* (2018). By its nature, the PIC solver can be viewed as a finite element solver of the Vlasov–Maxwell system using the *Lagrangian* (phase-space) flow specification – as opposed to Eulerian continuum solvers, where the (phase-space) flow is computed on a fixed grid.

[¶]Code documentation can be found at: <https://gkyl.readthedocs.io/en/latest/>.

Maxwell’s equations, (2.5), are solved on a grid of computational “cells”. The charge and current densities (2.6), are projected from the particles onto a staggered grid via the particle shape functions. The weighting and shape of the macroparticles allows the field–plasma interaction to emulate that of the simulated system. The PIC procedure thus consists of two operations: first, given the position and velocity of all particles, calculate the fields; then, given the fields and previous momenta of the particles, calculate the new position and momentum of the particles – commonly referred to as the *particle pusher*. These two operations are iterated back and forth for every simulated time step, and constitute the essence of a PIC code. In order to increase the numerical stability, more complex strategies are employed, such as the, de facto standard, “Boris (1970) pusher”.

The PIC method benefits from its conceptually simple algorithm. By relying on computing the trajectories of macroparticles, the method can aid the understanding of a physical problem by allowing particles to be followed through phase space – which would otherwise be challenging to do in a continuum framework. Furthermore, since every particle push occurs independently between the field calculations, PIC codes are naturally well-adapted for massively parallelized computation.

The main computational bottleneck for PIC simulations, however, is usually the number of macroparticles in the simulation. Since PIC codes do not have to include momentum space in their computational grid, they are not as weighed down by higher dimensions as Vlasov–Maxwell solvers can be. One way of viewing PIC codes is that they solve for a random statistical sampling of the initial distribution function in all its dimensions, thus breaking the “curse of dimensionality” with a limited number of statistical samples – the macroparticles. However, the limited number of macroparticles also usually results in rather noisy results due to a relatively coarse-grained projection of the particles onto the charge and current density grid. Unfortunately, due to the statistical nature of PIC simulations, the noise level only decreases as $\sim \bar{N}^{-1/2}$ with the number of macroparticles, \bar{N} .

The field–particle interaction is limited by the finite grid resolution of the fields, meaning that microscopic particle interactions mediated by the field – such as collisions – are similarly limited by the computational grid resolution. Due to computational constraints, the grid resolution is much too coarse to accurately capture collisional effects. Instead, Monte Carlo schemes are being used to emulate the “random kicks” the (micro) particles experience due to collisions. These schemes operate by

calculating the probability distribution for a certain angular deviation to the particle momentum due to collisions during one simulation time step. The most common method is to implement a scheme with binary collisions between macroparticles (Nanbu, 1997; Nanbu & Yonemura, 1998; Sentoku & Kemp, 2008; Pérez *et al.*, 2012), which are mutually scattered according to the scattering probability distribution, such that momentum and energy are being conserved – at least statistically.

The relatively simple basic principle of operation of PIC codes also means that there are a wide variety of different PIC codes available to use more or less freely – PIC codes are much more common than Vlasov–Maxwell codes. Together with the fact that PIC codes can readily handle relativistic particle motion, it is no surprise that the vast majority of laser-plasma simulations are done with PIC codes. As with binary collisions, PIC methods can more easily be adapted to emulate quantum mechanical effects on the macroparticles, such as interactions with photons (e.g. emission/absorption and quantum-electrodynamical effects) or ionization, all of which are highly non-trivial to implement in a continuum framework and may be of great importance to laser–plasma interactions. An even remotely extensive account of studies performed with PIC codes would be prohibitively long; in fact, PIC simulations have become so ubiquitous that nowadays they accompany almost all experimental findings in laser-plasma physics (Faure *et al.*, 2004; Haberberger *et al.*, 2012; Higginson *et al.*, 2018; Fiuza *et al.*, 2020).

Smilei

The main plasma-simulation tool used in papers B through E has been Smilei[‡] (Derouillat *et al.*, 2018). It is co-developed by high-performance-computing specialists and physicists, in order to be as modular as possible and perform efficiently on large-scale supercomputers. Smilei is complemented by a large set of run-time diagnostics (based on the HDF5 file format) and user-friendly (Python) post-processing tools complements the code. The modularity of Smilei gives it access to various additional physics modules, among which are field ionization, binary collisions and collisional impact ionization – all of which are of high relevance to the work included in this thesis.

[‡]Code documentation can be found at: <https://smileipic.github.io/Smilei/>.

We may find illustrations of the highest doctrines of science in games and gymnastics, in travelling by land and by water, in storms of the air and of the sea, and wherever there is matter in motion.

James Clerk Maxwell (1871)

Chapter 3

Laser–plasma interactions

We have now had a brief overview of plasma physics in general, in chapter 2; in this chapter, we will be diving into some more detail about the physics of the interaction between the laser and the plasma, which directly concerns all papers in this thesis, except paper A. There are, like with plasmas in general, many different kinds of laser plasmas, with different outcomes and applications in mind. Of course, what they all have in common, is that their behavior is dominated by a very high-intensity electromagnetic wave – the laser. The laser is capable of delivering a large amount of energy to the target in as little as a few femtoseconds, and we have to understand where that energy goes and how it affects the plasma. In this chapter, we will be reviewing some of the theory more specific to laser plasmas.

3.1 Basic concepts of laser–plasma interactions

In this section, we will review some of the basic concepts of the interaction between the laser and a plasma. As has been noted before in this thesis and elsewhere, the laser–plasma interaction is two way. The charged particles in the plasma react to the electromagnetic field of the laser, and in that process, they generate their own electromagnetic fields which affect the laser. We start this section by examining the effect of the laser fields on the charged particles in §3.1.1. We then move on to include the effects of the plasma on the laser in §§3.1.2 and 3.1.3 for under- and overcritical plasmas, respectively.

3.1.1 Particle motion in an electromagnetic plane wave

The first step in understanding laser–plasma interactions, is to study how a single particle reacts to an electromagnetic wave. Since laser light in many circumstances can be approximated as *plane waves*, we will here study the particle dynamics in such plane waves. We can describe the plane wave with the complex framework as

$$\mathbf{A} = A_0 \hat{\mathbf{e}} \exp(i\mathbf{x} \cdot \mathbf{k} - i\omega t), \quad (3.1)$$

with polarization $\hat{\mathbf{e}}$, amplitude A_0 , wave vector \mathbf{k} , and frequency ω . The vector potential in a *plane* wave stays constant along the *planes* perpendicular to the direction of propagation $\hat{\mathbf{k}} = \mathbf{k}/|\mathbf{k}|$.

Using the Lagrangian framework for a charged particle in an electromagnetic field (c.f. Jackson, 1999, ch. 12), it is possible to derive various constants of motion for a charged particle moving in a plane wave, like the *canonical momentum* $\mathbf{P} = \mathbf{p} + eZ\mathbf{A}$, from which the particle momentum \mathbf{p} can be deduced. In a plane wave, the components of the canonical momentum perpendicular to the direction of propagation, \mathbf{P}_\perp , will be conserved due to the translational symmetry in these directions. The parallel component of the canonical momentum $P_\parallel = \mathbf{P} \cdot \hat{\mathbf{k}}$ is, however, generally not conserved. It is, nonetheless, possible to find a relation for the parallel momentum component in a plane wave. The relations for the transverse and parallel momenta can be summarized as

$$\mathbf{p}_\perp = -eZ\mathbf{A} \quad (3.2a)$$

and

$$p_\parallel = \frac{p_\perp^2}{2mc} = \frac{(eZA)^2}{2mc} \quad (3.2b)$$

for a particle initially at rest, $\mathbf{p}_{\text{init}} = 0$, without any initial fields, $\mathbf{A}_{\text{init}} = 0$, in a plane wave field that is slowly (adiabatically) brought up in amplitude. Note that these relations holds for motion in any longitudinally modulated plane wave field ($A_\parallel = 0$), since the longitudinal modulation can be described via a Fourier expansion of plane waves with the same $\hat{\mathbf{k}}$. These expressions might seem suspiciously simple, but in reality their dependence on the longitudinal position $\hat{\mathbf{k}} \cdot \mathbf{x}$ of \mathbf{A} will make the full particle trajectory more complicated to disentangle.

In laser-plasma physics, the particles that are affected most by the laser are the electrons, due to their high charge-to-mass ratio. It is therefore natural to normalize the induced momenta, and thereby wave

amplitude, to $m_e c$, which gives the *normalized relativistic amplitude*

$$a_0 = \frac{eA_0}{m_e c} = \frac{eE_0}{m_e c\omega} \quad (3.3)$$

for a plane wave in vacuum with vector-potential amplitude A_0 , which gives the corresponding electric-field amplitude $E_0 = \omega A_0$. This provides a measure of how large relativistic effects will be on the electron motion. Additionally, from (3.2b), we see that the longitudinal motion $p_{\parallel} \sim m_e c a_0^2$ is negligible for small $a_0 \ll 1$.

So far, we have been working with the vector potential \mathbf{A} , but in practice the *intensity* is normally the measure used for the “strength” of a laser pulse. The intensity is defined through the cycle-averaged square of the (real) electric field

$$\begin{aligned} I \equiv c\epsilon_0 \left\langle |\operatorname{Re}\{\mathbf{E}\}|^2 \right\rangle_{\tau} &= \frac{c\epsilon_0}{\tau} \int_0^{\tau} dt |\operatorname{Re}\{\mathbf{E}(t)\}|^2 = \frac{c\epsilon_0}{2} \left(\frac{m_e c \omega a_0}{e} \right)^2 \\ &\approx 1.4 \times 10^{18} \text{ W cm}^{-2} \times a_0^2 \left(\frac{\lambda}{1 \mu\text{m}} \right)^{-2} \end{aligned} \quad (3.4)$$

where $\tau = 2\pi/\omega$ is one laser cycle, $\lambda = 2\pi c/\omega$ is the laser wavelength, and $\mathbf{E} = -\partial\mathbf{A}/\partial t$ for a plane wave (3.1) in vacuum.

When introducing the intensity together with a_0 , as we have done above, we should also clarify the convention that we use for the polarization vector $\hat{\mathbf{e}}$. Maxwell’s equations in vacuum only allow polarizations perpendicular to the propagation of direction $\hat{\mathbf{e}} \cdot \hat{\mathbf{k}} = 0$, so we may express the polarization as

$$\hat{\mathbf{e}} = \cos(\vartheta) e^{i\varphi_1} \hat{\mathbf{e}}_1 + \sin(\vartheta) e^{i\varphi_2} \hat{\mathbf{e}}_2, \quad (3.5)$$

where $\hat{\mathbf{e}}_1$ and $\hat{\mathbf{e}}_2$ are orthogonal unit vectors spanning the plane perpendicular to the direction of wave propagation, $\hat{\mathbf{e}}_1 \cdot \hat{\mathbf{e}}_2 = \hat{\mathbf{e}}_1 \cdot \hat{\mathbf{k}} = \hat{\mathbf{e}}_2 \cdot \hat{\mathbf{k}} = 0$. The angles ϑ and $\varphi_{1,2}$ are related to the ellipticity of the polarization; for $\varphi_1 = \varphi_2$ we have *linear polarization* (LP), and for $\vartheta = \pi/4$ and $|\varphi_1 - \varphi_2| = \pi/2$ the wave has *circular polarization* (CP). Importantly, with this convention, the amplitude of the wave is such that the intensity is given by the expression in (3.4), regardless of polarization*.

*This convention also means that a circularly polarized wave of amplitude a_0 will only trace a circle with (normalized) radius $a_0/\sqrt{2}$.

Ponderomotive force

The final single-particle phenomenon that we will discuss in this section regards the effect of the laser-pulse envelope – modulating the pulse in both the longitudinal and transverse directions. We have only considered electromagnetic plane waves so far, which can somewhat easily be generalized to any longitudinal modulation, but the conservation of transverse canonical momentum breaks down when we add a transverse modulation to the wave. However, for sufficiently slow-varying modulations – with a modulation length scale much larger than the transverse movement of the particle – the relations in (3.2) present good approximations for the particle dynamics.

Consider that the particle in question has an oscillatory motion in the perpendicular direction. If the particle moves to a region of lower amplitude during its oscillation, it will lose a little energy and not be able to return to its original position, which will manifest as a tendency to move away from regions of high intensity. Using the momentum relations (3.2), we can express the kinetic energy of the particle, which can be averaged over one laser cycle to yield

$$\langle \mathcal{E}_{\text{kin}} \rangle_{\tau} = \frac{e^2 Z^2}{2m} \langle A^2 \rangle_{\tau} = \frac{e^2 Z^2}{2m c \epsilon_0 \omega^2} I, \quad (3.6)$$

where I is the intensity given by (3.4). What this equation tells us is that the cycle-averaged energy of a particle is proportional to the *local* intensity. From this relation, we can express the above mentioned tendency to move away from regions of high intensity as a force, given by the gradient of the average kinetic energy

$$\mathbf{F}_{\text{PM}} = -\nabla \langle \mathcal{E}_{\text{kin}} \rangle_{\tau} = -\frac{e^2 Z^2}{2m} \nabla \langle A^2 \rangle_{\tau} = -\frac{e^2 Z^2}{2\epsilon_0 c m \omega^2} \nabla I, \quad (3.7)$$

which we call the *ponderomotive force*. For more details on the ponderomotive force the reader is referred to, e.g., the books by Gibbon (2005) or Macchi (2013); Quesnel & Mora (1998) also present a thorough analytical and numerical treatment of the ponderomotive force in the relativistic regime.

The ponderomotive force plays a key role in many laser–plasma interactions, perhaps most prominently in laser wakefield acceleration (Tajima, Yan & Ebisuzaki, 2020), where the ponderomotive force expels electrons to create the charge separation that generate the accelerating field. From the expression in (3.7), we can make a few observations about the ponderomotive force. First, it acts to expel particles away from regions of

high intensity, both transversely and longitudinally in front of the pulse, and it does so independently of the sign of the charge. Second, since the ponderomotive force has an inverse dependence of the mass of the particle, electrons will be most strongly affected by it in a laser plasmas.

3.1.2 Laser interaction with undercritical plasmas

We briefly, in §2.1.3, already touched upon the fact that the electron density determines whether or not a plasma allows propagation of electromagnetic waves. For a laser of frequency ω impinging on a plasma with density $n_e < n_c$, where n_c given by (2.17) is the critical density associated with ω , the plasma is said to be *undercritical* and the laser can propagate through it. For a typical laser wavelength of $\lambda = 800$ nm, the critical density is $n_c \simeq 1.74 \times 10^{21} \text{ cm}^{-3}$. In order to achieve plasmas with densities below that, gas-jet targets are normally used (Semushin & Malka, 2001) since most solid-density materials have significantly higher electron densities. Applications employing undercritical plasmas include LWFA (Tajima, Yan & Ebisuzaki, 2020), shock acceleration of ions (Wei *et al.*, 2004), generation of strong magnetic fields (Léczi *et al.*, 2016), and plasma-based laser amplification (Riconda *et al.*, 2014; Sundström *et al.*, 2022*b* – paper E).

When the laser pulse passes through an underdense plasmas, it is, however, not completely unaffected. In the case with a low-amplitude wave – such that the wave itself does not significantly affect the plasma – the plasma dispersion relation (2.16) give rise to a frequency dependent phase and group velocities

$$v_{\text{ph}} = \frac{\omega}{k} = c \left(1 - \frac{\tilde{\omega}_{\text{p}}^2}{\omega^2} \right)^{-1/2} \quad \text{and} \quad v_{\text{gr}} = \frac{\partial \omega}{\partial k} = c \left(1 - \frac{\tilde{\omega}_{\text{p}}^2}{\omega^2} \right)^{1/2}, \quad (3.8)$$

respectively. Because of this frequency dependence, different frequency components of a pulse will propagate at different velocities, thus *dispersing* the pulse. The shorter a laser pulse is, the broader its frequency spectrum will be, and thereby more affected by dispersion. In general, for a pulse to have a short duration – compared to its central-frequency period – the phases of each frequency components must be related in a very specific manner; as soon the pulse propagates through a dispersive medium, these phases start to drift relative to each other, and the pulse duration increases. In the next chapter, we will go into further detail on the dispersion of short-duration pulses in plasmas, which constitute the

basis of the plasma-density diagnostics technique presented in paper D. In short, since the dispersion depends on $\tilde{\omega}_p^2$ which depends on n_e , we can infer some information on the density profile if the relative phases of the pulse before and after dispersion are known.

Next, if the intensity of the laser pulse is sufficiently high that the plasma density is significantly affected, we may encounter other phenomena, such as wakes behind the laser and the growth of plasma waves. The laser wake is created by the electrons being expelled from the laser region by the ponderomotive force. Behind the pulse, the ions – which are much less affected by the ponderomotive force – that are left behind create a bubble of strong positive charge, which attract electrons back. This electrostatic field in the wake also has a strong longitudinal component, which is the accelerating force in a laser wakefield accelerator (LWFA).

Laser-induced electron waves

If we stay with moderately high-amplitude waves, we may use a perturbative approach to solve the electromagnetic wave equation in a plasma (2.14). Since the effect of the wave on the plasma is no longer negligible, we will consider a plasma frequency with a perturbation

$$\omega_p^2(x, t) = \omega_{p,0}^2 + \omega_{p,1}^2(x, t) = \omega_{p,0}^2 \left[1 + \frac{n_{e,1}(x, t)}{n_{e,0}} \right], \quad (3.9)$$

where $n_{e,1}$ is the perturbed electron density and $\omega_{p,0}$ and $n_{e,0}$ are the unperturbed (constant) plasma frequency and electron density, respectively. We may then write the electron-wave equation (2.14) as

$$c^2 \frac{\partial^2 \mathbf{A}_\perp}{\partial x^2} - \frac{\partial^2 \mathbf{A}_\perp}{\partial t^2} - \omega_{p,0}^2 \mathbf{A}_\perp = \omega_{p,0}^2 \frac{n_{e,1}}{n_{e,0}} \mathbf{A}_\perp, \quad (3.10)$$

where we have ignored the relativistic effects in $\bar{\gamma}_e$.

The term on the right-hand side is due to the (longitudinal) waves in the electron density, n_1 , induced by \mathbf{A} . To find how n_1 is affected by \mathbf{A} , we may use the same fluid framework as for the electrostatic electron waves derived in §2.2.3. We must, however, modify the approach to account for the electromagnetic wave \mathbf{A}_\perp that is present. To simplify the calculations, we again ignore relativistic effects[†]. In the perturbed

[†]Which might be somewhat dubious, given the “moderately high amplitude” of the waves. However, for our purposes, the amplitudes considered in paper E can be considered sufficiently small so that relativistic effects can be ignored.

momentum equation (2.23b), we must now account for the background transverse fields \mathbf{E}_\perp and \mathbf{B}_\perp .

The transverse electric field does, however, not directly affect the (longitudinal) electron wave since we still consider a 1D geometry. The induced transverse electron velocity, $\mathbf{v}_{e,\perp} = e\mathbf{A}_\perp/m_e$ from (3.2a), together with the magnetic field does, however, contribute with a longitudinal component in the Lorentz force. From this longitudinal component, it is possible to modify (2.29) to account for the effect of the electromagnetic wave (c.f. Kruer, 2003, ch. 7). The modified electron-wave equation thus becomes

$$\left[\frac{\partial^2}{\partial t^2} - 3v_{te}^2 \frac{\partial^2}{\partial x^2} + \omega_{p,0}^2 \right] n_1 = \frac{e^2 n_0}{2m_e^2} \frac{\partial^2 (\mathbf{A}_\perp^2)}{\partial x^2}. \quad (3.11)$$

We remind the reader that $v_{te} = (T_e/m_e)^{1/2}$ is the thermal velocity of the electrons. Notably, the driving force term has the same form as an instantaneous (non-averaged) ponderomotive force (3.7), which has an intuitive explanation: The ponderomotive force acts to expel particles from local regions of high (instantaneous) intensity, which in a plane wave becomes a force away from its crests and troughs that will then drive longitudinal density waves.

The driven wave will, however, be quite weak in most cases because the electromagnetic and electron waves do not resonate – resonant driving requires matching phase velocities. For a laser pulse of frequency ω , propagating through an undercritical plasma, its phase velocity (3.8) is $v_{ph}^{(EM)} \geq c$, while the electron wave driven by it (at frequency 2ω) will have a phase velocity near that of the non-driven electron wave $v_{ph}^{(e)} \simeq \sqrt{3} v_{te} (1 - \omega_{p,0}^2/4\omega^2)^{-1/2}$. Next, since $v_{te} \ll c$ (in the vast majority of cases), the phase velocities are similarly far apart, $v_{ph}^{(e)} \ll v_{ph}^{(EM)}$. The two waves are thus far away from being resonant with each other[‡]. Therefore, single laser pulses propagating through a plasma generally do not generate any significant (longitudinal) electron-wave response. However, if there are two electromagnetic waves of different frequencies in the plasma, a resonance can arise through one of the heterodyne frequencies in the \mathbf{A}_\perp^2 term. This effect is one of the cornerstones of stimulated Raman scattering (SRS), which plays a central role in paper E, and will be discussed further in §4.2.

[‡]Another way of viewing this (failed) resonance is that, since the electromagnetic wave is much faster than the electron thermal velocity, *Landau* damping is ineffective and the electromagnetic wave does not lose much energy to the plasma that way.

3.1.3 Laser interaction with overcritical plasmas

The work in papers B and C concerns collisional effects in solid-density plasmas irradiated by high-intensity laser pulses. The electron densities considered in these papers are well above the critical density of the laser employed. In this section, we will therefore briefly go over how the interaction between the laser light and an overcritical plasma; more specifically, we will only consider plasmas with a sharp vacuum–plasma interface, i.e. the plasma density ramp is much shorter than the laser wavelength. For a deeper treatment of the subject, the reader may refer to the reviews by Kemp *et al.* (2014) or Kaw (2017).

As noted before, laser light (in general) cannot propagate through an overdense plasma, but that does not mean that the field does not penetrate the overdense region at all. As demonstrated by the electromagnetic plasma dispersion relation (2.16), there are no real solutions for k when $\omega < \omega_p$, which means that there are no propagating wave solutions in the plasma. There will, however, be an evanescent field with an exponentially decaying amplitude profile in the so called *skin region*. For a normally incident laser on a semi-infinite plasma occupying the space $x \geq 0$, we have an amplitude profile inside the plasma given by

$$A_{\text{plasma}}(x) = A_1 \exp(-x/l_s), \quad (3.12)$$

where l_s is called the *skin depth* and is given by (Ch. 7.5, Jackson, 1999)

$$l_s = \frac{c}{\omega_p} \left(1 - \frac{\omega^2}{\omega_p^2}\right)^{-1/2} = \frac{\lambda}{2\pi} \sqrt{\frac{n_c}{n_e}} \left(1 - \frac{n_c}{n_e}\right)^{-1/2}, \quad (3.13)$$

where λ is the laser wavelength (in vacuum).

Next, since the light is reflected from the plasma, a standing wave is generated in the vacuum region which will have an amplitude profile of

$$A_{\text{vacuum}}(x) = 2A_0 \sin(-kx + \varphi), \quad (3.14)$$

where A_0 is the (unaffected) amplitude of the incoming wave, $k = 2\pi/\lambda$ is the vacuum wavenumber and φ is a constant phase. By matching the values and derivatives of $A(x)$ at $x = 0$ between (3.12) and (3.14) at $x = 0$, we obtain the amplitude relation and phase

$$\begin{cases} A_1 = 2A_0(n_c/n_e)^{1/2}, \\ \tan \varphi = kl_s = (n_c/n_e)^{1/2}(1 - n_c/n_e)^{-1/2}. \end{cases} \quad (3.15)$$

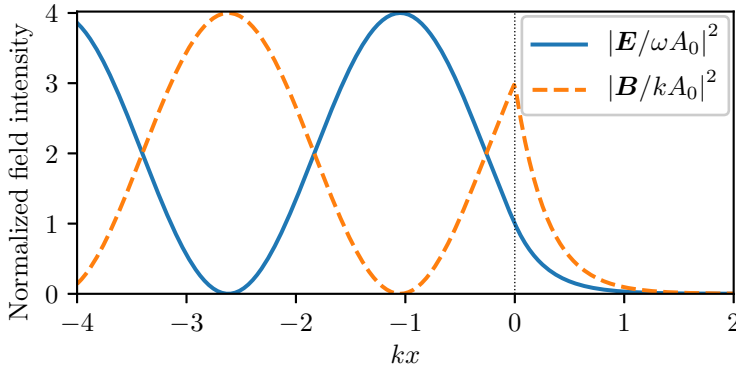


Figure 3.1: Illustration of the standing wave field intensity for a plane wave field normally incident on a plasma occupying the space $x \geq 0$ with density $n_e = 4n_c$, giving a skin-depth of $kl_s \approx 0.6$. Note the discontinuity in the gradient of the amplitude of the B field.

The full vector potential of the standing and evanescent wave can therefore be written as $\mathbf{A}_\perp = -iA(x)\hat{\mathbf{e}} \exp(-i\omega t)$ with the amplitude envelope

$$A(x) = 2A_0 \times \begin{cases} \sin(-kx + \varphi), & x < 0, \\ \left(\frac{n_c}{n_e}\right)^{1/2} e^{-x/l_s}, & x \geq 0. \end{cases} \quad (3.16)$$

An example of the fields from such a standing wave is shown in Fig. 3.1, where the normalized field intensity of E and B are plotted. Note the discontinuity in the gradient of the B field amplitude at $x = 0$, which is due to the discontinuity in \mathbf{j} at the surface of the plasma.

The standing wave discussed above is what would arise from a laser hitting a static plasma target, and we can use these calculations to gain a few insights. First, the laser field penetrates the overcritical plasma over a few skin depths, l_s , where it has a possibility to impart energy onto the electrons (mainly). Second, the on-target intensity, at the plasma surface, is a factor $(A_1/A_0)^2 = 4n_c/n_e$ lower than the initial unaffected laser intensity, which means that the higher the plasma density is, the lower the field will be on the plasma surface as well as inside the skin region.

While the model calculations above are useful to gain some insights, in reality, however, the plasma is not static and will react to the laser light. There are a couple of effects at play. First, in real laser systems, the main laser pulse will be preceded by a parasitic *prepulse*, which is often much longer than the main pulse. The prepulse will heat the

plasma, causing the plasma pressure to increase and the plasma to hydrodynamically expand out into the vacuum region. Many laser plasmas therefore have a region where the plasma density ramps up, called the *preplasma*. There are various ways of minimizing the preplasma, but a perfectly sharp plasma–vacuum boundary is not possible. Next, even if the preplasma is minimized, rapid heating from the main pulse will also dramatically increase the plasma pressure in the skin region, causing plasma expansion which will also alter the laser–plasma interaction.

Radiation pressure and the laser piston

The hydrodynamic expansion out the front of the plasma due to the high plasma pressure is, however, counteracted by the laser itself. Electromagnetic waves have been known for almost 150 years to carry momentum proportional to their intensity. As the laser pulse is either absorbed or reflected, its momentum is transferred to the target acting as a *radiation pressure*. The exact strength of the radiation pressure depends on the reflected, transmitted and absorbed fractions of the laser pulse, but for simplicity in the discussion here, we will assume that the pulse is fully reflected. This is a fairly decent assumption for laser pulses normally incident onto a highly overcritical ($n_e \gg n_c$) plasma.

For a plasma with a sharp boundary, as studied above in this section, we can actually find the strength of the radiation pressure \mathcal{P}_R from the ponderomotive force (3.7) generated by the evanescent field (3.12) inside the plasma (Ch. 5.7, Macchi, 2013)

$$\mathcal{P}_R = \int_0^{\infty} n_e F_{\text{PM}}(x) dx = \frac{n_e e^2}{2m_e} \int_0^{\infty} -\frac{\partial}{\partial x} \left[\frac{1}{2} A_1^2 e^{-2x/l_s} \right] dx, \quad (3.17)$$

where we have only considered the ponderomotive force on the electrons due to the inverse-mass dependence of F_{PM} ; the additional factor 1/2 inside the brackets stem from the cycle average in the ponderomotive force. Solving the integral and expanding A_1 from (3.15) gives

$$\mathcal{P}_R = \frac{n_c e^2 A_0^2}{m_e} = \frac{2I_0}{c}, \quad (3.18)$$

where I_0 is the intensity (3.4) of the incoming laser light. Note that this expression for the radiation pressure is valid for any fully reflective target at normal incidence.

For the laser intensities considered in this thesis, the radiation pressure far overpowers the electron pressure, and the laser pulse will push the electrons deeper inside the target. The ions, which are much heavier, are left behind, which sets up a *charge separation layer* at the target surface. The charge separation creates an electrostatic field which, eventually, will start accelerating the ions as well. The electrostatic field also acts to decelerate the electrons that are pushed by the radiation pressure, and a steady state is reached where the laser acts as a piston flying into the plasma at a constant velocity u_P , and the momentum from the laser is now transferred to the ions instead of the electrons.

The ions accelerated by the *laser piston* reach twice the velocity of the piston $2u_P$, in a process very similar to electrostatic shock acceleration – discussed further in paper A. In fact, if the piston is faster than the ion-acoustic speed, $u_P > c_s$, the disturbance created by the piston can set up an electrostatic shock wave that continues to propagate and accelerate ions (Denavit, 1992; Silva *et al.*, 2004), and is also observed in paper C. The piston velocity, can be found through a simple momentum balance between the rate of momentum gained by the accelerated ions, $2u_P m_i \times n_i u_P$ (ignoring relativistic effects), and the radiation pressure \mathcal{P}_R , which yields

$$u_P = \left(\frac{\mathcal{P}_R}{2m_i n_i} \right)^{1/2} = a_0 c \left(\frac{Z_i m_e n_c}{m_i n_e} \right)^{1/2} = a_0 c \frac{\omega}{\omega_p} \left(\frac{Z_i m_e}{m_i} \right)^{1/2}, \quad (3.19)$$

where a_0 is the normalized amplitude (3.3) of the incoming laser light, and where we have used the ion charge Z_i to express $n_e = Z_i n_i$. Note that, in this picture, the ions accelerated by the piston, are the ones that are in front of and subsequently hit by the laser piston; this model does not account for the acceleration of the ions in the charge separation layer behind the piston. For a more detailed (and relativistic) derivation and discussion of such *radiation pressure acceleration* (RPA), see e.g. (Macchi, 2013).

Various forms of RPA has been used for ion-acceleration, either via the laser piston, also called *hole-boring* regime, at the target front surface (Macchi *et al.*, 2005; Robinson, 2011), or by accelerating ultra-thin targets as a whole, in the so called *light sail* regime (Esirkepov *et al.*, 2004; Macchi, 2014). As mentioned, if the laser piston is supersonic, it can create an electrostatic shock (Denavit, 1992; Silva *et al.*, 2004; Habara *et al.*, 2004), which is another way of accelerating ions. Such a formation, along with the subsequent decay, of an electrostatic shock wave in highly collisional plasmas is studied in paper A.

3.2 Laser-induced plasma heating

As discussed in the introduction to this thesis (§1.2), isochoric plasma heating can be used to create and study warm/hot dense matter (W/HDM), which has many further applications. In order to make these kinds of studies, the plasma must first be heated, which means that energy must be coupled from the laser to the plasma. In overcritical plasmas, the interaction between the laser and the plasma mostly occurs in the skin layer, which limits the efficiency with which the energy transfer occurs. Over the years, various laser-plasma heating mechanisms have been described, such as the *anomalous skin effect* (Weibel, 1967), described in great detail by Rozmus & Tikhonchuk (1990), *sheath inverse bremsstrahlung* (Catto & More, 1977), and *not-so-resonant, resonant heating* (Brunel, 1987). Both these mechanisms are based on the fact that electrons, coming from the inside of the plasma, are reflected back by the strong electromagnetic fields with slightly more energy, thus carrying energy deeper inside the plasma.

The above effects are valid in sharp plasma–vacuum boundaries. If instead the plasma has a long density ramp compared to the laser wavelength, such that the laser penetrates the plasma in the gradient region, the laser electric field – if it has a component normal to the plasma surface – can drive longitudinal electron waves deeper inside the plasma in what is called *resonant absorption* (Freidberg *et al.*, 1972). Instead of relying on the electric field, Kruer & Estabrook (1985) suggested that the $\mathbf{v} \times \mathbf{B}$ component of the Lorentz force – the amplitude of which varies longitudinally along the plasma-density gradient – would also periodically direct electrons back into the plasma, setting up the same kind of longitudinal electron waves; this mechanism is now known as *$j \times B$ heating*. Similar to the *$j \times B$ heating*, but acting on plasmas with sharp boundaries, the so called *vacuum heating*, described by Bauer & Mulser (2007) and May *et al.* (2011), relies on reasonably fast electrons flying out into the vacuum region, where they are subject to much stronger fields. These electrons are energized by the electric field before they are launched back into the plasma by the magnetic forces – as bunches of high-energy electrons.

Because of the limited penetration depth of the laser light, many laser-based isochoric heating experiments have exploited the high-energy electrons generated through *$j \times B$ heating* or vacuum heating to heat the core of the plasma (Martinolli *et al.*, 2006; Chen *et al.*, 2007; Nilson *et al.*, 2010; Pérez *et al.*, 2010; Schönlein *et al.*, 2016; Santos *et al.*, 2017). The heat-

ing of the plasma is caused by the interaction of the fast electrons with the bulk plasma via various mechanisms. The most direct mechanism is heating via collisions between the fast electrons and the background plasma (Robinson *et al.*, 2014); although, due to the decreasing collisionality with temperature and particle energy, this mechanism gets increasingly weaker for higher electron energies and as the plasma is heated. When the fast electrons rush into the plasma, there is also a return current of slower electrons to ensure quasi-neutrality; ohmic (collisional) dissipation of this return current will also contribute to heat the bulk plasma (Lovelace & Sudan, 1971; Guillory & Benford, 1972; Bell & Kingham, 2003; Robinson *et al.*, 2014). Lastly, since the fast electrons come in bunches at twice the laser frequency, they can drive plasma waves which are collisionally damped and dissipated as heat (Sherlock *et al.*, 2014).

Usually, however, the heating from fast electrons results in poor spatial uniformity (Dervieux *et al.*, 2015) and relatively slow thermalization (\sim ps). The slow thermalization of the fast electrons is simply a consequence of the decreased effects of collisions at higher energies. However, because some applications – such as verification of high-energy-density (HED) atomic physics models (Hoarty *et al.*, 2013a; Faussurier & Blancard, 2019) or HED states of matter models (Renaudin *et al.*, 2003; Nettelmann *et al.*, 2008) – may require a well-thermalized, Maxwellian plasma, the fast-electron methods may not be ideal since the timescale for thermalization can be comparable to that of hydrodynamic expansion. One of the motivations behind the work in paper **B** was to examine a way of generating well-thermalized, solid-density plasmas.

This is the key of modern science and is the beginning of the true understanding of nature. This idea. That to look at the things, to record the details, and to hope that in the information thus obtained, may lie a clue to one or another of a possible theoretical interpretation.

Richard Feynman (1964)

Chapter 4

Plasma diagnostics using attosecond pulses

In the previous chapter, we have had a short review of some of the aspects of the interaction between a high-intensity laser and a plasma, both analytically and numerically. In this chapter, we will discuss the final research topic covered in this thesis: diagnosing the laser plasma. In particular we will discuss the techniques presented in papers **D** and **E**, which both concern the use of short-duration extreme-ultraviolet (XUV) pulses to measure the density of a solid-density plasma. In paper **D**, the dispersion of such a pulse, as it passes through the plasma, is used to infer non-localized information about the electron-density profile along the path of the XUV pulse. While in paper **E**, we employ stimulated Raman scattering, which occurs between two counterpropagating laser beams, to devise a method that allows for localized, in-depth measurements of the electron density.

4.1 Diagnosing electron density with dispersion

We have seen how the plasma density – through the plasma frequency – affects the laser propagation properties through the plasma. The most prominent effect is if the plasma frequency is higher than that of the laser, then the laser pulse cannot propagate through the plasma. However, even if the plasma is undercritical, and thus transparent to the laser light, the pulse is still affected by the plasma. In particular, the dispersion relation (2.16) shows that the speed of propagation will be frequency dependent, thus causing dispersion. The dispersion of the pulse depends

on the plasma frequency $\tilde{\omega}_p$, so a natural question to ask is if we can solve the inverse problem: *Given a pulse that has been dispersed a certain amount, can we infer any information about $\tilde{\omega}_p$?* This is the topic of paper D.

In this section, we will present some details on how to measure and quantify dispersion, especially how to handle the complications that arise in the numerical treatment due to the finite step size. Then we present a short overview of the *pseudo-spectral wave solver*, that can be used to compute the wave propagation with minimal phase shifts due to numerical errors – *numerical dispersion*.

4.1.1 Quantifying dispersion using group delay

Our casual understanding of dispersion is that when different frequency components of a pulse propagate at different velocities, they fall out of phase with each other, thus spreading out the pulse, see Fig. 4.1(a). In order to then use the dispersion as a diagnostic, we must be able to quantify it in a manner that is also practical for experimental measurements. On a more formal mathematical basis, the dispersion affects the complex phase of the Fourier transform of the pulse. It is, however, impossible to measure the absolute phase of the Fourier transform, ϕ , except wrapped on the interval 0 to 2π . This phenomenon is illustrated in Fig. 4.1(b), and we can conclude that this representation of ϕ is not particularly useful for a human observer, even though the phase information contained in this representation is sufficient to exactly reconstruct the real-space waveform. There are, however, phase-unwrapping methods available, and one such technique used here is based on the so-called *relative group delay*,

$$\tau \equiv \frac{\partial \phi}{\partial \omega}, \quad (4.1)$$

which is a measure of the delay of each frequency component relative to each other. Since the group delay is based on the rate of change of ϕ , there is no need to know the absolute phase ϕ , and we obtain a much clearer picture of the effects of dispersion, as illustrated in Fig. 4.1(c).

In the concrete problem that we solve in paper D, we need to compare the group delays of the initial and transmitted attosecond pulses, which are *numerically computed*. In this discrete case, the real-space field, $E(x)$, is linked to its discrete Fourier spectrum, \hat{E}_k , through

$$E(x; t) = \sum_k \hat{E}_k(t) e^{ikx}, \quad (4.2)$$

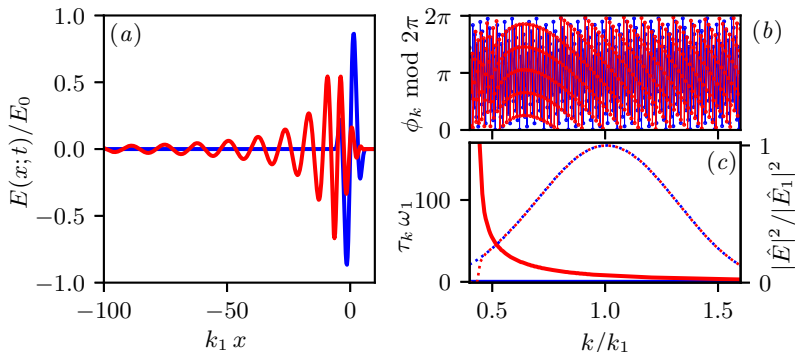


Figure 4.1: Illustration of the effects of dispersion. (a) The real space field E , normalized to the envelope peak amplitude E_0 , before (blue) and after (red) propagation through a plasma slab. (b) The phase angle ϕ_k of the different wavenumber components. Because the values are wrapped onto the interval 0 to 2π , it becomes very difficult to deduce any information about the dispersion from this representation. (c) The group delay τ_k (solid lines), normalized with the central frequency ω_1 , and spectral intensity $|\hat{E}|^2$ (dotted lines), normalized to that of the central frequency $|\hat{E}_1|^2$. Comparing the group delays before (blue) and after (red) propagation through a plasma slab.

where the sum is taken in discrete wavenumber steps $\Delta k = 2\pi/L$ with L being the length of the numerical box. The complex spectral phase $\mathcal{P}_k = \hat{E}_k/|\hat{E}_k| = \exp[i\phi_k]$ can easily be obtained from the Fourier spectrum, but, as illustrated in Fig. 4.1(b), it is non-trivial to correctly unwrap ϕ_k if taken directly from \mathcal{P}_k , and therefore difficult to calculate the rate of change in ϕ_k directly. We can instead consider

$$\psi_k = \frac{\Delta \mathcal{P}_k}{i \mathcal{P}_k} = \frac{\mathcal{P}_{k+\Delta k} - \mathcal{P}_k}{i \mathcal{P}_k} = \sin(\Delta \phi_k) - i[1 - \cos(\Delta \phi_k)], \quad (4.3)$$

which provides a way of extracting $\Delta \phi_k = \phi_{k+\Delta k} - \phi_k$. Note that ψ_k is also a periodic expression, and hence potentially suffers the same problems as \mathcal{P}_k . However, since ψ_k is 2π periodic in $\Delta \phi_k$, we can mitigate the periodicity-induced ambiguity by choosing a sufficiently large numerical resolution so that $|\Delta \phi_k| \ll \pi$. Finally, to calculate the discrete group delay, we can simply use $\tau_k = \Delta \phi_k / (c \Delta k)$.

In the above treatment, we have used the spatial, rather than temporal, Fourier transform – for reasons that will be apparent in the following subsection. Because of this choice of transform, there is one more effect on the phases that we must consider in the numerical treatment: that of the pulse position relative to the simulation box. This effect can be

understood in terms of vacuum propagation, where the pulse is simply advected, without any dispersion or changes to the shape of the pulse. If a pulse with real-space waveform $E(x; 0)$ at time $t = 0$ propagates (in the positive x direction) through vacuum for a time t , the propagated waveform is described by $E(x; t) = E(x - ct; 0)$, which in the spatial Fourier spectrum entails a shift in each phase by e^{-ikct} . In paper D we compensate for this vacuum-propagation phase shift by multiplying each wavenumber component e^{+ikct} in order to be able to compare the transmitted (propagated) and initial pulses.

4.1.2 The pseudo-spectral wave solver

The goal when creating a synthetic dispersion diagnostic is to accurately simulate the propagation of the attosecond XUV pulse through the plasma, especially the phases of each frequency component. It is therefore important to eliminate so called *numerical dispersion*, which is unphysical dispersion caused by numerical errors in the partial-differential-equation (PDE) solver – in our case the PDE of interest is the wave equation (2.14). Most PIC codes employ so called *finite-difference time-domain* (FDTD) Maxwell solvers, due to their relative simplicity and suitability for the temporally and spatially varying charge and current densities. These FDTD solvers are however susceptible to numerical dispersion. While there exists various FDTD methods that try to combat the effects of numerical dispersion (Nuter *et al.*, 2014), none of them are suitable for our purposes as the resolution requirements would be prohibitively high.

An alternative to FDTD are *spectral solvers* where we solve the time evolution of each spectral component separately. We can use the same transform (4.2) on $A(x; t) \mapsto \hat{A}_k(t)$ and $\tilde{\omega}_p^2(x; t) \mapsto \hat{\omega}_{p,k}^2(t)$, to transform the wave equation (2.14) into a set of coupled ordinary differential equations for each spectral component

$$\frac{\partial^2 \hat{A}_k}{\partial t^2} + c^2 k^2 \hat{A}_k = - \sum_{k'} \hat{\omega}_{p,k'}^2(t) \hat{A}_{k-k'}(t). \quad (4.4)$$

Since these are non-stiff ordinary differential equations, there are numerous highly accurate numerical methods available that can be used to find the solutions. Importantly, since the time evolution of each frequency component is accurately calculated, there is virtually no numerical dispersion with a spectral solver.

One issue with the spectral solver is the convolution on the right-hand side of (4.4) that couples every frequency component to each other, which can be very costly computationally. Instead of performing the costly convolution in each time step, the process can be sped up by utilizing the fast-Fourier-transform (FFT) algorithm, whereby $\hat{\omega}_{p,k}^2$ and \hat{A}_k are first individually transformed to real space and multiplied before being transformed back to wavenumber space as a single source term. When done this way, the method is called *pseudo-spectral*, since it involves operations in real space. In practice, for our purposes in paper D, $\tilde{\omega}_p^2(x; t)$ is already given in real space, so there is never a need to transform it individually.

While the pseudo-spectral solver can be very powerful at solving the wave equation, and pseudo-spectral PIC solvers have gained interest in recent years (Yu *et al.*, 2014; Lehe *et al.*, 2016; Blaclard *et al.*, 2017; Jalias *et al.*, 2017), there are also some drawbacks that make its use less frequent in PIC codes than FDTD methods. Firstly the method is significantly more costly than FDTD, even with the speedup granted by the FFT-base convolution. Next, the FDTD is much simpler to implement than any spectral solver – a reason which cannot be understated with respect to the relative frequency of use – and FDTD more readily lends itself to the PIC loop, where the real-space fields are used to push the particles, and the current and charge densities enter the FDTD scheme without complicated alterations. Finally, the spectral method requires a periodic domain, which may not suit all simulation cases. There are methods that can be used for non-periodic domains, but they risk introducing aliasing or spectral leakage, which then defeats the purpose of a spectral solver – the high accuracy.

4.2 Using stimulated Raman scattering to measure density

Another method for measuring the electron density in a plasma considered in this thesis uses stimulated Raman scattering (SRS). The SRS mechanism relies on the scattering of a pump laser pulse against Langmuir electron waves. Although, as was alluded to in §3.1.2, a single electromagnetic wave cannot effectively induce such electron waves. The driving term on the right-hand side of (3.11) is far from resonant with the electron wave. However, as that driving term has an A_{\perp}^2 dependence, if there are two waves with different frequencies present – e.g. by adding

a so called seed pulse – the square term will cause frequency mixing that can drive an electron wave. Or in other words, if the beating frequency between the two waves are close to the plasma frequency, that beating can induce electron waves.

The theory of SRS, based on a three-wave interaction, was developed by Forslund, Kindel & Lindman (1975), and detailed accounts of this theory can be found in text books on laser–plasma interactions, e.g. the one by Kruer (2003). For our purposes, we will only note that the phase-matching condition that arises from the cross term of A_{\perp}^2 in (3.11) becomes

$$\omega_0 - \omega_1 = \omega_e \approx \omega_{p,0} \quad \text{and} \quad \mathbf{k}_0 + \mathbf{k}_1 = \mathbf{k}_e, \quad (4.5)$$

where $\omega_{0,1}$ and $\mathbf{k}_{0,1}$ are the frequencies and wave vectors of the pump (0) and seed (1) laser pulses, respectively; ω_e and \mathbf{k}_e are the frequency and wave vector of the induced electron wave, respectively, and $\omega_{p,0}$ is the unperturbed plasma frequency. While the phase-matching condition (4.5) is stated for a 3D (or 2D) geometry, we will only consider the 1D case in this thesis. Therefore, further considering the condition that the phase velocities of the electron wave and the pump–seed beating should match, it is possible to conclude that k_0 and k_1 must have different signs, i.e. that the waves must be *counterpropagating*.

Since the phase-matching condition (4.5) determines the optimal frequency shift $\Delta\omega = \omega_0 - \omega_1$ with the strongest SRS coupling, and $\Delta\omega \approx \omega_{p,0} \propto n_e^{1/2}$, it becomes possible to use this relation to gauge the electron density n_e . Indeed this density-measurement scheme was proposed by Jang *et al.* (2008), and experimentally demonstrated by Vieux *et al.* (2013) using short duration optical-frequency laser pulses. In order for this method to work, the bandwidth of the seed and pump pulses must be wide. Because if two monochromatic pulses are used, it is impossible to determine the optimum frequency shift $\Delta\omega$ unless it is swept over several shots.

If broad-band seed and pump pulses are used, we find that the SRS interaction can cause the spectrum of the pump pulse to be *imprinted* onto the seed pulse, with a frequency shift $\Delta\omega \approx \omega_{p,0}$. Note here the conceptual change of perspective with respect to $\Delta\omega$. Before, $\Delta\omega$ was a part of the phase-matching condition to reach an optimal coupling between the Langmuir and electromagnetic waves. Whereas, now, with broad-band pump and seed pulses, $\Delta\omega$ represents a frequency shift observed when the spectrum of the pump pulse is imprinted onto that of the seed pulse. Now, by comparing the spectra of the pump pulse and

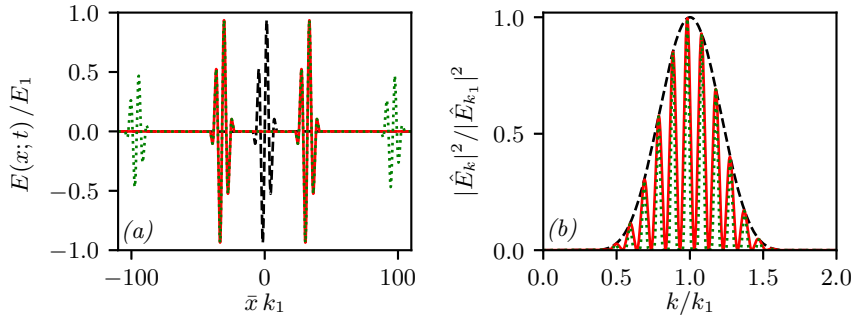


Figure 4.2: The real-space waveforms (a) and their corresponding spectra (b), illustrating of the spectral fringes that occurs in a pulse train. The single pulse (black dashed lines) has a continuous spectrum, where as the two- (solid red lines) and four-pulse (dotted green lines) trains have very distinct spectral fringes. The longer the train is the narrower the fringes become.

the amplified seed pulse, it is possible to determine $\Delta\omega \approx \omega_{p,0}$ and hence the electron density n_e in the region of the SRS interaction.

There is, however, an apparent problem with using broad-band seed and pump pulses. The accuracy of the value of $\Delta\omega$, and thereby also n_e , is determined by the widths of the spectral peaks – a wider peak results in a lower accuracy in the measured density. One possible solution to this problem, that we demonstrate in paper E, is to use a train of pulse as the pump. Each individual pulse in the train can have a very short duration, and thereby cover a broad spectral band, but when combined in a pulse train, the spectrum develops fringes, as shown in Fig. 4.2. This type of pulse trains naturally arise in high-order harmonic generation (HHG), and the XUV frequencies that are generated in this manner makes it possible to probe solid-density plasmas. Note however, that the seed should be an isolated pulse, as the continuous spectrum of the isolated pulse provides a good background onto which the pump spectrum can be imprinted.

When the spectrum of a pulse train is imprinted onto the amplified seed pulse, the accuracy of the frequency shift $\Delta\omega$ is determined by the width of the spectral fringes, which is much narrower than the bandwidth covered by the pulse train spectrum. The spectral width of the fringes is determined by the number of pulses in the pulse train – a longer train results in narrower fringes. It is, however, not necessarily desirable to have excessively long pulse trains, as that negatively impacts another desirable feature of SRS-based density diagnostic, namely that

this technique provides a *localized* measurement. Since the SRS mechanism require both the pump and seed pulses, the SRS process will only occur in the region where the pump and seed interact. It is therefore possible to control at which depth in the plasma the electron density is measured, which is not possible in most other diagnostic techniques, e.g. the dispersion diagnostics of paper **D**.

Another aspect of having excessively long pulse-train pumps is that if the seed is amplified beyond a certain amplitude, the SRS interaction can become non-linear (Chen *et al.*, 2007; Trines *et al.*, 2020). This regime is well suited for producing short-duration high-intensity pulses (Trines *et al.*, 2011*a,b*; Weber *et al.*, 2013). However, for density-measurement purposes, in the non-linear amplification regime, which includes compression of the seed pulse, the spectral details are lost (paper **E**). The amplitudes of the seed and pump pulses should therefore be chosen such that the SRS interaction stays in the linear regime. If HHG in gas targets is used to generate the seed and pump pulses, the risk of reaching the non-linear SRS regime is minimal.

*The Road goes ever on and on
Down from the door where it began.
Now far ahead the Road has gone,
And I must follow, if I can,
Pursuing it with eager feet,
Until it joins some larger way
Where many paths and errands meet.
And whither then? I cannot say.*

Bilbo's song, from *The Lord of the Rings*

Chapter 5

Summary and outlook

In the previous chapters, the focus has been on the underlying physics. In this chapter, we will instead, focus on and summarize the content of the papers and give an outlook of possible directions of future research on the topics covered.

5.1 Summary of papers

The themes of the included papers, can be divided into two categories. In the first category, we find papers **A** through **C**, which study collisional effects in laser-plasma settings – laser-plasma heating and electrostatic shocks. In the second category, with papers **D** and **E**, we present two plasma diagnostic methods based on attosecond XUV laser pulses.

In paper A, we expand upon a semi-analytical model from Cairns *et al.* (2014, 2015) and Pusztai *et al.* (2018), to include velocity diffusion due to ion–ion collisions in a single-ion-species plasma. The model is based upon a perturbative treatment in the smallness of the collisionality, $\nu\lambda_D/c_s \ll 1$, and is thus only suitable for electrostatic shocks in rather weakly collisional plasmas, such as space plasmas and perhaps low-density (gas-jet) laser-target plasmas.

The collisional velocity diffusion causes ions to enter regions of phase space where they become trapped due to the electrostatic potential oscillation in the shock downstream. The accumulation of ions in the trapped regions upsets the charge balance of the electrostatic shock, causing the downstream oscillations to grow. Since shocks can be long-lived – especially in space plasmas – and the effect of the collisional diffusion is

cumulative, and collisions can become important for the shock dynamics, even though the collisionality is very weak.

As a complement to the semi-analytical model, we also performed kinetic simulation using the Vlasov–Maxwell solver in the `Gkeyll` code framework. At the time, `Gkeyll` only had support for the Dougherty (or Lenard–Bernstein) operator, which lacks the velocity dependence that the Fokker–Planck operator. The consequence was that the collisional coupling between populations separated by a large velocity difference became artificially strong, which quickly broke down the shock structure. These results show a cautionary example on the importance of choosing a collision operator suited for the situation being modeled.

In paper B, we revisit inverse bremsstrahlung as a possible energy-absorption mechanism for an ultraintense and ultrashort laser pulse hitting a solid copper target, using the Smilei particle-in-cell simulations. The electrons are heated to temperatures of several keV. By using a circularly polarized laser pulse, the number of high-energy electrons is reduced compared to linear polarization, which in turn leads to a faster thermalization of the electrons. The creation of well-thermalized, hot and dense plasmas is attractive for warm-dense-matter studies. From comparisons to simulations with collisions disabled, we find that inverse bremsstrahlung is responsible for most of the energy absorption.

A crucial element as to why collisions become important is the fact that the copper plasma was ionized to a relatively high level of $Z^* = 27$. To test this assumed ionization level, an additional simulation was performed, where the ionization of the individual macro-particle ions was self-consistently simulated, using both collisional impact ionization and field ionization. In this simulation, the laser field quickly ionizes the skin-layer ions to $Z^* \gtrsim 20$, and collisional impact ionization then gradually brings up the ionization level to $Z^* \simeq 27$ in the whole plasma, which justifies the assumed $Z^* = 27$ in the other simulations. Importantly, since the ionization quickly reaches relatively high levels in the skin region, where the absorption happens, the absorbed energy becomes comparable to that of the fixed-ionization simulation.

Collisional absorption was also studied with respect to variations in the laser parameters through a wide scan in laser intensity and pulse duration. A power-law scaling is found, and the absorption efficiency is found to scale as (pulse amplitude)^{-0.52} × (pulse duration)^{0.13}. Therefore, at fixed laser pulse energy, increasing the pulse duration rather than the intensity leads to a higher electron temperature. Furthermore, the

collisional absorption was also tested against transverse plasma instabilities by performing a two-dimensional simulation, which showed very similar behavior as its one-dimensional counterpart.

In paper C, we investigate the impact of collisions on the ion dynamics in solid density caesium hydride and copper targets irradiated by high-intensity and ultrashort-duration circularly polarized laser pulses. As in paper B, the study was performed using particle-in-cell simulations employing the Smilei PIC code. Since both target materials have a relatively high Z^* , collisions significantly enhance the electron heating, as discussed in paper B, which creates more favorable conditions for shock formation. In comparison, simulations made without collisions show signs of a shock as well, although with much lower speed and amplitude than the corresponding collisional simulations.

In the caesium hydride (CsH) target, the protons are favored in the shock reflection mechanism due to their high charge-to-mass ratio. With the copper targets, we find that the lack of embedded protons results in the launch of a shock-like perturbation which initially is not capable of reflecting ions. With both target materials, after the first few ions are reflected, collisional heating between the reflected and incoming upstream ion populations play an important role in steadily increasing the fraction of reflected ions. This self-amplification leads to the shock ion reflection bootstrapping itself. At later times, the energy lost by the shock to the increasing fraction of reflected ions results in a demise of the shock, which transforms into a hydrodynamic blast wave.

In paper D, we present a new technique for diagnosing the electron density of a solid-density plasma, based on the dispersion of an attosecond XUV pulse. Since the propagation of an electromagnetic wave in an undercritical plasma is affected by the plasma frequency ω_p , which in turn depends on the electron density n_e , it is possible to infer information about the plasma density based on the relative phases of the frequency components in the dispersed laser pulse. By using attosecond XUV pulses, we are able to probe solid-density plasmas, and the few-cycle duration of the pulse results in a broad spectrum over which dispersion can act, giving more available dispersion data that can be used to infer more information about the plasmas. The technique was inspired by the work by López-Martens *et al.* (2005), wherein the naturally arising chirp of attosecond pulses generated through HHG was counteracted through dispersion in an aluminium foil. However, instead

of using a chosen dispersive medium to alter the pulse into a desired shape, we use the altered shape of the pulse to determine properties of the dispersive medium.

In our paper, we present the dispersion diagnostic as a synthetic diagnostic that can be used on the output of a PIC simulation. However, the experimental techniques RABBIT (Paul *et al.*, 2001) and attosecond streak-camera (Itatani *et al.*, 2002) make it possible to apply our diagnostic technique in experiments as well. If that is done, the dispersion obtain in the experiment can then be compared to the synthetic diagnostic from the PIC simulation, in order to validate the PIC code or the experimental setup. For instance, this diagnostic can be used to gauge the height of a density peak in a shock wave, which may be significantly affected by the strength of collisions, as we saw with the issue of different PIC collision models raised in paper C.

Since the synthetic dispersion diagnostic relies on the dispersion of the probe pulse, we must be careful in the way that the propagation of the probe is computed. Many numerical schemes for solving partial differential equations suffer from *numerical dispersion*; notably, the finite difference methods used in most PIC codes suffer from numerical dispersion. It is therefore not possible to just use the normal PIC approach when we want to compute the probe-pulse dispersion here, unless the resolution is increased far beyond what is normally used to resolve a certain pulse. We, instead, use a *pseudo-spectral solver*, which is essentially free of numerical dispersion, to calculate the propagation of the probe pulse, based on the plasma profile obtained from a separate PIC simulation. In other words, the physics is simulated with PIC, and then the dispersion diagnostics is computed externally, with the pseudo-spectral solver. Not only does this significantly reduce the numerical cost, it also allows us to study arbitrarily many different probe pulses for the same physics simulation – which is often the most computationally demanding step.

In paper E, we study how XUV pulse trains can be used in stimulated Raman scattering (SRS), and in doing so we continue on the trail of using XUV pulses to diagnose solid-density plasmas. In SRS, the interaction between a seed pulse and a counterpropagating pump pulse in a plasma, which induces a plasma electron wave, results in an energy transfer from the pump to the seed pulse. Normally, the SRS interaction is well understood for single seed and pump pulses, but it is not obvious how the interaction should work if the pump pulse is replaced by a train of short

pulses, e.g. as generated in different HHG schemes. We have therefore studied the amplification of a single attosecond XUV seed pulse with an XUV pulse-train pump through SRS.

Initially, we investigated the use of pulse-train SRS to amplify isolated attosecond pulses, because of the limited availability of suitable pump pulses in the XUV frequency range. Our simulations show that it is possible to use pulse-train pumps to amplify short-duration seed pulses, despite the broad spectral width of both the seed and pump. In order to reach an efficient non-linear amplification regime, the amplitude of the pulse-train pump should be $a_0 \gtrsim 0.2$. However, the amplitude of the amplified seed pulse saturates when it reaches that of the pump, which is not the case when comparable flat-top pump pulses were used. The amplitude saturation is mostly due to spontaneous Raman scattering interfering with the stimulated scattering and also depleting the pump of energy prematurely. Spontaneous Raman scattering is found to affect the pulse-train more than the flat-top pump due to the broader spectral range of the pulse train.

If the linear SRS regime, the amplification is not as efficient, but the result can instead be used as an electron-density diagnostic. Since the seed and pump pulses interact via an induced electron wave, the SRS interaction is strongest if the seed and pump frequencies have an offset equal to the plasma frequency. It is therefore possible to imprint the spectrum of the pump pulse(s) onto the amplified-seed pulse with a frequency shift $\Delta\omega = \omega_p$. Thus, by comparing the spectra of the pump and the amplified-seed pulses, it becomes possible to deduce the local plasma density. Like in paper D, the use of XUV frequencies allows for the probing of solid-density plasmas. Furthermore, since the spectrum of a pulse train is highly peaked, the spectral imprint on the amplified pulse can be very clear and give a precise value of $\Delta\omega$, which allow for a high accuracy in the density measurement. However, unlike other schemes, such as transmission spectroscopy, wavefront sensing, and the dispersion diagnostic in paper D, which give a line-of-sight integrated measurement, this SRS diagnostics scheme provides a longitudinally resolved measurement of the electron density at the site of the SRS interaction.

5.2 Outlook

Beginning with the use of inverse bremsstrahlung for isochoric heating in paper B, there are a number of parameters and settings which were left out from the study. For instance, the laser-plasma interaction can change quite drastically depending on the plasma-density profile at the

target front surface. It would therefore be valuable to study the sensitivity of inverse bremsstrahlung heating with respect to the preplasma size – both in terms of energy-absorption efficiency and how it affects the thermalization of the electrons. Preliminary simulations indicate that the absorption efficiency is negatively affected by including a preplasma for circularly polarized laser pulses.

In addressing ionization, we found that ionization injection of electrons into the vacuum region with strong laser fields impacts the thermalization of the plasma. While this does not detract from the statement that circular polarization (CP) produces a more thermalized plasma than linear polarization (LP) – since the same ionization injection would happen with LP as well – this generation of high-energy electrons might be considered for other applications where such electrons are desirable. In general, the effect and dynamics of field ionization as a fast electron source has received little research attention and could be studied more thoroughly, not only in the context of laser absorption.

From a broader perspective, the collisional heating could be studied in combination with more exotic targets. For example, only using a layered target, with a high- Z^* material in the front to provide electron heating, combined with another material optimized for other purposes, such as to produce electrostatic shocks. Since electrostatic shocks require a high electron temperature, but also more preferably accelerate protons, the heating from a thin (tens of nanometers) copper target could perhaps be combined with a plastic target in order to generate a stronger (proton-accelerating) shock than either of the target materials on their own.

Continuing with the semi-analytical studies of electrostatic shocks in paper A. While this study of velocity diffusion leads to some more general conclusions about the effects of collisions on the shocks, our description is restricted to one type of collisions, and only in a limited region of phase space. There is still room for further analytical developments, such as multi-species collisions or considering the effects of collisional friction between the incoming and reflected ions, especially with respect to the observations of self-amplifying ion reflection made in paper C. Both cases would require improving the model to capture the effect of a varying collision frequency. The latter case would furthermore require a refinement with a velocity dependent collision frequency; the effects of which could also be studied with respect to the diffusion and trapping in the downstream region.

Next, we consider the simulation study in paper C, of the collisional effects on the ion and shock dynamics. Like with paper B, further studies on the sensitivity of the problem to its dimensionality would be valuable. Electrostatic shocks are indeed expected to be highly sensitive to transverse non-uniformities, in particular due to the development of the strongly oblique ion–ion instability (Dieckmann *et al.*, 2013). Thanks to the similarities, the simulations required can likely be shared with those required to study higher-dimensional effects to the inverse bremsstrahlung heating.

It would be interesting to study the effects of collisions in a slightly weaker collisionality regime, such as lower-charge materials. In fact, from a scan in Z^* (artificially chosen at four fixed values) performed for paper B, we can find qualitatively different shock behaviors likely due to variations in the plasma collisionality with Z^* . A closer examination throughout the range of collisionality could shed light on the plasma conditions for which collisions can be neglected in shock studies. In addition, one could investigate the impact of the laser parameters and the plasma density profile.

Regarding the dispersion-based diagnostic presented in paper D, there are a number of interesting possibilities for further investigation; the most interesting of which would be to experimentally test this method in a laser-plasma experiment. That could be done in a setup like the example of a thin-foil target presented in the paper, or perhaps measuring the density of the expanding plasma pulse in front of or behind a laser target. Note that, while we presented the dispersion diagnostic using a single attosecond probe pulse, it is just as possible to use an attosecond pulse-train probe, the latter being much easier to create experimentally. With that said, using this diagnostics method on solid target might prove experimentally challenging due to the large number of repetitions required to accurately measure the relative group delays of the probe.

The alternative to solid target is gas-jet targets, which allow a much higher repetition rate, but the low density means that the dispersion of the XUV probe is low and the diagnostic becomes ineffective. We have performed preliminary studies on the use of the dispersion diagnostic on LWFA plasmas, but with poor results when using a single attosecond probe pulse. However, if two or more probe pulses are used in a pulse train, differential dispersion due to different pulses experiencing different electron densities can lead to shifts in the pulse-train spectrum, which

can easily be detected experimentally. This possible avenue of research is especially interesting since (i) it allows for rapid repetition rates; (ii) it will be easier to perform experimentally, both because the pulse-train probe is simpler to generate than a single attosecond pulse and that the spectral shifts are easier to detect than the group delays; and (iii) it has a concrete application in diagnosing LWFA plasmas.

Finally, the studies of pulse-train SRS in paper E are far from exhaustive. It would be interesting to further investigate the diagnostic power of the spectral imprinting that we saw, e.g. in non-homogeneous plasmas or perhaps using a pulse-train seed as well as pump. Besides further simulation studies, it would also be interesting –and likely not too difficult – to investigate if the well understood theory for monochromatic SRS can be generalized to the broad-spectrum pulse that we consider here. Better theoretical understanding of the nature of broad-spectrum SRS, could help guide further development of this diagnostic technique.

References

- ALBERT, F. & THOMAS, A. G. R. 2016 “Applications of laser wakefield accelerator-based light sources”. *Plasma Physics and Controlled Fusion* **58** (10), 103 001, DOI: 10.1088/0741-3335/58/10/103001
- ALLEN, C. H., OLIVER, M., DIVOL, L., LANDEN, O. L., PING, Y., SCHÖLMECH, M., WALLACE, R., EARLEY, R., THEOBALD, W., WHITE, T. G. & DÖPPNER, T. 2022 “Toward an integrated platform for characterizing laser-driven, isochorically heated plasmas with 1 μm spatial resolution”. *Appl. Opt.* **61** (8), 1987–1993, DOI: 10.1364/AO.446182
- ALLMANN-RAHN, F., TROST, T. & GRAUER, R. 2018 “Temperature gradient driven heat flux closure in fluid simulations of collisionless reconnection”. *Journal of Plasma Physics* **84** (3), 905840 307, DOI: 10.1017/S002237781800048X
- AMIRANOFF, F., BATON, S., BERNARD, D. *et al.* 1998 “Observation of laser wakefield acceleration of electrons”. *Phys. Rev. Lett.* **81**, 995–998, DOI: 10.1103/PhysRevLett.81.995
- ANTICI, P., BOELLA, E., CHEN, S. N. *et al.* 2017 “Acceleration of collimated 45 MeV protons by collisionless shocks driven in low-density, large-scale gradient plasmas by a 10^{20} W/cm², 1 μm laser”. *Scientific Reports* **7** (1), 1–9, DOI: 10.1038/s41598-017-15449-8
- AREFIEV, A., STARK, D. J., TONCIAN, T. & MURAKAMI, M. 2020 “Birefringence in thermally anisotropic relativistic plasmas and its impact on laser–plasma interactions”. *Physics of Plasmas* **27** (6), 063 106, DOI: 10.1063/5.0008018
- BAILEY, J. E., ROCHAU, G. A., IGLESIAS, C. A. *et al.* 2007 “Iron-plasma transmission measurements at temperatures above 150 eV”. *Phys. Rev. Lett.* **99**, 265 002, DOI: 10.1103/PhysRevLett.99.265002
- BARGSTEN, C., HOLLINGER, R., CAPELUTO, M. G. *et al.* 2017 “Energy penetration into arrays of aligned nanowires irradiated with relativistic intensities: Scaling to terabar pressures”. *Sci. Adv.* **3**, e1601 558, DOI: 10.1126/sciadv.1601558
- BAUER, D. & MULSER, P. 2007 “Vacuum heating versus skin layer absorption of intense femtosecond laser pulses”. *Physics of Plasmas* **14** (2), 023 301, DOI: 10.1063/1.2435326
- BELL, A. R. & KINGHAM, R. J. 2003 “Resistive collimation of electron beams in laser-produced plasmas”. *Phys. Rev. Lett.* **91**, 035 003, DOI: 10.1103/PhysRevLett.91.035003
- BHATNAGAR, P. L., GROSS, E. P. & KROOK, M. 1954 “A model for collision processes in gases. I. small amplitude processes in charged and neutral one-

- component systems”. *Phys. Rev.* **94**, 511–525, DOI: 10.1103/PhysRev.94.511
- BLACLARD, G., VINCENTI, H., LEHE, R. & VAY, J. L. 2017 “Pseudospectral Maxwell solvers for an accurate modeling of Doppler harmonic generation on plasma mirrors with particle-in-cell codes”. *Phys. Rev. E* **96**, 033305, DOI: 10.1103/PhysRevE.96.033305
- BOGOLJUBOV, N. N. 1960 Problems of a dynamical theory in statistical physics. Geophysics Research Directorate, AF Cambridge Research Laboratories, Air Force Research Division, United States
- BOLTZMANN, L. 1868 “Studien über das Gleichgewicht der lebendigen Kraft zwischen bewegten materiellen Punkten”. *Wissenschaftliche Abhandlungen* **1**, 49–96. In German, English title roughly “Studies on the balance of living force between moving material points”.
- BOLTZMANN, L. 1872 “Weitere Studien über das Wärmegleichgewicht unter Gasmolekülen (Eng. Further studies on the thermal equilibrium of gas molecules)”. *Sitzungsberichte der Kaiserlichen Akademie der Wissenschaften* **66**, 275–370. An English translation can be found at DOI: 10.1142/9781848161337_0015.
- BORGHESI, M., CAMPBELL, D. H., SCHIAVI, A. *et al.* 2002 “Electric field detection in laser-plasma interaction experiments via the proton imaging technique”. *Physics of Plasmas* **9** (5), 2214–2220, DOI: 10.1063/1.1459457
- BORIS, J. P. 1970 “Relativistic plasma simulation-optimization of a hybrid code”. In “Proceedings, Fourth Conference on Numerical Simulation of Plasmas”, (3–8)
- BORN, M. & GREEN, H. 1946 “A general kinetic theory of liquids I. The molecular distribution functions”. *Proceedings of the Royal Society of London. Series A.* **188** (1012), 10–18, DOI: 10.1098/rspa.1946.0093
- BOTT, A. F. A., TZEFERACOS, P., CHEN, L. *et al.* 2021 “Time-resolved turbulent dynamo in a laser plasma”. *Proceedings of the National Academy of Sciences* **118** (11), e2015729118, DOI: 10.1073/pnas.2015729118
- BROOKNER, E. 1985 “Phased-array radars”. *Scientific American* **252** (2), 94–103, DOI: 10.2307/24967572
- BROWN, C. R. D., HOARTY, D. J., JAMES, S. F. *et al.* 2011 “Measurements of electron transport in foils irradiated with a picosecond time scale laser pulse”. *Phys. Rev. Lett.* **106**, 185003, DOI: 10.1103/PhysRevLett.106.185003
- AN DER BRÜGGE, D., KUMAR, N., PUKHOV, A. & RÖDEL, C. 2012 “Influence of surface waves on plasma high-order harmonic generation”. *Phys. Rev. Lett.* **108**, 125002, DOI: 10.1103/PhysRevLett.108.125002
- BRUNEL, F. 1987 “Not-so-resonant, resonant absorption”. *Phys. Rev. Lett.* **59**, 52–55, DOI: 10.1103/PhysRevLett.59.52
- BULANOV, S. V., ESIRKEPOV, T. ZH., KHOROSHKOV, V. S., KUZNETSOV, A. V. & PEGORARO, F. 2002 “Oncological hadrontherapy with laser ion accelerators”. *Physics Letters A* **299** (2), 240 – 247, DOI: 10.1016/S0375-9601(02)00521-2
- CAGAS, P., HAKIM, A., SCALES, W. & SRINIVASAN, B. 2017 “Nonlinear saturation of the weibel instability”. *Physics of Plasmas* **24** (11), 112116, DOI: 10.1063/1.4994682
- CAIRNS, R. A., BINGHAM, R., NORREYS, P. & TRINES, R. G. M. 2014 “Laminar shocks in high power laser plasma interactions”. *Physics of Plasmas* **21** (2), 022112, DOI: 10.1063/1.4864328

- CAIRNS, R. A., BINGHAM, R., TRINES, R. G. M. & NORREYS, P. 2015 “Weak collisionless shocks in laser-plasmas”. *Plasma Physics and Controlled Fusion* **57** (4), 044008, DOI: 10.1088/0741-3335/57/4/044008
- CALEGARI, F., SANSONE, G., STAGIRA, S., VOZZI, C. & NISOLI, M. 2016 “Advances in attosecond science”. *Journal of Physics B: Atomic, Molecular and Optical Physics* **49** (6), 062001, DOI: 10.1088/0953-4075/49/6/062001
- CASEY, D. T., SAYRE, D. B., BRUNE, C. R. *et al.* 2017 “Thermonuclear reactions probed at stellar-core conditions with laser-based inertial-confinement fusion”. *Nature Physics* **13** (12), 1227–1231, DOI: 10.1038/nphys4220
- CATTO, P. J. & MORE, R. M. 1977 “Sheath inverse bremsstrahlung in laser produced plasmas”. *The Physics of Fluids* **20** (4), 704–705, DOI: 10.1063/1.861930
- CHAN, Y. W. 1971 “Ultra-intense laser radiation as a possible energy booster for relativistic charged particle”. *Physics Letters A* **35** (4), 305–306, DOI: 10.1016/0375-9601(71)90397-5
- CHEN, S. N., GREGORI, G., PATEL, P. K. *et al.* 2007 “Creation of hot dense matter in short-pulse laser-plasma interaction with tamped titanium foils”. *Physics of Plasmas* **14** (10), 102701, DOI: 10.1063/1.2777118
- CHENG, W., AVITZOUR, Y., PING, Y., SUCKEWER, S., FISCH, N. J., HUR, M. S. & WURTELE, J. S. 2005 “Reaching the nonlinear regime of Raman amplification of ultrashort laser pulses”. *Phys. Rev. Lett.* **94**, 045003, DOI: 10.1103/PhysRevLett.94.045003
- CHRISTOV, I. P., MURNANE, M. M. & KAPTEYN, H. C. 1997 “High-harmonic generation of attosecond pulses in the “single-cycle” regime”. *Phys. Rev. Lett.* **78**, 1251–1254, DOI: 10.1103/PhysRevLett.78.1251
- COWAN, T. E., FUCHS, J., RUHL, H. *et al.* 2004 “Ultralow emittance, multi-MeV proton beams from a laser virtual-cathode plasma accelerator”. *Phys. Rev. Lett.* **92**, 204801, DOI: 10.1103/PhysRevLett.92.204801
- DAIDO, H., NISHIUCHI, M. & PIROZHKOV, A. S. 2012 “Review of laser-driven ion sources and their applications”. *Reports on progress in physics* **75** (5), 056401, DOI: 10.1088/0034-4885/75/5/056401
- DENAVIT, J. 1992 “Absorption of high-intensity subpicosecond lasers on solid density targets”. *Phys. Rev. Lett.* **69**, 3052–3055, DOI: 10.1103/PhysRevLett.69.3052
- DEROULLAT, J., BECK, A., PÉREZ, F. *et al.* 2018 “Smilei: A collaborative, open-source, multi-purpose particle-in-cell code for plasma simulation”. *Comput. Phys. Commun.* **222**, 351, DOI: 10.1016/j.cpc.2017.09.024
- DERVIEUX, V., LOUPIAS, B., BATON, S. *et al.* 2015 “Characterization of near-LTE, high-temperature and high-density aluminum plasmas produced by ultra-high intensity lasers”. *High Energy Density Physics* **16**, 12 – 17, DOI: 10.1016/j.hedp.2015.04.009
- DESCAMPS, D., LYNGÅ, C., NORIN, J., L’HULLIER, A., WAHLSTRÖM, C.-G., HERGOTT, J.-F., MERDJI, H., SALIÈRES, P., BELLINI, M. & HÄNSCH, T. 2000 “Extreme ultraviolet interferometry measurements with high-order harmonics”. *Optics letters* **25** (2), 135–137, DOI: 10.1364/OL.25.000135
- DI PIAZZA, A., MÜLLER, C., HATSAGORTSYAN, K. Z. & KEITEL, C. H. 2012 “Extremely high-intensity laser interactions with fundamental quantum systems”. *Rev. Mod. Phys.* **84**, 1177–1228, DOI: 10.1103/RevModPhys.84.1177

- DIECKMANN, M. E., SARRI, G., DORIA, D., POHL, M. & BORGHESI, M. 2013 “Modification of the formation of high-Mach number electrostatic shock-like structures by the ion acoustic instability”. *Physics of Plasmas* **20** (10), 102112, DOI: 10.1063/1.4825339
- DOBOSZ, S., DOUMY, G., STABILE, H., D’OLIVEIRA, P., MONOT, P., RÉAU, F., HÜLLER, S. & MARTIN, P. 2005 “Probing hot and dense laser-induced plasmas with ultrafast XUV pulses”. *Phys. Rev. Lett.* **95**, 025001, DOI: 10.1103/PhysRevLett.95.025001
- DOUGHERTY, J. P. 1964 “Model Fokker–Planck equation for a plasma and its solution”. *The Physics of Fluids* **7** (11), 1788–1799, DOI: 10.1063/1.2746779
- DOUGHERTY, J. P. & WATSON, S. R. 1967 “Model Fokker–Planck equations: Part 2. The equation for a multicomponent plasma”. *Journal of Plasma Physics* **1** (3), 317–326, DOI: 10.1017/S0022377800003329
- DRAKE, R. P. 2018 “A journey through high-energy-density physics”. *Nuclear Fusion* **59** (3), 035001, DOI: 10.1088/1741-4326/aaf0e3
- DYER, G. M., BERNSTEIN, A. C., CHO, B. I., OSTERHOLZ, J., GRIGSBY, W., DALTON, A., SHEPHERD, R., PING, Y., CHEN, H., WIDMANN, K. & DITMIRE, T. 2008 “Equation-of-state measurement of dense plasmas heated with fast protons”. *Phys. Rev. Lett.* **101**, 015002, DOI: 10.1103/PhysRevLett.101.015002
- ESIRKEPOV, T., BORGHESI, M., BULANOV, S. V., MOUROU, G. & TAJIMA, T. 2004 “Highly efficient relativistic-ion generation in the laser-piston regime”. *Phys. Rev. Lett.* **92**, 175003, DOI: 10.1103/PhysRevLett.92.175003
- EVANS, R., BADGER, A. D., FALLIÈS, F., MAHDIEH, M., HALL, T. A., AUDEBERT, P., GEINDRE, J.-P., GAUTHIER, J.-C., MYSYROWICZ, A., GRILLON, G. & ANTONETTI, A. 1996 “Time- and space-resolved optical probing of femtosecond-laser-driven shock waves in aluminum”. *Phys. Rev. Lett.* **77**, 3359–3362, DOI: 10.1103/PhysRevLett.77.3359
- EVANS, R. G., CLARK, E. L., EAGLETON, R. T. *et al.* 2005 “Rapid heating of solid density material by a petawatt laser”. *Applied Physics Letters* **86** (19), 191505, DOI: 10.1063/1.1920422
- FAURE, J., GLINEC, Y., PUKHOV, A., KISELEV, S., GORDIENKO, S., LEFEBVRE, E., ROUSSEAU, J.-P., BURG, F. & MALK, V. 2004 “A laser–plasma accelerator producing monoenergetic electron beams”. *Nature* **431** (7008), 541–544, DOI: 10.1038/nature02963
- FAUSSURIER, G. & BLANCARD, C. 2019 “Pressure in warm and hot dense matter using the average-atom model”. *Phys. Rev. E* **99**, 053201, DOI: 10.1103/PhysRevE.99.053201
- FERNÁNDEZ, J. C., CORT GAUTIER, D., HUANG, C. *et al.* 2017 “Laser-plasmas in the relativistic-transparency regime: Science and applications”. *Physics of Plasmas* **24** (5), 056702, DOI: 10.1063/1.4983991
- FERRAY, M., L’HUILIER, A., LI, X. F., LOMP, L. A., MAINFRAY, G. & MANUS, C. 1988 “Multiple-harmonic conversion of 1064 nm radiation in rare gases”. *Journal of Physics B: Atomic, Molecular and Optical Physics* **21** (3), L31–L35, DOI: 10.1088/0953-4075/21/3/001
- FERRI, J., CORDE, S., DÖPP, A., LIFSCHITZ, A., DOCHE, A., THAURY, C., TA PHUOC, K., MAHIEU, B., ANDRIYASH, I. A., MALK, V. & DAVOINE, X. 2018 “High-brilliance betatron γ -ray source powered by laser-accelerated elec-

- trons". *Phys. Rev. Lett.* **120**, 254802, DOI: 10.1103/PhysRevLett.120.254802
- FEYNMAN, R. 1964 "The character of physical law". A lecture series given at Cornell University.
- FIUZA, F., STOCKEM, A., BOELLA, E., FONSECA, R. A., SILVA, L. O., HABERBERGER, D., TOCHITSKY, S., GONG, C., MORI, W. B. & JOSHI, C. 2012 "Laser-driven shock acceleration of monoenergetic ion beams". *Phys. Rev. Lett.* **109**, 215001, DOI: 10.1103/PhysRevLett.109.215001
- FIUZA, F., SWADLING, G. F., GRASSI, A. *et al.* 2020 "Electron acceleration in laboratory-produced turbulent collisionless shocks". *Nature Physics* (1–5), DOI: 10.1038/s41567-020-0919-4
- FORSLUND, D. W. & SHONK, C. R. 1970 "Formation and structure of electrostatic collisionless shocks". *Phys. Rev. Lett.* **25**, 1699, DOI: 10.1103/PhysRevLett.25.1699
- FORSLUND, D. W., KINDEL, J. M. & LINDMAN, E. L. 1975 "Theory of stimulated scattering processes in laser-irradiated plasmas". *The Physics of Fluids* **18** (8), 1002–1016, DOI: 10.1063/1.861248
- FREIDBERG, J. P., MITCHELL, R. W., MORSE, R. L. & RUDSINSKI, L. I. 1972 "Resonant absorption of laser light by plasma targets". *Phys. Rev. Lett.* **28**, 795–799, DOI: 10.1103/PhysRevLett.28.795
- FUJIOKA, S., TAKABE, H., YAMAMOTO, N. *et al.* 2009 "X-ray astronomy in the laboratory with a miniature compact object produced by laser-driven implosion". *Nat. Phys.* **8**, 821, DOI: 10.1038/NPHYS1402
- GAUMNITZ, T., JAIN, A., PERTOT, Y., HUPPERT, M., JORDAN, I., ARDANA-LAMAS, F. & WÖRNER, H. J. 2017 "Streaking of 43-attosecond soft-X-ray pulses generated by a passively CEP-stable mid-infrared driver". *Opt. Express* **25** (22), 27506–27518, DOI: 10.1364/OE.25.027506
- GIBBON, P. 1996 "Harmonic generation by femtosecond laser-solid interaction: A coherent "water-window" light source?" *Phys. Rev. Lett.* **76**, 50–53, DOI: 10.1103/PhysRevLett.76.50
- GIBBON, P. 2005 *Short Pulse Laser Interactions with Matter*. London: Imperial College Press, DOI: 10.1142/p116
- GITOMER, S. J., JONES, R. D., BEGAY, F., EHLER, A. W., KEPHART, J. F. & KRISTAL, R. 1986 "Fast ions and hot electrons in the laser-plasma interaction". *The Physics of Fluids* **29** (8), 2679–2688, DOI: 10.1063/1.865510
- GIULIETTI, A. & TAJIMA, T. 2016 "Lasers Offer New Tools to Radiobiology and Radiotherapy". In "Laser-Driven Particle Acceleration Towards Radiobiology and Medicine", (ed. A. Giulietti), Biological and Medical Physics, Biomedical Engineering, Springer International Publishing, ISBN 978-3-319-31563-8, DOI: 10.1007/978-3-319-31563-8_1
- GONOSKOV, A. A., KORZHIMANOV, A. V., KIM, A. V., MARKLUND, M. & SERGEEV, A. M. 2011 "Ultrarelativistic nanoplasmonics as a route towards extreme-intensity attosecond pulses". *Phys. Rev. E* **84**, 046403, DOI: 10.1103/PhysRevE.84.046403
- GORDIENKO, S., PUKHOV, A., SHOROKHOV, O. & BAEVA, T. 2004 "Relativistic Doppler effect: Universal spectra and zeptosecond pulses". *Phys. Rev. Lett.* **93**, 115002, DOI: 10.1103/PhysRevLett.93.115002

- GREEN, H. S. 1952 The molecular theory of fluids. North-Holland
- GREGORI, G., HANSEN, S. B., CLARKE, R. *et al.* 2005 “Experimental characterization of a strongly coupled solid density plasma generated in a short-pulse laser target interaction”. *Contributions to Plasma Physics* **45** (3-4), 284–292, DOI: 10.1002/ctpp.200510032
- GREMILLET, L. & LEMOINE, M. 2020 “Miniature supernova shock waves”. *Nature Physics* **16** (9), 901–903, DOI: 10.1038/s41567-020-0951-4
- GUILLORY, J. & BENFORD, G. 1972 “Estimates of dense plasma heating by stable intense electron beams”. *Plasma Physics* **14** (12), 1131–1138, DOI: 10.1088/0032-1028/14/12/007
- GUILLOT, T. 1999 “A comparison of the interiors of jupiter and saturn”. *Planetary and Space Science* **47** (10), 1183–1200, ISSN 0032-0633, DOI: 10.1016/S0032-0633(99)00043-4
- HABARA, H., LANCASTER, K. L., KARSCH, S. *et al.* 2004 “Ion acceleration from the shock front induced by hole boring in ultraintense laser-plasma interactions”. *Phys. Rev. E* **70**, 046 414, DOI: 10.1103/PhysRevE.70.046414
- HABERBERGER, D., TOCHITSKY, S., FIUZA, F., GONG, C., FONSECA, R. A., SILVA, L. O., MORI, W. B. & JOSHI, C. 2012 “Collisionless shocks in laser-produced plasma generate monoenergetic high-energy proton beams”. *Nat. Phys.* **8**, 95–99, DOI: 10.1038/nphys2130
- HAKIM, A., LOVERICH, J. & SHUMLAK, U. 2006 “A high resolution wave propagation scheme for ideal two-fluid plasma equations”. *Journal of Computational Physics* **219** (1), 418–442, DOI: 10.1016/j.jcp.2006.03.036
- HAKIM, A., FRANCISQUEZ, M., JUNO, J. & HAMMETT, G. W. 2020 “Conservative discontinuous Galerkin schemes for nonlinear Dougherty–Fokker–Planck collision operators”. *Journal of Plasma Physics* **86** (4), 905860 403, DOI: 10.1017/S0022377820000586
- HAMMOND, T. J., BROWN, G. G., KIM, K. T., VILLENEUVE, D. M. & CORKUM, P. B. 2016 “Attosecond pulses measured from the attosecond lighthouse”. *Nature Photonics* **10** (3), 171–175, DOI: 10.1038/nphoton.2015.271
- HARGROVE, L. E., FORK, R. L. & POLLACK, M. A. 1964 “Locking of He–Ne laser modes induced by synchronous intracavity modulation”. *Applied Physics Letters* **5** (1), 4–5, DOI: 10.1063/1.1754025
- HELANDER, P. & SIGMAR, D. J. 2002 Collisional Transport in Magnetized Plasmas, vol. 4 of *Cambridge Monographs on Plasma Physics*. Cambridge University Press, ISBN 978-0-521-02098-5
- HENIG, A., KIEFER, D., MARKEY, K. *et al.* 2009 “Enhanced laser-driven ion acceleration in the relativistic transparency regime”. *Phys. Rev. Lett.* **103**, 045 002, DOI: 10.1103/PhysRevLett.103.045002
- HENTSCHEL, M., KIENBERGER, R., SPIELMANN, C., REIDER, G. A., MILOSEVIC, N., BRABEC, T., CORKUM, P., HEINZMANN, U., DRESCHER, M. & KRAUSZ, F. 2001 “Attosecond metrology”. *Nature* **414** (6863), 509–513, DOI: 10.1038/35107000
- HERGOTT, J.-F., SALIÈRES, P., MERDJI, H. *et al.* 2001 “XUV interferometry using high-order harmonics: Application to plasma diagnostics”. *Laser and Particle Beams* **19** (1), 35–40, DOI: 10.1017/S0263034601191056

- HERGOTT, J.-F., AUGUSTE, T., SALIÈRES, P., LE DÉROFF, L., MONOT, P., D'OLIVEIRA, P., CAMPO, D., MERDJI, H. & CARRÉ, B. 2003 “Application of frequency-domain interferometry in the extreme-ultraviolet range by use of high-order harmonics”. *JOSA B* **20** (1), 171–181, DOI: 10.1364/JOSAB.20.000171
- HIGGINSON, A., GRAY, R. J., KING, M. *et al.* 2018 “Near-100 MeV protons via a laser-driven transparency-enhanced hybrid acceleration scheme”. *Nat. Commun.* **9** (1), 724, DOI: 10.1038/s41467-018-03063-9
- HOARTY, D. J., ALLAN, P., JAMES, S. F. *et al.* 2013a “Observations of the effect of ionization-potential depression in hot dense plasma”. *Phys. Rev. Lett.* **110**, 265003, DOI: 10.1103/PhysRevLett.110.265003
- HOARTY, D. J., ALLAN, P., JAMES, S. F. *et al.* 2013b “The first data from the Orion laser; measurements of the spectrum of hot, dense aluminium”. *High Energy Density Physics* **9** (4), 661 – 671, DOI: 10.1016/j.hedp.2013.06.005
- HOGSTROM, K. R. & ALMOND, P. R. 2006 “Review of electron beam therapy physics”. *Physics in Medicine and Biology* **51** (13), R455–R489, DOI: 10.1088/0031-9155/51/13/r25
- HORNÝ, V., KRŮS, M., YAN, W. & FÜLÖP, T. 2020 “Attosecond betatron radiation pulse train”. *Scientific Reports* **10**, 15074, DOI: 10.1038/s41598-020-72053-z
- HOSKIN, P. J. & BHATTACHARYA, I. S. 2014 “Protons and more: state of the art in radiotherapy”. *Clinical Medicine* **14** (Suppl 6), s61–s65, DOI: 10.7861/clinmedicine.14-6-s61
- HUNANA, P., ZANK, G. P., LAURENZA, M., TENERANI, A., WEBB, G. M., GOLDSTEIN, M. L., VELLI, M. & ADHIKARI, L. 2018 “New closures for more precise modeling of Landau damping in the fluid framework”. *Phys. Rev. Lett.* **121**, 135101, DOI: 10.1103/PhysRevLett.121.135101
- ITATANI, J., QUÉRÉ, F., YUDIN, G. L., IVANOV, M. Y., KRAUSZ, F. & CORKUM, P. B. 2002 “Attosecond streak camera”. *Phys. Rev. Lett.* **88**, 173903, DOI: 10.1103/PhysRevLett.88.173903
- IZZO, V. A., PUSZTAI, I., SÄRKIMÄKI, K., SUNDRÖM, A., GARNIER, D. T., WEISBERG, D., TINGUELY, R. A., PAZ-SOLDAN, C., GRANETZ, R. S. & SWEENEY, R. 2022 “Runaway electron deconfinement in SPARC and DIII-D by a passive 3D coil”. *Nuclear Fusion* **62** (9), 096029, DOI: 10.1088/1741-4326/ac83d8
- JACKSON, J. D. 1999 *Classical Electrodynamics*. 3rd edn., Wiley, ISBN 978-0-471-30932-1
- JALAS, S., DORNMAIR, I., LEHE, R., VINCENTI, H., VAY, J.-L., KIRCHEN, M. & MAIER, A. R. 2017 “Accurate modeling of plasma acceleration with arbitrary order pseudo-spectral particle-in-cell methods”. *Physics of Plasmas* **24** (3), 033115, DOI: 10.1063/1.4978569
- JANG, H., HUR, M. S., LEE, J. M., CHO, M. H., NAMKUNG, W. & SUK, H. 2008 “A method to measure the electron temperature and density of a laser-produced plasma by Raman scattering”. *Applied Physics Letters* **93** (7), 071506, DOI: 10.1063/1.2973395
- JOSHI, C., MORI, W. B., KATSIOULEAS, T., DAWSON, J. M., KINDEL, J. M. & FORSLUND, D. W. 1984 “Ultra-high gradient particle acceleration by intense laser-driven plasma density waves”. *Nature* **311** (5986), 525–529, DOI: 10.1038/311525a0

- JUNO, J. 2020 “A deep dive into the distribution function: Understanding phase space dynamics with continuum Vlasov–Maxwell simulations”. PhD thesis, University of Maryland, College Park, Maryland. <https://arxiv.org/abs/2005.13539>
- JUNO, J., HAKIM, A., TENBARGE, J., SHI, E. & DORLAND, W. 2018 “Discontinuous galerkin algorithms for fully kinetic plasmas”. *Journal of Computational Physics* **353**, 110 – 147, DOI: 10.1016/j.jcp.2017.10.009
- JUNO, J., SWISDAK, M. M., TENBARGE, J. M., SKOUTNEV, V. & HAKIM, A. 2020 “Noise-induced magnetic field saturation in kinetic simulations”. *Journal of Plasma Physics* **86** (4), 175860 401, DOI: 10.1017/S0022377820000707
- JÜTTNER, F. 1911 “Das Maxwellsche Gesetz der Geschwindigkeitsverteilung in der Relativtheorie”. *Annalen der Physik* **339** (5), 856–882, DOI: 10.1002/andp.19113390503. In German, English title roughly “The Maxwellian law of the velocity distribution in the theory of relativity”.
- KARSCH, L., BEYREUTHER, E., ENGHARDT, W., GOTZ, M., MASOOD, U., SCHRAMM, U., ZEIL, K. & PAWELKE, J. 2017 “Towards ion beam therapy based on laser plasma accelerators”. *Acta Oncologica* **56** (11), 1359–1366, DOI: 10.1080/0284186X.2017.1355111
- KAW, P. K. 2017 “Nonlinear laser–plasma interactions”. *Reviews of Modern Plasma Physics* **1** (1), 1–42, DOI: 10.1007/s41614-017-0005-2
- KAW, P. & DAWSON, J. 1970 “Relativistic nonlinear propagation of laser beams in cold overdense plasmas”. *The Physics of Fluids* **13** (2), 472–481, DOI: 10.1063/1.1692942
- KEMP, A. J., FIUZA, F., DEBAYLE, A., JOHZAKI, T., MORI, W. B., PATEL, P. K., SENTOKU, Y. & SILVA, L. O. 2014 “Laser–plasma interactions for fast ignition”. *Nuclear Fusion* **54** (5), 054002, DOI: 10.1088/0029-5515/54/5/054002
- KIM, I. J., PAE, K. H., CHOI, I. W. *et al.* 2016 “Radiation pressure acceleration of protons to 93 MeV with circularly polarized petawatt laser pulses”. *Physics of Plasmas* **23** (7), 070 701, DOI: 10.1063/1.4958654
- KIRKWOOD, J. G. 1946 “The statistical mechanical theory of transport processes I. General theory”. *The Journal of Chemical Physics* **14** (3), 180–201, DOI: 10.1063/1.1724117
- KLUGE, T., RÖDEL, M., METZKES-NG, J. *et al.* 2018 “Observation of ultrafast solid-density plasma dynamics using femtosecond x-ray pulses from a free-electron laser”. *Phys. Rev. X* **8**, 031 068, DOI: 10.1103/PhysRevX.8.031068
- KNUDSON, M. D., DESJARLAIS, M. P. & DOLAN, D. H. 2008 “Shock-wave exploration of the high-pressure phases of carbon”. *Science* **322** (5909), 1822–1825, DOI: 10.1126/science.1165278
- KOLIYADU, J. C. P., KÜNZEL, S., WODZINSKI, T. *et al.* 2017 “Optimization and characterization of high-harmonic generation for probing solid density plasmas”. *Photonics* **4** (2), 25, DOI: 10.3390/photonics4020025
- KRUEER, W. L. 2003 *The Physics Of Laser Plasma Interactions*. 1st edn., CRC Press, ISBN 0-8133-4083-7
- KRUEER, W. L. & ESTABROOK, K. 1985 “J×B heating by very intense laser light”. *The Phys. of Fluids* **28**, 430–432, DOI: 10.1063/1.865171
- LANGDON, A. B. 2014 “Evolution of Particle-in-Cell plasma simulation”. *IEEE Transactions on Plasma Science* **42** (5), 1317–1320, DOI: 10.1109/TPS.2014.2314615

- LANGMUIR, I. 1928 “Oscillations in ionized gases”. *Proceedings of the National Academy of Sciences* **14** (8), 627–637, DOI: 10.1073/pnas.14.8.627
- LAW, K. F. F., ABE, Y., MORACE, A. *et al.* 2020 “Relativistic magnetic reconnection in laser laboratory for testing an emission mechanism of hard-state black hole system”. *Phys. Rev. E* **102**, 033202, DOI: 10.1103/PhysRevE.102.033202
- LE PAPE, S., BERZAK HOPKINS, L. F., DIVOL, L. *et al.* 2018 “Fusion energy output greater than the kinetic energy of an imploding shell at the national ignition facility”. *Phys. Rev. Lett.* **120**, 245003, DOI: 10.1103/PhysRevLett.120.245003
- LEĆZ, Z., KONOPLEV, I. V., SERGI, A. & ANDREEV, A. 2016 “GigaGauss solenoidal magnetic field inside bubbles excited in under-dense plasma”. *Scientific reports* **6** (1), 1–11, DOI: 10.1038/srep36139
- LEHE, R., KIRCHEN, M., ANDRIYASH, I. A., GODFREY, B. B. & VAY, J.-L. 2016 “A spectral, quasi-cylindrical and dispersion-free Particle-In-Cell algorithm”. *Computer Physics Communications* **203**, 66–82, DOI: <https://doi.org/10.1016/j.cpc.2016.02.007>
- LENARD, A. & BERNSTEIN, I. B. 1958 “Plasma oscillations with diffusion in velocity space”. *Phys. Rev.* **112**, 1456–1459, DOI: 10.1103/PhysRev.112.1456. URL <https://link.aps.org/doi/10.1103/PhysRev.112.1456>
- LIAO, G.-Q. & LI, Y.-T. 2019 “Review of intense terahertz radiation from relativistic laser-produced plasmas”. *IEEE Transactions on Plasma Science* **47** (6), 3002–3008, DOI: 10.1109/TPS.2019.2915624
- LINLOR, W. I. 1963 “Ion energies produced by laser giant pulse”. *Applied Physics Letters* **3** (11), 210–211, DOI: 10.1063/1.1753852
- LINZ, U. & ALONSO, J. 2007 “What will it take for laser driven proton accelerators to be applied to tumor therapy?” *Phys. Rev. ST Accel. Beams* **10**, 094801, DOI: 10.1103/PhysRevSTAB.10.094801
- LOBET, M., D’HUMIÈRES, E., GRECH, M., RUYER, C., DAVOINE, X. & GREMILLET, L. 2016 “Modeling of radiative and quantum electrodynamics effects in PIC simulations of ultra-relativistic laser-plasma interaction”. *Journal of Physics: Conference Series* **688**, 012058, DOI: 10.1088/1742-6596/688/1/012058
- LÓPEZ-MARTENS, R., VARJÚ, K., JOHNSON, P., MAURITSSON, J., MAIRESSE, Y., SALIÈRES, P., GAARDE, M. B., SCHAFER, K. J., PERSSON, A., SVANBERG, S., WAHLSTRÖM, C.-G. & L’HUILIER, A. 2005 “Amplitude and phase control of attosecond light pulses”. *Phys. Rev. Lett.* **94**, 033001, DOI: 10.1103/PhysRevLett.94.033001
- LOVELACE, R. V. & SUDAN, R. N. 1971 “Plasma heating by high-current relativistic electron beams”. *Phys. Rev. Lett.* **27**, 1256–1259, DOI: 10.1103/PhysRevLett.27.1256
- LUNDH, O., LIM, J., RECHATIN, C., AMMOURA, L., BEN-ISMAÏL, A., DAVOINE, X., GALLOT, G., GODDET, J.-P., LEFEBVRE, E., MALKA, V. & FAURE, J. 2011 “Few femtosecond, few kiloampere electron bunch produced by a laser–plasma accelerator”. *Nature Physics* **7** (3), 219–222, DOI: 10.1038/nphys1872
- MACCHI, A. 2013 *A Superintense Laser–Plasma Interaction Theory Primer*. 1st edn., Springer, ISBN 978-94-007-6124-7
- MACCHI, A. 2014 “Theory of light sail acceleration by intense lasers: an overview”. *High Power Laser Science and Engineering* **2**, e10, DOI: 10.1017/hpl.2014.13

- MACCHI, A., CATTANI, F., LISEYKINA, T. V. & CORNOLTI, F. 2005 “Laser acceleration of ion bunches at the front surface of overdense plasmas”. *Phys. Rev. Lett.* **94**, 165 003, DOI: 10.1103/PhysRevLett.94.165003
- MACCHI, A., BORGHESI, M. & PASSONI, M. 2013 “Ion acceleration by superintense laser-plasma interaction”. *Rev. Mod. Phys.* **85**, 751–793, DOI: 10.1103/RevModPhys.85.751
- MAIER, M., KAISER, W. & GIORDMAINE, J. A. 1966 “Intense light bursts in the stimulated Raman effect”. *Phys. Rev. Lett.* **17**, 1275–1277, DOI: 10.1103/PhysRevLett.17.1275
- MAIMAN, T. H. 1960 “Stimulated optical radiation in ruby”. *Nature* **187** (4736), 493–494, DOI: 10.1038/187493a0
- MALKO, S., CAYZAC, W., OSPINA-BOHORQUEZ, V., BHUTWALA, K., BAILLY-GRANDVAUX, M., MCGUFFEY, C., FEDOSEJEVS, R., VAISSEAU, X., TAUSCHWITZ, A., APIÑANIZ, J. *et al.* 2022 “Proton stopping measurements at low velocity in warm dense carbon”. *Nature Communications* **13** (1), 1–12, DOI: 10.1038/s41467-022-30472-8
- MANSCHWETUS, B., RADING, L., CAMPI, F. *et al.* 2016 “Two-photon double ionization of neon using an intense attosecond pulse train”. *Phys. Rev. A* **93**, 061 402, DOI: 10.1103/PhysRevA.93.061402
- MANČIĆ, A., LÉVY, A., HARMAND, M. *et al.* 2010 “Picosecond short-range disordering in isochorically heated aluminum at solid density”. *Phys. Rev. Lett.* **104**, 035 002, DOI: 10.1103/PhysRevLett.104.035002
- MARTINEZ, B., CHEN, S. N., BOLAÑOS, S. *et al.* 2022 “Numerical investigation of spallation neutrons generated from petawatt-scale laser-driven proton beams”. *Matter and Radiation at Extremes* **7** (2), 024 401, DOI: 10.1063/5.0060582
- MARTINOLLI, E., KOENIG, M., BATON, S. D. *et al.* 2006 “Fast-electron transport and heating of solid targets in high-intensity laser interactions measured by K α fluorescence”. *Phys. Rev. E* **73**, 046 402, DOI: 10.1103/PhysRevE.73.046402
- MATSUO, K., HIGASHI, N., IWATA, N. *et al.* 2020 “Petapascal pressure driven by fast isochoric heating with a multipicosecond intense laser pulse”. *Phys. Rev. Lett.* **124**, 035 001, DOI: 10.1103/PhysRevLett.124.035001
- MAXWELL, J. C. 1860 “V. Illustrations of the dynamical theory of gases.—Part I. on the motions and collisions of perfectly elastic spheres”. *The London, Edinburgh, and Dublin Philosophical Magazine and Journal of Science* **19** (124), 19–32, DOI: 10.1080/14786446008642818
- MAXWELL, J. C. 1865 “VIII. A dynamical theory of the electromagnetic field”. *Philosophical Transactions of the Royal Society of London* **155**, 459–512, DOI: 10.1098/rstl.1865.0008
- MAXWELL, J. C. 1871 Introductory lecture on experimental physics, held at Cambridge in October 1871.
- MAY, J., TONGE, J., FIUZA, F., FONSECA, R. A., SILVA, L. O., REN, C. & MORI, W. B. 2011 “Mechanism of generating fast electrons by an intense laser at a steep overdense interface”. *Phys. Rev. E* **84**, 025 401, DOI: 10.1103/PhysRevE.84.025401
- MCCCLUNG, F. J. & HELLWARTH, R. W. 1962 “Giant optical pulsations from ruby”. *Journal of Applied Physics* **33** (3), 828–829, DOI: 10.1063/1.1777174

- MERDJI, H., SALIÈRES, P., LE DÉROFF, L. *et al.* 2000 “Coherence properties of high-order harmonics: Application to high-density laser–plasma diagnostic”. *Laser and Particle Beams* **18** (3), 495–502, DOI: 10.1017/S026303460018320X
- MODENA, A., NAJMUDIN, Z., DANGOR, A. E., CLAYTON, C. E., MARSH, K. A., JOSHI, C., MALKA, V., DARROW, C. B., DANSON, C., NEELY, D. & WALSH, F. N. 1995 “Electron acceleration from the breaking of relativistic plasma waves”. *Nature* **377** (6550), 606–608, DOI: 10.1038/377606a0
- MOISEEV, S. S. & SAGDEEV, R. Z. 1963 “Collisionless shock waves in a plasma in a weak magnetic field”. *Journal of Nuclear Energy Part C* **5** (1), 43–47, DOI: 10.1088/0368-3281/5/1/309
- NANBU, K. 1997 “Theory of cumulative small-angle collisions in plasmas”. *Phys. Rev. E* **55**, 4642–4652, DOI: 10.1103/PhysRevE.55.4642
- NANBU, K. & YONEMURA, S. 1998 “Weighted particles in Coulomb collision simulations based on the theory of a cumulative scattering angle”. *Journal of Computational Physics* **145** (2), 639 – 654, ISSN 0021-9991, DOI: 10.1006/jcph.1998.6049
- NEELY, D., FOSTER, P., ROBINSON, A., LINDAU, F., LUNDH, O., PERSSON, A., WAHLSTRÖM, C.-G. & MCKENNA, P. 2006 “Enhanced proton beams from ultrathin targets driven by high contrast laser pulses”. *Applied Physics Letters* **89** (2), 021 502, DOI: 10.1063/1.2220011
- NETTELMANN, N., HOLST, B., KIETZMANN, A., FRENCH, M., REDMER, R. & BLASCHKE, D. 2008 “Ab initio equation of state data for hydrogen, helium, and water and the internal structure of Jupiter”. *The Astrophysical Journal* **683** (2), 1217–1228, DOI: 10.1086/589806
- NILSON, P. M., WILLINGALE, L., KALUZA, M. C. *et al.* 2006 “Magnetic reconnection and plasma dynamics in two-beam laser–solid interactions”. *Phys. Rev. Lett.* **97**, 255 001, DOI: 10.1103/PhysRevLett.97.255001
- NILSON, P. M., THEOBALD, W., MYATT, J. F., STOECKL, C., STORM, M., ZUEGEL, J. D., BETTI, R., MEYERHOFER, D. D. & SANGSTER, T. C. 2009 “Bulk heating of solid-density plasmas during high-intensity-laser plasma interactions”. *Phys. Rev. E* **79**, 016 406, DOI: 10.1103/PhysRevE.79.016406
- NILSON, P. M., SOLODOV, A. A., MYATT, J. F. *et al.* 2010 “Scaling hot-electron generation to high-power, kilojoule-class laser–solid interactions”. *Phys. Rev. Lett.* **105**, 235 001, DOI: 10.1103/PhysRevLett.105.235001
- NÜRNBERG, F., SCHOLLMEIER, M., BRAMBRINK, E. *et al.* 2009 “Radiochromic film imaging spectroscopy of laser-accelerated proton beams”. *Review of Scientific Instruments* **80** (3), 033 301, DOI: 10.1063/1.3086424
- NUTER, R., GREMILLET, L., LEFEBVRE, E., LÉVY, A., CECCOTTI, T. & MARTIN, P. 2011 “Field ionization model implemented in particle in cell code and applied to laser-accelerated carbon ions”. *Physics of Plasmas* **18** (3), 033 107, DOI: 10.1063/1.3559494
- NUTER, R., GRECH, M., DE ALAIZA MARTINEZ, P. G., BONNAUD, G. & D’HUMIERES, E. 2014 “Maxwell solvers for the simulations of the laser–matter interaction”. *The European Physical Journal D* **68** (6), 1–9, DOI: 10.1140/epjd/e2014-50162-y
- PAK, A., KERR, S., LEMOS, N. *et al.* 2018 “Collisionless shock acceleration of narrow energy spread ion beams from mixed species plasmas using 1 μm lasers”. *Phys.*

- Rev. Accel. Beams* **21**, 103401, DOI: 10.1103/PhysRevAccelBeams.21.103401
- PALMER, R. B. 1972 “Interaction of relativistic particles and free electromagnetic waves in the presence of a static helical magnet”. *Journal of Applied Physics* **43** (7), 3014–3023, DOI: 10.1063/1.1661650
- PAQUETTE, C., PELLETIER, C., FONTAINE, G. & MICHAUD, G. 1986 “Diffusion Coefficients for Stellar Plasmas”. *The Astrophysical Journal Supplement Series* **61**, 177, DOI: 10.1086/191111
- PASCAL, B. 1657 Les Provinciales, ou les Lettres écrites par Louis de Montalte a un provincial de ses amis & aux RR. PP. Iesuites: sur le sujet de la Morale & de la Politique de ces Peres. 1st edn., Cologne: Pierre de la Vallee
- PATEL, P. K., MACKINNON, A. J., KEY, M. H., COWAN, T. E., FOORD, M. E., ALLEN, M., PRICE, D. F., RUHL, H., SPRINGER, P. T. & STEPHENS, R. 2003 “Isochoric heating of solid-density matter with an ultrafast proton beam”. *Phys. Rev. Lett.* **91**, 125004, DOI: 10.1103/PhysRevLett.91.125004
- PAUL, P. M., TOMA, E. S., BREGER, P., MULLOT, G., AUGÉ, F., BALCOU, PH., MULLER, H. G. & AGOSTINI, P. 2001 “Observation of a train of attosecond pulses from high harmonic generation”. *Science* **292** (5522), 1689–1692, DOI: 10.1126/science.1059413
- PÉREZ, F., GREMILLET, L., KOENIG, M. *et al.* 2010 “Enhanced isochoric heating from fast electrons produced by high-contrast, relativistic-intensity laser pulses”. *Phys. Rev. Lett.* **104**, 085001, DOI: 10.1103/PhysRevLett.104.085001
- PÉREZ, F., GREMILLET, L., DECOSTER, A., DROUIN, M. & LEFEBVRE, E. 2012 “Improved modeling of relativistic collisions and collisional ionization in particle-in-cell codes”. *Phys. of Plasmas* **19**, 083104, DOI: 10.1063/1.4742167
- PING, Y., GELTNER, I., FISCH, N. J., SHVETS, G. & SUCKEWER, S. 2000 “Demonstration of ultrashort laser pulse amplification in plasmas by a counterpropagating pumping beam”. *Phys. Rev. E* **62**, R4532–R4535, DOI: 10.1103/PhysRevE.62.R4532
- PUKHOV, A. 2016 “Particle-in-cell codes for plasma-based particle acceleration”. In “Proceedings of the 2014 CAS-CERN Accelerator School: Plasma Wake Acceleration”, (ed. B. Holzer), vol. 1, (181–206), DOI: 10.5170/CERN-2016-001.181
- PURVIS, M. A., SHLYAPTSEV, V. N., HOLLINGER, R., BARGSTEN, C., PUKHOV, A., PRIETO, A., WANG, Y., LUTHER, B. M., YIN, L., WANG, S. & ROCCA, J. J. 2013 “Relativistic plasma nanophotonics for ultrahigh energy density physics”. *Nat. Photonics* **7**, 796–800, DOI: 10.1038/nphoton.2013.217
- PUSZTAI, I., TENBARGE, J. M., CSAPÓ, A. N., JUNO, J., HAKIM, A., YI, L. & FÜLÖP, T. 2018 “Low Mach-number collisionless electrostatic shocks and associated ion acceleration”. *Plasma Physics and Controlled Fusion* **60**, 035004, DOI: 10.1088/1361-6587/aaa2cc
- PUSZTAI, I., JUNO, J., BRANDENBURG, A., TENBARGE, J. M., HAKIM, A., FRANCISQUEZ, M. & SUNDSTRÖM, A. 2020 “Dynamo in weakly collisional nonmagnetized plasmas impeded by Landau damping of magnetic fields”. *Physical Review Letters* **124**, 255102, DOI: 10.1103/PhysRevLett.124.255102
- PUYUELO-VALDES, P., HENARES, J. L., HANNACHI, F. *et al.* 2019 “Proton acceleration by collisionless shocks using a supersonic H₂ gas-jet target and high-power infrared laser pulses”. *Physics of Plasmas* **26** (12), 123109, DOI: 10.1063/1.5116337

- QUESNEL, B. & MORA, P. 1998 “Theory and simulation of the interaction of ultraintense laser pulses with electrons in vacuum”. *Phys. Rev. E* **58**, 3719–3732, DOI: 10.1103/PhysRevE.58.3719
- RABAUD, M. & MOISY, F. 2013 “Ship wakes: Kelvin or mach angle?” *Phys. Rev. Lett.* **110**, 214503, DOI: 10.1103/PhysRevLett.110.214503
- REMINGTON, B. A. 2005 “High energy density laboratory astrophysics”. *Plasma Phys. and Control. Fusion* **47**, A191–A203, DOI: 10.1088/0741-3335/47/5a/014
- REMINGTON, B. A., ARNETT, D., PAUL, R. & TAKABE, H. 1999 “Modeling astrophysical phenomena in the laboratory with intense lasers”. *Science* **284** (5419), 1488–1493, DOI: 10.1126/science.284.5419.1488
- REN, J., CHENG, W., LI, S. & SUCKEWER, S. 2007 “A new method for generating ultraintense and ultrashort laser pulses”. *Nature Physics* **3** (10), 732–736, DOI: 10.1038/nphys717
- RENAUDIN, P., BLANCARD, C., CLÉROUIN, J., FAUSSURIER, G., NOIRET, P. & RECOULES, V. 2003 “Aluminum equation-of-state data in the warm dense matter regime”. *Phys. Rev. Lett.* **91**, 075002, DOI: 10.1103/PhysRevLett.91.075002
- RENNER, O. & ROSMEJ, F. B. 2019 “Challenges of x-ray spectroscopy in investigations of matter under extreme conditions”. *Matter and Radiation at Extremes* **4** (2), 024201, DOI: 10.1063/1.5086344
- RICHTER, C., KALUZA, M., KARSCH, L., SCHLENVOIGT, H.-P., SCHÜRER, M., SOBIELLA, M., WOITHE, J. & PAWELKE, J. 2011 “Dosimetry of laser-accelerated electron beams used for in vitro cell irradiation experiments”. *Radiation Measurements* **46** (12), 2006–2009, ISSN 1350-4487, DOI: 10.1016/j.radmeas.2011.04.019. Proceedings of the 16th Solid State Dosimetry Conference
- RICONDA, C., WEBER, S., LANCIA, L., MARQUÈS, J.-R., MOUROU, G. & FUCHS, J. 2014 “Plasma-based creation of short light pulses: analysis and simulation of amplification and focusing”. *Plasma Physics and Controlled Fusion* **57** (1), 014002, DOI: 10.1088/0741-3335/57/1/014002
- RINCON, F., CALIFANO, F., SCHEKOCIHIN, A. A. & VALENTINI, F. 2016 “Turbulent dynamo in a collisionless plasma”. *Proceedings of the National Academy of Sciences* **113** (15), 3950–3953, DOI: 10.1073/pnas.1525194113
- RIVAS, D. E., BOROT, A., CARDENAS, D. E. *et al.* 2017 “Next generation driver for attosecond and laser-plasma physics”. *Scientific reports* **7** (1), 1–8, DOI: 10.1038/s41598-017-05082-w
- ROBINSON, A. P. L. 2011 “Production of high energy protons with hole-boring radiation pressure acceleration”. *Physics of Plasmas* **18** (5), 056701, DOI: 10.1063/1.3562551
- ROBINSON, A. P. L., STROZZI, D. J., DAVIES, J. R., GREMILLET, L., HONRUBIA, J. J., JOHZAKI, T., KINGHAM, R. J., SHERLOCK, M. & SOLODOV, A. A. 2014 “Theory of fast electron transport for fast ignition”. *Nucl. Fusion* **54** (5), 054003, DOI: 10.1088/0029-5515/54/5/054003
- ROMAGNANI, L., FUCHS, J., BORGHESI, M. *et al.* 2005 “Dynamics of electric fields driving the laser acceleration of multi-MeV protons”. *Phys. Rev. Lett.* **95**, 195001, DOI: 10.1103/PhysRevLett.95.195001
- ROMAGNANI, L., BULANOV, S. V., BORGHESI, M., AUDEBERT, P., GAUTHIER, J. C., LÖWENBRÜCK, K., MACKINNON, A. J., PATEL, P., PRETZLER, G.,

- TONCIAN, T. & WILLI, O. 2008 “Observation of collisionless shocks in laser-plasma experiments”. *Phys. Rev. Lett.* **101**, 025 004, DOI: 10.1103/PhysRevLett.101.025004
- ROSS, M. 1981 “The ice layer in Uranus and Neptune—diamonds in the sky?” *Nature* **292** (5822), 435–436, DOI: 10.1038/292435a0
- ROTH, M., JUNG, D., FALK, K. *et al.* 2013 “Bright laser-driven neutron source based on the relativistic transparency of solids”. *Phys. Rev. Lett.* **110**, 044 802, DOI: 10.1103/PhysRevLett.110.044802
- ROUSSE, A., PHUOC, K. T., SHAH, R., PUKHOV, A., LEFEBVRE, E., MALKA, V., KISELEV, S., BURG, F., ROUSSEAU, J.-P., UMSTADTER, D. & HULIN, D. 2004 “Production of a keV x-ray beam from synchrotron radiation in relativistic laser-plasma interaction”. *Phys. Rev. Lett.* **93**, 135 005, DOI: 10.1103/PhysRevLett.93.135005
- ROZMUS, W. & TIKHONCHUK, V. T. 1990 “Skin effect and interaction of short laser pulses with dense plasmas”. *Phys. Rev. A* **42**, 7401, DOI: 10.1103/PhysRevA.42.7401
- SALIÈRES, P., LE DÉROFF, L., AUGUSTE, T., MONOT, P., D’OLIVEIRA, P., CAMPO, D., HERGOTT, J.-F., MERDJI, H. & CARRÉ, B. 1999 “Frequency-domain interferometry in the XUV with high-order harmonics”. *Phys. Rev. Lett.* **83**, 5483–5486, DOI: 10.1103/PhysRevLett.83.5483
- SANTOS, J. J., VAUZOUR, B., TOUATI, M. *et al.* 2017 “Isochoric heating and strong blast wave formation driven by fast electrons in solid-density targets”. *New Journal of Physics* **19** (10), 103 005, DOI: 10.1088/1367-2630/aa806b
- SÄVERT, A., MANGLES, S. P. D., SCHNELL, M. *et al.* 2015 “Direct observation of the injection dynamics of a laser wakefield accelerator using few-femtosecond shadowgraphy”. *Phys. Rev. Lett.* **115**, 055 002, DOI: 10.1103/PhysRevLett.115.055002
- SAWADA, H., SENTOKU, Y., YABUCHI, T., ZASTRAU, U., FÖRSTER, E., BEG, F. N., CHEN, H., KEMP, A. J., MCLEAN, H. S., PATEL, P. K. & PING, Y. 2019 “Monochromatic 2D $K\alpha$ emission images revealing short-pulse laser isochoric heating mechanism”. *Phys. Rev. Lett.* **122**, 155 002, DOI: 10.1103/PhysRevLett.122.155002
- SCHWAB, M. B., SÄVERT, A., JÄCKEL, O., POLZ, J., SCHNELL, M., RINCK, T., VEISZ, L., MÖLLER, M., HANSINGER, P., PAULUS, G. G. & KALUZA, M. C. 2013 “Few-cycle optical probe-pulse for investigation of relativistic laser-plasma interactions”. *Applied Physics Letters* **103** (19), 191 118, DOI: 10.1063/1.4829489
- SCHÖNLEIN, A., BOUTOUX, G., PIKUZ, S. *et al.* 2016 “Generation and characterization of warm dense matter isochorically heated by laser-induced relativistic electrons in a wire target”. *Europhysics Letters* **114** (4), 45 002, DOI: 10.1209/0295-5075/114/45002
- SEMUSHIN, S. & MALKA, V. 2001 “High density gas jet nozzle design for laser target production”. *Review of Scientific Instruments* **72** (7), 2961–2965, DOI: 10.1063/1.1380393
- SENTOKU, Y. & KEMP, A. J. 2008 “Numerical methods for particle simulations at extreme densities and temperatures: Weighted particles, relativistic collisions and reduced currents”. *J. of Comput. Phys.* **227** (14), 6846–6861, DOI: 10.1016/

- j.jcp.2008.03.043
- SHERLOCK, M., HILL, E. G., EVANS, R. G., ROSE, S. J. & ROZMUS, W. 2014 “In-depth plasma-wave heating of dense plasma irradiated by short laser pulses”. *Phys. Rev. Lett.* **113**, 255 001, DOI: 10.1103/PhysRevLett.113.255001
- SHOUCRI, M. M. 2011 Eulerian codes for the numerical solution of the kinetic equations of plasmas. Nova Science Publishers, ISBN 9781613245613
- SILVA, L. O., MARTI, M., DAVIES, J. R., FONSECA, R. A., REN, C., TSUNG, F. S. & MORI, W. B. 2004 “Proton shock acceleration in laser-plasma interactions”. *Phys. Rev. Lett.* **92**, 015 002, DOI: 10.1103/PhysRevLett.92.015002
- SIMINOS, E., GRECH, M., SKUPIN, S., SCHLEGEL, T. & TIKHONCHUK, V. T. 2012 “Effect of electron heating on self-induced transparency in relativistic-intensity laser-plasma interactions”. *Phys. Rev. E* **86**, 056 404, DOI: 10.1103/PhysRevE.86.056404
- SIMINOS, E., SKUPIN, S., SÄVERT, A., COLE, J. M., MANGLES, S. P. D. & KALUZA, M. C. 2016 “Modeling ultrafast shadowgraphy in laser-plasma interaction experiments”. *Plasma Physics and Controlled Fusion* **58** (6), 065 004, DOI: 10.1088/0741-3335/58/6/065004
- SKOUTNEV, V., HAKIM, A., JUNO, J. & TENBARGE, J. M. 2019 “Temperature-dependent saturation of Weibel-type instabilities in counter-streaming plasmas”. *The Astrophysical Journal Letters* **872** (2), L28, DOI: 10.3847/2041-8213/ab0556
- STARK, D. J., BHATTACHARJEE, C., AREFIEV, A. V., TONCIAN, T., HAZELTINE, R. D. & MAHAJAN, S. M. 2015 “Relativistic plasma polarizer: Impact of temperature anisotropy on relativistic transparency”. *Phys. Rev. Lett.* **115**, 025 002, DOI: 10.1103/PhysRevLett.115.025002
- STRICKLAND, D. & MOUROU, G. 1985 “Compression of amplified chirped optical pulses”. *Opt. Commun.* **56** (3), 219 – 221, DOI: 10.1016/0030-4018(85)90120-8
- SUNDSTRÖM, A., JUNO, J., TENBARGE, J. M. & PUSZTAI, I. 2019 “Effect of a weak ion collisionality on the dynamics of kinetic electrostatic shocks”. *Journal of Plasma Physics* **85** (1), 905850 108, DOI: 10.1017/S0022377819000023
- SUNDSTRÖM, A., GREMILLET, L., SIMINOS, E. & PUSZTAI, I. 2020a “Fast collisional electron heating and relaxation with circularly polarized ultraintense short-pulse laser”. *Journal of Plasma Physics* **86** (2), 755860 201, DOI: 10.1017/S0022377820000264
- SUNDSTRÖM, A., GREMILLET, L., SIMINOS, E. & PUSZTAI, I. 2020b “Collisional effects on the ion dynamics in thin-foil targets driven by an ultraintense short pulse laser”. *Plasma Physics and Controlled Fusion* **62** (8), 085 015, DOI: 10.1088/1361-6587/ab9a62
- SUNDSTRÖM, A., PUSZTAI, I., ENG-JOHNSON, P. & FÜLÖP, T. 2022a “Attosecond dispersion as a diagnostics tool for solid-density laser-generated plasmas”. *Journal of Plasma Physics* **88** (2), 905880 211, DOI: 10.1017/S0022377822000307
- SUNDSTRÖM, A., GRECH, M., PUSZTAI, I. & RICONDA, C. 2022b “Stimulated-Raman-scattering amplification of attosecond XUV pulses with pulse-train pumps and application to local in-depth plasma-density measurement”. *Physical Review E* **106**, 045 208, DOI: 10.1103/PhysRevE.106.045208
- SVEDUNG WETTERVIK, B., DUBOIS, T. C. & FÜLÖP, T. 2016 “Vlasov modelling

- of laser-driven collisionless shock acceleration of protons". *Physics of Plasmas* **23** (5), 053103, DOI: 10.1063/1.4948424
- TAJIMA, T. & DAWSON, J. M. 1979 "Laser electron accelerator". *Phys. Rev. Lett.* **43**, 267–270, DOI: 10.1103/PhysRevLett.43.267
- TAJIMA, T., YAN, X. Q. & EBISUZAKI, T. 2020 "Wakefield acceleration". *Reviews of Modern Plasma Physics* **4** (1), 1–72, DOI: 10.1007/s41614-020-0043-z
- TAKABE, H. & KURAMITSU, Y. 2021 "Recent progress of laboratory astrophysics with intense lasers". *High Power Laser Science and Engineering* **9**, e49, DOI: 10.1017/hpl.2021.35
- THIELE, I., ZHOU, B., NGUYEN, A., SMETANINA, E., NUTER, R., KALTENECKER, K. J., DE ALAIZA MARTÍNEZ, P. G., DÉCHARD, J., BERGÉ, L., JEPSEN, P. U. & SKUPIN, S. 2018 "Terahertz emission from laser-driven gas plasmas: a plasmonic point of view". *Optica* **5**, 1617, DOI: 10.1364/OPTICA.5.001617
- TINGUELY, R. A., IZZO, V. A., GARNIER, D. T., SUNDSTRÖM, A., SÄRKIMÄKI, K., EMBRÉUS, O., FÜLÖP, T., GRANETZ, R. S., HOPPE, M., PUSZTAI, I. & SWEENEY, R. 2021 "Modeling the complete prevention of disruption-generated runaway electron beam formation with a passive 3D coil in SPARC". *Nuclear Fusion* **61** (12), 124003, DOI: 10.1088/1741-4326/ac31d7
- TINGUELY, R. A., PUSZTAI, IZZO, V. A., , SÄRKIMÄKI, K., FÜLÖP, T., GARNIER, D. T., GRANETZ, R. S., HOPPE, M., PAZ-SOLDAN, C., SUNDSTRÖM, A. & SWEENEY, R. 2022 "On the minimum transport required to passively suppress runaway electrons in SPARC". *Submitted to Plasma Physics and Controlled Fusion*
- TONKS, L. & LANGMUIR, I. 1929 "Oscillations in ionized gases". *Phys. Rev.* **33**, 195–210, DOI: 10.1103/PhysRev.33.195
- TREACY, E. B. 1968 "Compression of picosecond light pulses". *Physics Letters A* **28** (1), 34–35, ISSN 0375-9601, DOI: 10.1016/0375-9601(68)90584-7
- TRINES, R. M. G. M., FIÚZA, F., BINGHAM, R., FONSECA, R. A., SILVA, L. O., CAIRNS, R. A. & NORREYS, P. A. 2011a "Production of picosecond, kilojoule, and petawatt laser pulses via Raman amplification of nanosecond pulses". *Phys. Rev. Lett.* **107**, 105002, DOI: 10.1103/PhysRevLett.107.105002
- TRINES, R. M. G. M., FIÚZA, F., BINGHAM, R., FONSECA, R. A., SILVA, L. O., CAIRNS, R. A. & NORREYS, P. A. 2011b "Simulations of efficient Raman amplification into the multipetawatt regime". *Nature Physics* **7** (1), 87–92, DOI: 10.1038/nphys1793
- TRINES, R. M. G. M., ALVES, E. P., WEBB, E., VIEIRA, J., FIÚZA, F., FONSECA, R. A., SILVA, L. O., CAIRNS, R. A. & BINGHAM, R. 2020 "New criteria for efficient Raman and Brillouin amplification of laser beams in plasma". *Scientific reports* **10** (1), 1–10, DOI: 10.1038/s41598-020-76801-z
- TZEFERACOS, P., RIGBY, A., BOTT, A. F. A. *et al.* 2018 "Laboratory evidence of dynamo amplification of magnetic fields in a turbulent plasma". *Nature communications* **9** (1), 1–8
- VIEUX, G., ERSFELD, B., FARMER, J. P., HUR, M. S., ISSAC, R. C. & JAROSZYNSKI, D. A. 2013 "Plasma density measurements using chirped pulse broad-band Raman amplification". *Applied Physics Letters* **103** (12), 121106, DOI: 10.1063/1.4821581

- VLASOV, A. A. 1968 “The vibrational properties of an electron gas”. *Soviet Physics Uspekhi* **10** (6), 721–733, DOI: 10.1070/PU1968v010n06ABEH003709
- WAGNER, F., DEPERT, O., BRABETZ, C., FIALA, P., KLEINSCHMIDT, A., POTH, P., SCHANZ, V. A., TEBARTZ, A., ZIELBAUER, B., ROTH, M., STÖHLKER, T. & BAGNOUD, V. 2016 “Maximum proton energy above 85 MeV from the relativistic interaction of laser pulses with micrometer thick CH₂ targets”. *Phys. Rev. Lett.* **116**, 205 002, DOI: 10.1103/PhysRevLett.116.205002
- WANG, L., HAKIM, A. H., NG, J., DONG, C. & GERMASCHEWSKI, K. 2020 “Exact and locally implicit source term solvers for multifluid-Maxwell systems”. *Journal of Computational Physics* **415**, 109 510, DOI: 10.1016/j.jcp.2020.109510
- WEBER, S., RICONDA, C., LANCIA, L., MARQUÈS, J.-R., MOUROU, G. A. & FUCHS, J. 2013 “Amplification of ultrashort laser pulses by Brillouin backscattering in plasmas”. *Phys. Rev. Lett.* **111**, 055 004, DOI: 10.1103/PhysRevLett.111.055004
- WEI, M. S., MANGLES, S. P. D., NAJMUDIN, Z. *et al.* 2004 “Ion acceleration by collisionless shocks in high-intensity-laser–underdense-plasma interaction”. *Phys. Rev. Lett.* **93**, 155 003, DOI: 10.1103/PhysRevLett.93.155003
- WEIBEL, E. S. 1967 “Anomalous skin effect in a plasma”. *The Physics of Fluids* **10** (4), 741–748, DOI: 10.1063/1.1762185
- WHEELER, J. A., BOROT, A., MONCHOCÉ, S., VINCENTI, H., RICCI, A., MALVACHE, A., LOPEZ-MARTENS, R. & QUÉRÉ, F. 2012 “Attosecond lighthouses from plasma mirrors”. *Nature Photonics* **6** (12), 829–833, DOI: 10.1038/nphoton.2012.284
- WILKS, S. C., LANGDON, A. B., COWAN, T. E., ROTH, M., SINGH, M., HATCHETT, S., KEY, M. H., PENNINGTON, D., MACKINNON, A. & SNAVELY, R. A. 2001 “Energetic proton generation in ultra-intense laser–solid interactions”. *Physics of Plasmas* **8** (2), 542–549, DOI: 10.1063/1.1333697
- WILLIAMS, G. O., CHUNG, H.-K., VINKO, S. M., KÜNZEL, S., SARDINHA, A. B., ZEITOUN, PH. & FAJARDO, M. 2013 “Method of time resolved refractive index measurements of x-ray laser heated solids”. *Physics of Plasmas* **20** (4), 042 701, DOI: 10.1063/1.4794964
- XUE, B., TAMARU, Y., FU, Y., YUAN, H., LAN, P., MÜCKE, O. D., SUDA, A., MIDORIKAWA, K. & TAKAHASHI, E. J. 2020 “Fully stabilized multi-TW optical waveform synthesizer: Toward gigawatt isolated attosecond pulses”. *Science Advances* **6** (16), eaay2802, DOI: 10.1126/sciadv.aay2802
- YI, L. 2021 “High-harmonic generation and spin-orbit interaction of light in a relativistic oscillating window”. *Phys. Rev. Lett.* **126**, 134 801, DOI: 10.1103/PhysRevLett.126.134801
- YI, L. & FÜLÖP, T. 2019 “Coherent diffraction radiation of relativistic terahertz pulses from a laser-driven microplasma waveguide”. *Phys. Rev. Lett.* **123**, 094 801, DOI: 10.1103/PhysRevLett.123.094801
- YI, L., SHEN, B., PUKHOV, A. & FÜLÖP, T. 2018 “Relativistic magnetic reconnection driven by a laser interacting with a micro-scale plasma slab”. *Nature Communications* **9**, 1601, DOI: 10.1038/s41467-018-04065-3
- YU, P., XU, X., DECYK, V. K., AN, W., VIEIRA, J., TSUNG, F. S., FONSECA, R. A., LU, W., SILVA, L. O. & MORI, W. B. 2014 “Modeling of laser wakefield acceleration in Lorentz boosted frame using EM-PIC code with spectral solver”.

- Journal of Computational Physics* **266**, 124–138, DOI: 10.1016/j.jcp.2014.02.016
- YVON, J. 1935 *La théorie statistique des fluides et l'équation d'état*, vol. 203. Hermann & cie
- ZEPF, M. 2011 “Powerful attosecond pulses from relativistic mirrors”. In “CLEO: 2011 – Laser Science to Photonic Applications”, DOI: 10.1364/QELS.2011.QTuC5
- ZHANG, H., SHEN, B. F., WANG, W. P. *et al.* 2017a “Collisionless shock acceleration of high-flux quasimonoenergetic proton beams driven by circularly polarized laser pulses”. *Phys. Rev. Lett.* **119**, 164801, DOI: 10.1103/PhysRevLett.119.164801
- ZHANG, C. J., HUA, J. F., WAN, Y. *et al.* 2017b “Femtosecond probing of plasma wakefields and observation of the plasma wake reversal using a relativistic electron bunch”. *Phys. Rev. Lett.* **119**, 064801, DOI: 10.1103/PhysRevLett.119.064801
- ZHONG, J., LI, Y., WANG, X. *et al.* 2010 “Modelling loop-top x-ray source and reconnection outflows in solar flares with intense lasers”. *Nature Physics* **6** (12), 984–987, DOI: 10.1038/nphys1790
- ZYLSTRA, A. B., HURRICANE, O. A., CALLAHAN, D. A. *et al.* 2022 “Burning plasma achieved in inertial fusion”. *Nature* **601** (7894), 542–548, DOI: 10.1038/s41586-021-04281-w